2021

Na/K-ATPase ALPHα1 Regulates Adipogenesis via Its Conserved Caveolin Binding Motif

Minqi Huang

NA/K-ATPASE ALPHA1 REGULATES ADIPOGENESIS VIA ITS CONSERVED CAVEOLIN BINDING MOTIF

A dissertation submitted to
the Graduate College of
Marshall University
In partial fulfillment of
the requirements for the degree of
Doctor of Philosophy
In
Biomedical Sciences
by
Minqi Huang
Approved by
Dr. Sandrine Pierre, Committee Chairperson
Dr. Liquan Cai
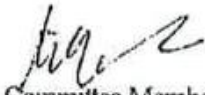Dr. Joseph Shapiro
Dr. Nalini Santanam
Dr. Gustavo Blanco
Dr. Komal Sodhi

Marshall University
July 2021

APPROVAL OF THESIS

We, the faculty supervising the work of Minqi Huang, affirm that the dissertation, [*Na/K-ATPase α1 Regulates Adipogenesis via Its Conserved Caveolin Binding Motif*], meets the high academic standards for original scholarship and creative work established by the [Biomedical Sciences Program] and the [Graduate School of Marshall University. This work also conforms to the editorial standards of our discipline and the Graduate College of Marshall University. With our signatures, we approve the manuscript for publication.

Dr. Sandrine Pierre	Committee Chairperson	5/25/21 Date
Dr. Liquan Cai	Committee Member	5/25/2021 Date
Dr. Joseph Shapiro	Committee Member	5/26/21 Date
Dr. Nalini Santanam	Committee Member	6/1/21 Date
Dr. Gustavo Blanco	Committee Member	5/26/21 Date
Dr. Komal Sodhi	Committee Member	5/27/21 Date

iii

I dedicate this work to Dr. Zijian Xie, a great scientist, mentor, and friend. I greatly appreciate his advice and support throughout the years of my Ph.D. training.

ACKNOWLEDGMENTS

TABLE OF CONTENTS

LIST OF TABLES

LIST OF FIGURES

ABSTRACT

The Na/K-ATPase (NKA) was identified in 1957 by Dr. Jens C. Skou. It belongs to the P-type ATPase family, which can actively transport ions across cell membranes by using the energy from adenosine triphosphate (ATP) hydrolysis. During the second half of the 20th century, the molecular mechanism of the NKA catalytic cycle was clarified, and the isoform diversity of NKA in different species and organs was identified. The active ion transport through NKA generates cell membrane ion gradients and the electric potential. Hence, the enzymatic function of NKA is critical for cell viability as well as multiple physiological processes including muscle contraction, renal sodium reabsorption, and nerve impulse transmission. Inhibition of NKA-mediated ion transport by cardiotonic steroids (CTS), which have long been used in the clinical treatment of heart failure, improves cardiac inotropy. Moreover, CTS at low concentrations were found to induce signal transduction through NKA, revealing its receptor signaling function. In addition to its role as an ion pump, the NKA α1 isoform forms a signal receptor complex with the non-receptor tyrosine kinase Src and the scaffolding protein caveolin-1 (Cav1). The gain of the caveolin binding motif (CBM) in the α1 NKA is required for the non-ion pumping function of NKA and the early stages of organogenesis in mice and C. elegans.

Considering the reported importance of NKA non-ion-pumping function in metabolic disorders, we further tested whether the loss of this CBM altered adiposity in mice and impaired adipogenesis in a human induced pluripotent stem cell (iPSC) model. At the age of 6-months, NKA CBM mutant (mCBM) heterozygous mice exhibit altered adiposity and reduced white adipose tissue (WAT) mass. The histology of mCBM WAT indicated tissue fibrosis and chronic inflammation, which may contribute to adipose tissue metabolic dysfunction. To further understand the molecular mechanism, we used an mCBM human iPSC model and a

differentiation protocol to mimic the adipogenesis process *in vitro*. These studies indicated that the loss of CBM function in NKA α1 in human iPSC induces extracellular matrix (ECM) fibrotic remodeling. The ECM remodeling does not block the commitment of stem cells into adipocytes. However, it results in increased oxidative stress, insulin resistance, chronic inflammation, and eventually metabolic dysfunction during adipogenesis.

Thus, we characterized a novel role of the non-ion pumping NKA and its interaction with Cav1 in the regulation of stem cell differentiation and adipogenesis. This provides novel insight into the complex dynamic of regulation of caveolar structure and function in the adipocyte and could be of therapeutic relevance in the management of fat-related disorders ranging from genetic lipodystrophies to metabolic syndromes.

CHAPTER 1

INTRODUCTION

The theory of active ion transport through the cell membrane was proposed in the 1940s. In 1957, Dr. Jens C. Skou first identified an ATPase enzyme that was activated in the presence of both Na^+ and K^+ ions and worked as an ion pump (Skou, 1957). Dr. Skou later named it Na/K-ATPase (NKA). The NKA belongs to the P-type ATPase family. Approximately 23% of the total ATP consumed in humans at rest is utilized by NKA. It plays a significant role in animal physiology by helping maintain resting potential, active transport, and cellular volume (Skou & Esmann, 1992). The NKA is a transmembrane protein with three subunits: α, β, and γ. The catalytic α subunit contains three domains, which allows active transport of three Na^+ and two K^+ through the conformational changes of NKA in one pump cycle (Lingrel & Kuntzweiler, 1994; Lingrel, Van Huysse, O'Brien, Jewell-Motz, Askew, et al., 1994; Morth et al., 2011). They are four isoforms of the NKA α subunit in mammalian species, and their sequences are highly homologous. The distribution of the α1 isoform is ubiquitous, and other isoforms are organ-specific (Blanco & Mercer, 1998). The α isoforms show different affinities for ions, substrate, and ligands (cardiotonic steroids, CTS) in different species and organs (Pressley, Duran, & Pierre, 2005), but the physiological relevance of this isoform diversity remains incompletely understood for the most part.

Studies in the 21st century have shown that NKA is not only an ion pump but also a signal transducer. By coupling with the scaffolding protein caveolin-1 (Cav1) and the protein tyrosine kinase Src, a pool of caveolae-localized NKA α1 can form a signaling complex that responds to low concentration of CTS by inducing signal transduction (Z. Xie, 2003; Z. Xie & Cai, 2003). The caveolin binding motif (CBM) on the N-terminus of NKA was identified as the NKA-Cav1

binding site and is conserved across species (Cai et al., 2008; H. Wang et al., 2004). The loss-of-function mutant NKA α1 CBM (mCBM) does not affect the enzymatic function of NKA, but disrupts NKA/Cav1/Src signalosome, perturbs human cell stemness markers, and is embryonically lethal in the mouse (Cai et al., 2008; X. Wang et al., 2020).

Early studies have shown that two isoforms of the NKA α subunit are expressed in adipocytes: α1 and α2 (Brodsky, 1990; Resh, 1982a, 1982b). It has also been known for some time that insulin stimulates ion transport through adipocyte NKA and that the two α isoforms have different sensitivity to insulin (Lytton, 1985; Lytton, Lin, & Guidotti, 1985; Resh, 1982a). More recently, we have learned that NKA α1 and α2 have different signaling properties (J. Xie et al., 2015). Moreover, there is genetic evidence that the α1 isoform-specific signaling function of NKA exhibits a distinct role in energy metabolism (Kutz et al., 2021) and pharmacological support for an effect in obesity and related complications (Sodhi et al., 2015; Sodhi et al., 2017). These features point to an important and specific physiological role of the caveolar α1 signaling in adipose physiology that has remained unexplored.

This led us to ask the question: is adipogenesis regulated by the non-ion pumping properties of α1 NKA? Using a genetic approach in the mCBM model, an NKA α1 signaling-null mutant model that does not affect the enzymatic function of NKA, we conducted a mechanistic investigation of the importance of the non-ion pumping scaffolding function of NKA in the regulation of adipogenesis in human induced pluripotent stem cells (iPSC).

I.   **Historical Background**

In the 1930s, it was generally recognized that the cell membrane is impermeable to Na^+. To explain the different electrochemical potential of Na^+ between inside and outside the cell, R. Dean first raised a hypothesis that there must be an ion pumping mechanism on the cell

membrane, which can pump Na^+ out and pump K^+ in (Dean, R. B. 1941). The concept of active transport developed during the 1940s and 1950s. By the research of short-circuit current in frog skin, Johnsen, et al. showed that the current is carried by active transport of Na^+. The influx of extracellular K^+ is essential for the efflux of Na^+ (Koefoed-Johnsen, Ussing, & Zerahn, 1952). A link between an active transport of Na^+ and K^+ was suggested (Skou & Esmann, 1992).

The finding that metabolic inhibitors impaired the active transport of Na^+ indicated that energy-rich triphosphate esters are the substrates of the active transport. In red blood cells, ATP was found to be able to support the influx of K^+. Furthermore, ATP was identified as the only substrate which can support active transport, as it could not be replaced by other triphosphates such as GTP, ITP, or UTP (Clarkson & Maizels, 1954; Gardos, 1954; Hoffman, 1962). The Na^+/K^+ stoichiometry was later determined in experiments in red blood cells and purified reconstituted systems. It was shown that 3 moles of Na^+ and 2 moles of K^+ are transported when 1.16 moles of ATP were hydrolyzed (C. B. Jorgensen, Levi, & Zerahn, 1954; A. K. Sen & Post, 1964; Skou & Esmann, 1992). In 1953, Schatzmann observed that CTS inhibit the active transport of Na^+ and K^+, which is specific to the Na/K pump. CTS had been used for the therapy of heart failure for over one hundred years, but the mechanism was still unrevealed (Schatzmann, 1953). The active transport of K^+ and Na^+ also generates an electric potential across the membrane, which is positive on the outside. The pumping of Na^+ and K^+ only adds a few millivolts to the membrane potential in normal cells with a high permeability to Cl^-, (Kernan, 1962; Thomas, 1969). However, this may be critical to the pulse transmission of synapses in the central nervous system (Skou & Esmann, 1992).

In 1957, Skou first identified a novel membrane-bound protein with ATPase properties from the crab nervous giant axon sheath (Skou, 1957). His finding suggested that this ATPase

3

was involved in the active transport of Na^+ and K^+. However, in the 1950s and 1960s, the models of the cell membrane structure were incomplete. For a transport system across the membrane, a protein must have access to both sides of the membrane. Thereby, without the recognition that membrane proteins are spanning the bilayer of lipids, it was difficult to reconcile the structure of an ion-pumping ATPase. The suitable model was introduced in 1972 as the fluid mosaic membrane model. (Singer & Nicolson, 1972; Skou & Esmann, 1992). Dr. Skou received the Nobel Prize in chemistry in 1997 for the first discovery of the ion-transporting enzyme Na/K-ATPase.

II. Structure of NKA

The NKA is a complex of two polypeptide subunits: α and β. The α-subunit contains the binding sites for cations and ATP. It couples ATP hydrolysis with the active transport of ions. The β subunit is essential for the assembly of a fully functional protein. The γ subunit, discovered later, is associated with the function of NKA in a tissue-specific manner (Lingrel & Kuntzweiler, 1994; Skou & Esmann, 1992).

The α-subunit contains about 1012 amino acids forming 10 transmembrane helices (M1-10). Both the N-terminus and C-terminus are on the intracellular side. The sequences of α-subunit from several species and different tissues are identical with more than 92% homology (Blanco & Mercer, 1998; Levenson, 1994). The membrane-spanning segments of the α subunit have an α-helical structure. The large intracellular loop between M4 and M5 is predominantly a β-sheet structure. The α-subunit has three functional domains: the actuator (A) domain includes the N-terminus and the second cytosolic domain (CD2) connected to M2 and M3, the phosphorylation (P) domain resides close to the membrane and is highly conserved, and the nucleotide-binding (N) domain and the C-terminus contains the ATP binding site (Blanco &

4

Mercer, 1998; Lingrel & Kuntzweiler, 1994; Lingrel, Van Huysse, O'Brien, Jewell-Motz,

Askew, et al., 1994; Lingrel, Van Huysse, O'Brien, Jewell-Motz, & Schultheis, 1994; Skou &

Esmann, 1992). In 3D orientation, transmembrane helices M1–M6 form the core of the

membrane transport domain and hold the main ion-binding sites. The C-terminal helices M7–

M10 bind to the core through interaction sites within M6-M7. Upon Na^+ binding, the conserved

aspartic acid residue of the P domain is auto-phosphorylated using ATP bound to the N domain.

Subsequently, K^+ binding stimulates the dephosphorylation of the P domain, which is catalyzed

by glutamic acid in the conserved TGE motif in the A domain (Fig. 1B), (Morth et al., 2011).
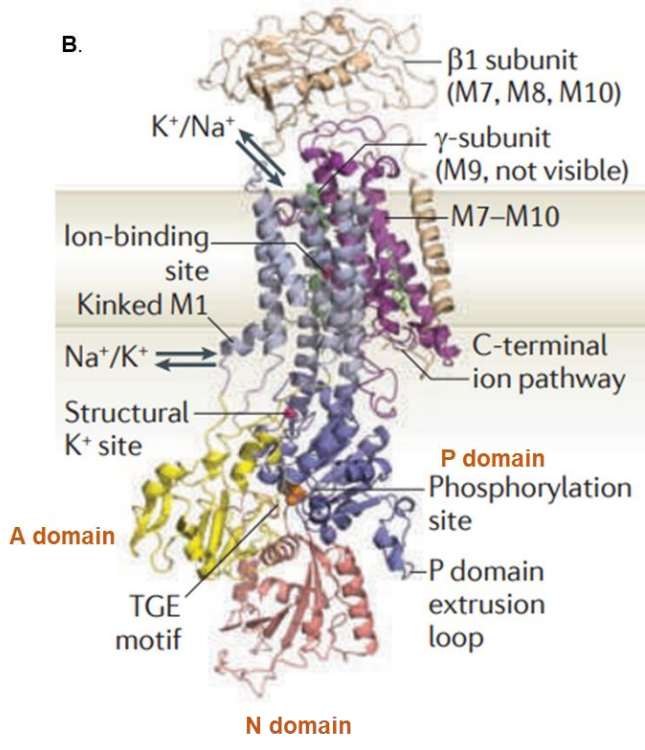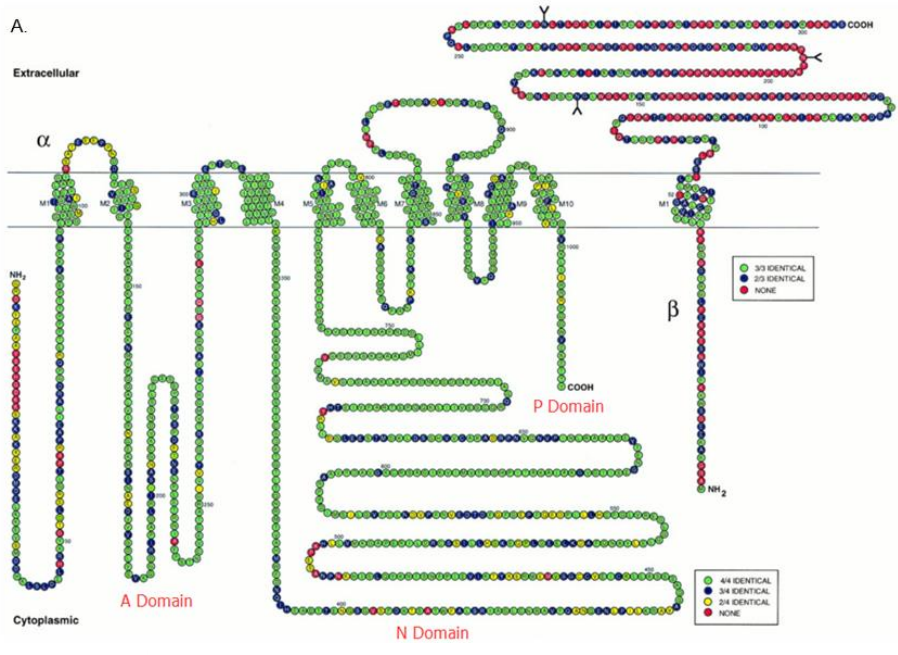
Figure 1. Structural and functional domains in NKA.
A. Schematic diagram of α and β subunits of NKA, adapted from Blanco G. et al. (Blanco & Mercer, 1998). B. Crystal structure and domain organization of NKA, adapted from Morth JP, et al. (Morth et al., 2011)

Four α isoforms are found in human tissues. They are expressed in a tissue-specific manner and regulated during ontogeny and diseases (Pressley et al., 2005). The α1 isoform is found in all cells, the α2 isoform is found in muscle and adipose tissue, and the α3 isoform is mainly found in the nervous tissue together with α1 and α2. The α4 isoform is in the testis and regulates sperm motility (Pressley et al., 2005). The four isoforms differ in their amino acid composition and sequence, with major differences observed in the N-terminal part (P. L. Jorgensen & Andersen, 1988). The four isoforms show different sensitivity towards cation concentration, ATP concentration, and CTS in different species and tissue (Table 1) (Blanco & Mercer, 1998; Lingrel & Kuntzweiler, 1994; Lingrel, Van Huysse, O'Brien, Jewell-Motz, Askew, et al., 1994; Lingrel, Van Huysse, O'Brien, Jewell-Motz, & Schultheis, 1994; Pressley et al., 2005).

Species and tissue	Major differences	Reference
Rodent brain	Affinity for CTS of NKA α2 and α3 is higher than α1	(Sweadner, 1985)
Rat enzyme expressed in HeLa cells	NKA α3 displays a higher affinity for extracellular K^+ and lower affinity for intracellular Na^+ relative to α1 and α2	(Munzer, Daly, Jewell-Motz, Lingrel, & Blostein, 1994)
Rat adipocyte	Insulin stimulates NKA α1 due to a small increase in Na^+ affinity and stimulates the α2 isoforms due to increased Na^+ affinity and an increase in the Vmax.	(McGill & Guidotti, 1991)
Rat enzyme expressed in HeLa cells and monkey kidney cells	The α2 isoform displays a faster rate of occluded K^+ release	(Daly, Lane, & Blostein, 1996; Petrosian, Carr, Guerrero, & Pressley, 1998)
Mammalian skeletal muscle	α2 isoform responds to insulin by translocation from an intracellular pool to the plasmalemma	(Hundal et al., 1992)

Table 1. Isoform-specific differences in NKA α-subunits.

The β-subunit contains about 300 amino acids (Shull, Schwartz, & Lingrel, 1985). There is one transmembrane segment near the N-terminus, and the C-terminus is located on the extracellular side (Fig. 1A) (Blanco & Mercer, 1998). The β-subunit is heavily glycosylated on the extracellular side, with a mass of sugar of about 10kD (Chow & Forte, 1995). There are three β-subunit isoforms. The sequences of β-subunit reveal a low homology between the isoforms (Blanco & Mercer, 1998). The β1 is the primary form in the mammalian kidney. The β2 was mainly isolated from the brain and it has been shown to play a role in cell-cell interaction. The β3 was later isolated from *Xenopus* (Sweadner, 1991).

Besides the protein subunits, negatively charged phospholipids are necessary for full NKA enzyme activity (Ottolenghi, 1979). The bilayer lipids act as a solvent for the protein and thus have a structural effect on the protein to perform the necessary conformation changes. A protective effect of negatively charged lipids has also been observed (Cornelius & Skou, 1988). It is generally accepted that the ratio between the two polypeptide chains is 1:1. The αβ-unit is the minimal functional unit of the enzyme, and higher oligomers have also been described (Maunsbach, Skriver, & Hebert, 1991). The higher oligomers are more stable than the αβ-structure. This implies that the enzyme has several different modes of organization within the membrane (Y. Hayashi, Mimura, Matsui, & Takagi, 1989).

III.   Catalytic Cycle of NKA

In the presence of Mg^{2+}, the hydrolysis of ATP by NKA is activated by a combined effect of Na^+ on the cytosolic side and K^+ on the extracellular side (Robinson, 1969, 1970). In contrast, the cytosolic K^+ and extracellular Na^+ act as inhibitors of the pumping cycle. At the extracellular sites, several monovalent cations can replace extracellular K^+ for action, but with decreasing affinity in the order: $K^+>Rb^+>NH4^+>Cs^+>Li^+>Na^+$. At the cytosolic sites, Li^+ is the only cation

that can replace Na^+ for action (Skou, 1988; Skou & Esmann, 1992). The ATP hydrolysis turnover number is about 10,000 per minute at 37 degrees Celsius. (Pollack, Tate, & Cook, 1981b)

NKA has two major conformations as the E1 and E2 forms. The catalytic cycle was first proposed by Albers and Post (Fig. 2) (Albers, Koval, & Siegel, 1968; Post, Kume, Tobin, Orcutt, & Sen, 1969). In the absence of Na^+ and K^+, the NKA is in the E2 form. Two K^+ binds to E2 (E2K2) and turns E2 into a new form with K^+ occluded (E2'K2). In the E2'K2 form, the K^+ binding is very stable (Karlish, Yates, & Glynn, 1976). Na^+ binding to the E2 form with the affinity $K_{0.5}$=5 mM turns the enzyme into the E1 form (Karlish et al., 1976). Then, three Na^+ bind the E1 form (E1Na3). ATP triggers the phosphorylation of E1Na3. In the presence of Mg^{2+}, the phosphate from ATP is transferred to Asp369 in the α subunit (E1PNa3) (Ohtsubo, Noguchi, Takeda, Morohashi, & Kawamura, 1990). The occlusion of Na^+ is the rate-limiting step in the phosphorylation reaction. In the following steps, Na^+ is released to the extracellular side and the E1PNa3 is converted to E2P form, which has a high affinity for K^+ and low affinity for Na^+. One of the three Na^+ is released, and then the phospho-enzyme with two occluded Na^+ undergoes the conformational change to the E2P form. E2P has a high affinity for extracellular K^+, it dephosphorylates rapidly upon K^+ binding. The dephosphorylation then leads to an occlusion of K^+ (E2'K2). ATP increases the rate of K^+ release to the intracellular side, it also increases the rate of transition to E1Na3MgATP in the presence of Na^+ (Lingrel & Kuntzweiler, 1994; Lingrel, Van Huysse, O'Brien, Jewell-Motz, Askew, et al., 1994; Morth et al., 2011; Skou & Esmann, 1992).
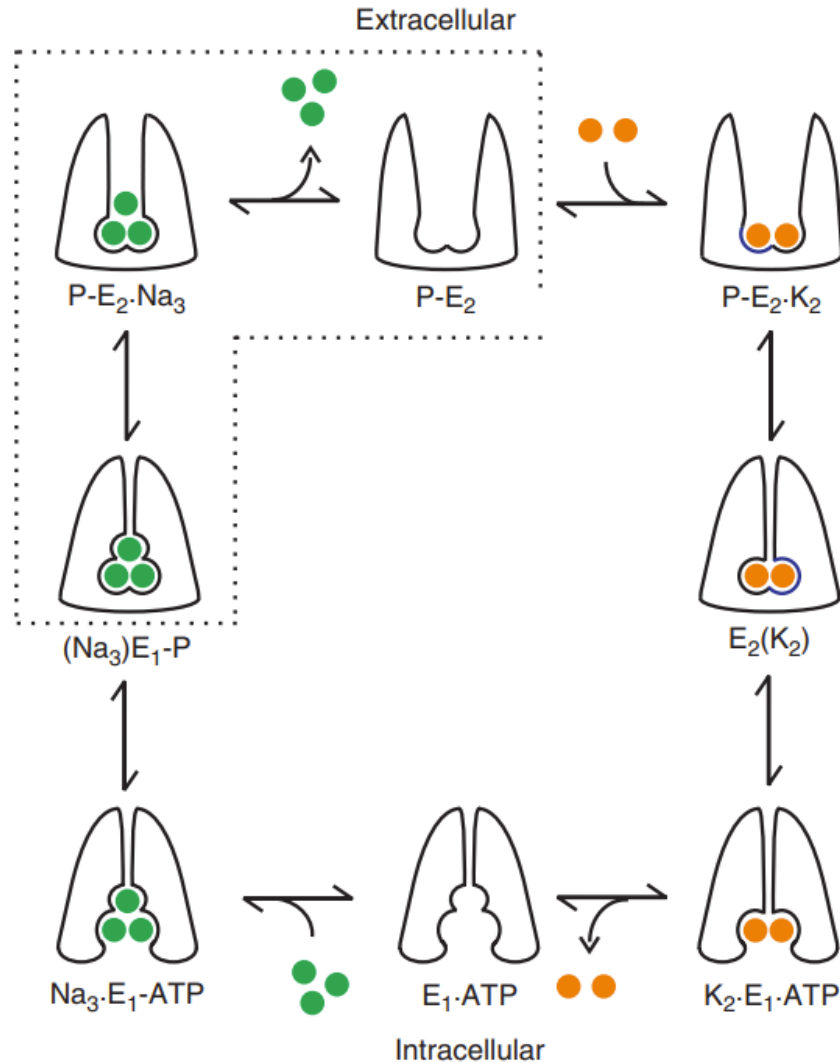
Figure 2. Albers-Post mechanism.
During a catalytic cycle, NKA undergoes conformational changes as E2-E1-E1P-E2P-E2 and actively transports three Na^+ and two K^+ across the cell membrane. Gadsby, et al. (Gadsby, Bezanilla, Rakowski, De Weer, & Holmgren, 2012)

IV.   Ligands of NKA

Cardiotonic steroids (CTS), a group of steroid compounds, were introduced into clinical practice over 1000 years ago (K. K. Chen & Kovarikova, 1967). The scientific study of CTS began with William Withering's clinical observation of foxglove in the 1780s (Whayne, 2018). CTS were identified as specific inhibitors of the NKA (Schatzmann, 1953; Skou, 1957). In the presence of Mg^{2+}, CTS can bind to the extracellular loops of the α subunit of NKA and inhibit

ion-pumping (Burns, Nicholas, & Price, 1996; Croyle, Woo, & Lingrel, 1997; Vasilets, Takeda, Kawamura, & Schwarz, 1998). CTS differ in their affinity for NKA. For a given CTS, the inhibitory effect on NKA varies for different species and different tissues (Blanco, Melton, Sanchez, & Mercer, 1999; O. V. Fedorova, Kolodkin, Agalakova, Lakatta, & Bagrov, 2001; O. V. Fedorova, Lakatta, & Bagrov, 2000; Geering, 2005; Mobasheri et al., 2000). The most widely used CTS, ouabain, originates from a plant and has a $K_{0.5}$ of $10^{-4} – 10^{-2}$ mM for NKA enzyme from most tissues (Bagrov, Shapiro, & Fedorova, 2009; Skou & Esmann, 1992). CTS includes two subfamilies, the cardenolides with a five-membered lactone ring, and the bufadienolides with a six-membered lactone ring (Fig. 3).

The NKA is the receptor for the inotropic effect of CTS in the heart. The inhibition of NKA increases intracellular Na^+, leading to a reduction of the sodium-calcium exchanger (NCX) activity and an enhanced Ca^{2+} influx. The increased intracellular Ca^{2+} leads to increased contractility by the heart muscle (Baker, Blaustein, Hodgkin, & Steinhardt, 1969; Blaustein & Hamlyn, 2020; Reuter et al., 2002).

The presence of an endogenous ouabain-like ligand in animals had been postulated since the 1950s (Blaustein, 2018). In 1961, the role of endogenous CTS in the pathogenesis of hypertension was implicated in a series of studies (De Wardener, Mills, Clapham, & Hayter, 1961; Gruber, Whitaker, & Buckalew, 1980; Hamlyn et al., 1982; Kojima, Yoshihara, & Ogata, 1982; Overbeck, Pamnani, Akera, Brody, & Haddy, 1976). In 1991, endogenous ouabain (EO) purified from human plasma was identified by mass spectrometry (Hamlyn et al., 1991; Ludens et al., 1991). The mammalian EO is identical to the plant-derived ouabain (Hamlyn et al., 1991; Schneider et al., 1998), and proposed to be synthesized in the adrenal medulla (Komiyama et al., 2001). Endogenous bufadienolides were also identified in mammalian species and human plasma

(Hilton et al., 1996; Lichtstein, Gati, & Ovadia, 1993; Sich, Kirch, Tepel, Zidek, & Schoner, 1996). Unlike ouabain that can produce weak vasoconstriction, the bufadienolide marinobufagenin produces rapid and strong vasoconstriction (Bagrov, Roukoyatkina, Pinaev, Dmitrieva, & Fedorova, 1995). The endogenous bufadienolides are synthesized by adrenocortical cells using cholesterol precursor, but unlike ouabain, this does not require cholesterol side-chain cleavage (Dmitrieva et al., 2000; Dmitrieva, Lalli, & Doris, 2005)

The plasma levels of EO in healthy humans is about 0.2 nM (Manunta et al., 1999; J. G. Wang et al., 2003), which is much lower than the IC_{50} of ATPase activity. Hence, a signaling effect of EO is thought to contribute to its role in physiological processes. EO was found to modulate cell Ca^{2+} signaling and peripheral vascular resistance via α2 NKA and NCX (Zhang et al., 2005). Moreover, the renal sodium handling function and EO related cardiac hypertrophy was linked to a signaling function of α1 NKA through tyrosine kinase Src and Mitogen-activated protein kinase (MAPK) pathway (Bagrov et al., 2009; Briones et al., 2006; Ferrandi et al., 2004; Hauptman & Kelly, 1999; Rossoni et al., 2002). Our recent study has shown that different CTS have biased effects on NKA-mediated signaling, which could explain some of the paradoxical effects of CTS. This NKA-mediated signal transduction will be discussed in detail in the next section.
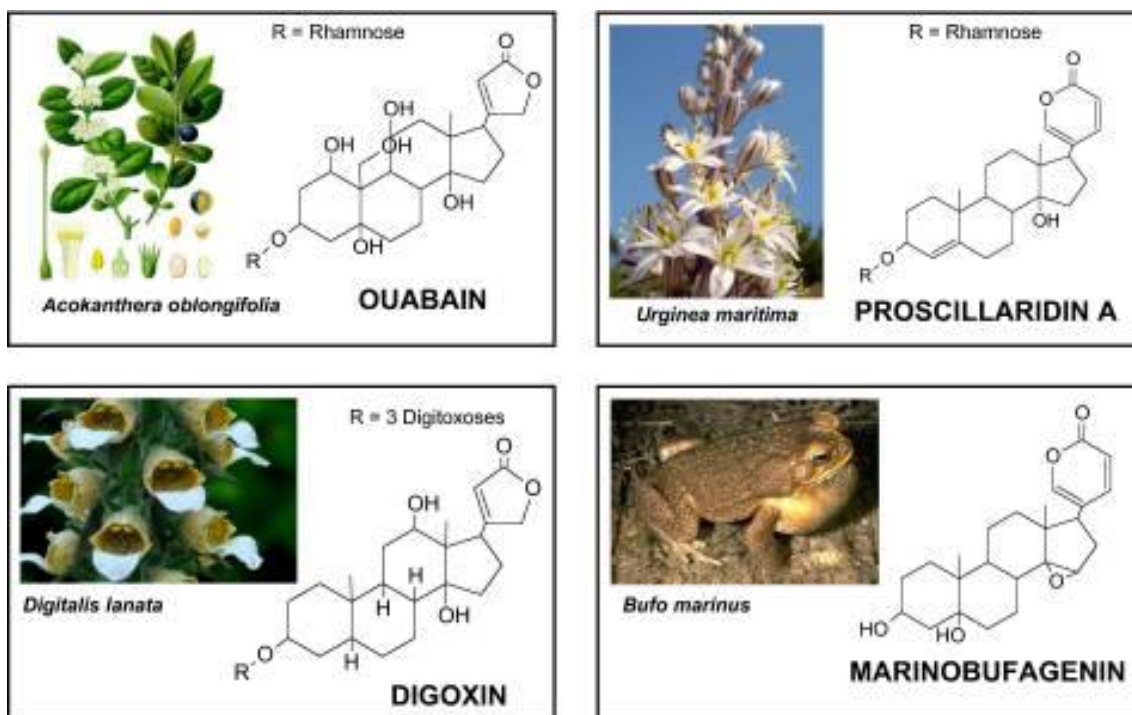
Figure 3. Molecular Structure of CTS.
Cardenolides ouabain and digoxin, and bufadienolides marinobufagenin and proscillaridin A are shown. Adapted from Bagrov, et al. (Bagrov et al., 2009)

V.   Signaling NKA

Overview of the Signaling NKA

In addition to the regulation of NKA enzymatic activity, CTS has also been reported to play an important role in the regulation of cell proliferation and differentiation since the 1970s. Ouabain at a very low concentration (nM range) was found to regulate gene expression and the mitogen-induced differentiation and proliferation of mouse lymphoblasts (Cuff & Lichtman, 1975; Kaplan, 1978; Pollack, Tate, & Cook, 1981a). Given the IC_{50} of ouabain for NKA in mouse lymphoblasts, the effect of nM concentrations of ouabain on lymphoblast proliferation and differentiation is unlikely due to the substantial inhibition of transmembrane ion transport via NKA, suggesting that additional mechanisms may be involved in CTS-induced regulation of cell proliferation and differentiation.

In the 1990s, a series of studies initiated by Xie and his colleagues revealed that CTS could induce protein tyrosine phosphorylation and several signaling pathways in a cell type- and tissue type-dependent manner (Haas, Askari, & Xie, 2000; Haas, Wang, Tian, & Xie, 2002; L. Huang, Li, & Xie, 1997; Kometiani et al., 1998; Z. Xie et al., 1999). This has now largely been confirmed by studies from other laboratories around the world (Bielawski, Winnicka, & Bielawska, 2006; Dmitrieva & Doris, 2003; Ferrandi et al., 2004; Golden & Martin, 2006; Kulikov, Eva, Kirch, Boldyrev, & Scheiner-Bobis, 2007; J. Li, Zelenin, Aperia, & Aizman, 2006; M. Li, Wang, & Guan, 2007; Lopez-Lazaro et al., 2005; Mijatovic et al., 2007; Ramirez-Ortega et al., 2006; Trevisi, Visentin, Cusinato, Pighin, & Luciani, 2004). These new findings suggest possible signaling functions of NKA in addition to its traditional ion-pumping function. These studies have suggested that there is a pool of caveolae localized non-pumping NKA that functions as a potential receptor (J. X. Xie, Li, & Xie, 2013; Z. Xie & Cai, 2003). They further suggested that a non-ion-pumping pool of $\alpha1$ NKA is concentrated in caveolae rafts, where it interacts with scaffolding protein Cav1 and tyrosine kinase Src to form an NKA/Src receptor complex. Src is then maintained inactive. Ouabain binding stabilizes the conformation of NKA. This binding further induces the formation of multiple signaling modules by changing the interaction of NKA with neighboring membrane proteins. This eventually results in the activation of Src, transactivation of the downstream mitogen-activated protein kinase (MAPK) pathway through Epidermal Growth Factor Receptor (EGFR), and reactive oxygen species (ROS) generation. (J. X. Xie et al., 2013; Z. Xie & Cai, 2003). This signaling cascade regulates multiple intracellular processes in cell physiology (Fig. 4).
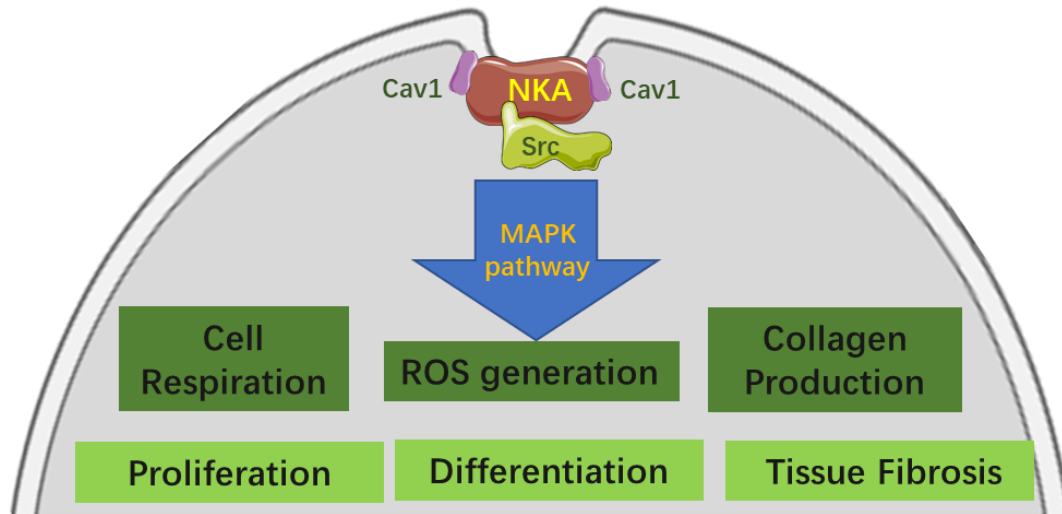
Figure 4. Schematic representation cellular processes regulated by Na/K ATPase/Src signalosome mediated signal transduction.

The signal transduction and heterogeneity of the NKA signalosome could explain the mechanism of low concentration CTS-mediated regulation of cell proliferation and vascular activity. Changes in NKA expression dictate the signaling effects of ouabain on cell proliferation (Tian, Li, et al., 2009). Moreover, the signaling function of NKA was found to be essential for ouabain's effect on cardiac myocytes (Tian, Gong, & Xie, 2001; Tian, Liu, Garlid, Shapiro, & Xie, 2003). Ouabain at 10 to 100 nM was sufficient to increase collagen production in mouse or rat cardiac fibroblasts (El-Okdi et al., 2008; Quintas et al., 2010), which is much lower than the NKA IC_{50} (about 100 μM) in mouse/rat fibroblasts and cannot be explained by inhibition of its ion-pumping property.

After the discovery of NKA-mediated signal transduction, follow-up studies by Wang et al., Yuan et al., and Chen et al. showed that NKA has a significant scaffolding function. NKA is capable of interacting with the scaffolding protein Cav1 (Y. Chen et al., 2008; H. Wang et al., 2004; Yuan et al., 2005). Such ability allows NKA to signal from caveolae. The NKA-caveolin

15

interaction is also critical for Cav1 membrane trafficking (Cai et al., 2008) (see next section for details).

The signaling function of NKA is isoform-specific. Using mRNA interference, Xie and his colleagues were able to knock down 90% of the endogenous NKA α subunit and express exogenous α isoforms of rodent NKA in pig kidney epithelial cell LLC-PK1 (Liang, Cai, Tian, Qu, & Xie, 2006). The CTS-induced Src activation and tyrosine phosphorylation is NKA α1 dependent (Liang et al., 2006; Liang et al., 2007). In a pig epithelial cell model with 90% endogenous NKA knockdown, expressing either rodent α1 or α2 NKA in the cells show no difference in NKA enzymatic function. However, the α2 rescued cells lack Src-dependent signal transduction. No difference in enzymatic kinetics was observed. Ouabain stimulated Src/ERK cascade in the α1 but not the α2 rescued cells (J. Xie et al., 2015). In the α3 rescued cells, CTS induced ERK activation through Src-independent pathways involving PI3K and PKC, which is distinct from that of cells expressing NKA α1 or α2 (Madan et al., 2017).

The NKA α1-mediated regulation of Src kinase activity is based on two Src-interacting domains. A peptide of 20 amino acids (Serine 415 to Glutamine 434) (NaKtide) derived from the nucleotide-binding domain of α1 NKA was shown to be able to bind and inhibit the kinase domain of Src (Z. Li et al., 2009). Expression of either A420P or A425P mutant α1 in endogenous NKA α subunit knockdown cells fully restored the α1 content and consequently the ATPase capacity of cells. However, the A420P and A425P mutants were incapable of interacting and regulating cellular Src (Lai et al., 2013). The second cytosolic (CD2) domain of the NKA α1 subunit can interact with the SH2 domain of Src, which recruits Src to specific signaling complexes. The Y260A mutation on NKA α1 CD2 abolished Src-dependent signal transduction in LLC-PK1 cells (Banerjee, Duan, & Xie, 2015). Moreover, by introducing the key residues of

NaKtide sequence and SH2 binding sequence into the NKA α2 sequence, the mutant α2 gained

α1-like signaling function, including Src interaction and CTS-induced Src/ERK activation (Yu et

al., 2018).

Caveolin and the Conserved NKA Caveolin Binding Motif

The cell membrane surface pit-like depression termed caveolae were first identified in the

mouse gall bladder epithelium in the mid-1950s (Yamada, 1955). However, the functions of

caveolae were not unveiled until the discovery of the first caveolae-associated structural protein,

Cav1, in the 1990s (Kurzchalia & Parton, 1999; Rothberg et al., 1992). Caveolae are flask-

shaped vesicular invaginations, consisting of approximately 140-150 Cav1 molecules (Parton &

Simons, 2007). The amount of caveolae structures varies remarkably in different cells. For

example, caveolae structures are nearly undetectable in lymphocytes (Fra, Williamson, Simons,

& Parton, 1995), but highly abundant in fibroblasts and adipocytes (Parton, 2003). Caveolae

participate in numerous cellular processes, including endocytosis, transcytosis, and signal

transduction (Kurzchalia & Parton, 1999; Sargiacomo et al., 1995; Williams & Lisanti, 2005).

Multiple signaling components are localized and concentrated within the cell membrane caveolar

structure (Fujimoto, Miyawaki, & Mikoshiba, 1995; Lockwich et al., 2000; Z. L. Tang, Scherer,

& Lisanti, 1994; H. Wang et al., 2004). Taken together, the membrane caveolar network serves

as a microdomain for compartmentalization of signal transduction, which facilitates signal

transduction events in a space-specific manner.

The caveolin proteins are the major components of caveolae (Williams & Lisanti, 2005).

Since the discovery of Cav1, a total of three caveolin genes have been found in mammals:

CAV1, CAV2, and CAV3, which encode four caveolin proteins: Cav1α, Cav1β, caveolin-2

(Cav2), and caveolin-3 (Cav3). Cav1 and Cav2 are co-expressed in most types of cells other than

myocytes, where Cav3 is the major isoform. Some types of cells, such as cardiomyocytes, express all three caveolins (Robenek, Weissen-Plenz, & Severs, 2008). Caveolin interacts with itself to form homo-oligomers via its cytoplasmic N-terminal domain interaction, and functions as a scaffolding protein to concentrate and organize signaling molecules within the caveolar structure (Sargiacomo et al., 1995). The N-terminal caveolin scaffolding domain (CSD, residues 82-101) of caveolin can interact with proteins' caveolin binding motif (CBM), whereas the intramembrane domain (residues 102-134) forms a unique α-helical hairpin that inserts into the cell membrane, thereby pinning signaling proteins within the membrane caveolae. (Aoki, Thomas, Decaffmeyer, Brasseur, & Epand, 2010; Ostermeyer, Ramcharan, Zeng, Lublin, & Brown, 2004; Parton, Hanzal-Bayer, & Hancock, 2006; Razani, Woodman, & Lisanti, 2002)

The functions of caveolae and caveolin proteins in cell biology have been studied extensively (Parton, 2003; Parton & del Pozo, 2013; Parton & Simons, 2007). Abnormalities of caveolins have been found in various human diseases. Mutations in the CAV3 gene were found to be associated with muscular dystrophy (Galbiati, Razani, & Lisanti, 2001). On the other hand, mutations in the CAV1 gene are associated with lipodystrophy (Garg & Agarwal, 2008; Garg et al., 2015; Schrauwen et al., 2015). This indicates the significant role of caveolin functions in the development of muscle and adipose tissue. Moreover, Cav1 expression is upregulated in patients with obesity-associated type 2 diabetes mellitus (Catalan et al., 2008), suggesting that Cav1 and related signaling events may be involved in adipose tissue metabolism and obesity development.

To further investigate the physiological relevance of caveolins, Dr. Lisanti and his colleagues have generated mice deficient in genes that encode caveolins. Additional research groups, using standard homologous recombination, have generated mice deficient in the Cav1 gene. As Cav1 is the major isoform in most types of cells, Cav1 knockout is sufficient to

eliminate the caveolae structure in non-muscle cells (Razani et al., 2001; Zhao et al., 2002). The Cav1 knockout mouse displays defects in lipid metabolism and adipocyte function, resulting in resistance to high fat diet-induced obesity (Razani, Combs, et al., 2002). In addition, the Cav1/Cav3 double knockout mouse lacks both muscle and non-muscle caveolae, which leads to the development of severe cardiomyopathy at the age of two months, probably due to hypertrophy, disorganization, and myocytes degeneration in the heart (Park et al., 2002).

The normal receptor function of NKA requires its localization in membrane caveolae, which provides the membrane microdomain that further allows protein-protein interaction (Z. Xie & Cai, 2003). Earlier studies in the 2000s have indicated that α1 NKA co-localizes with Src in caveolae, and that disruption of caveolae formation by either Cav1 knockdown or cholesterol depletion abolishes CTS-induced Src activation and downstream signal transduction (Cai et al., 2008; J. Liu et al., 2005; H. Wang et al., 2004). Hence, the scaffolding function of Cav1 is critical in the formation of the NKA signalosome.

The interaction of caveolin and other proteins commonly occurs between the caveolin scaffolding domain (CSD) on caveolin and the aromatic-rich CBM on its partner proteins. The CBM is identified as the consensus sequence: $\Phi XX\Phi XXXX\Phi$, $\Phi X\Phi XXXX\Phi$, or $\Phi X\Phi XXXX\Phi XX\Phi$, where Φ represents an aromatic amino acid residue and X represents any amino acid. (Anderson, 1998; Schlegel & Lisanti, 2001; Smart, Ying, Donzell, & Anderson, 1996). Two highly conserved potential CBM in the mammalian α1 NKA have been identified: FCROLFGGF at the N terminus and WWFCAFPY at the C-terminus (Fig. 5).
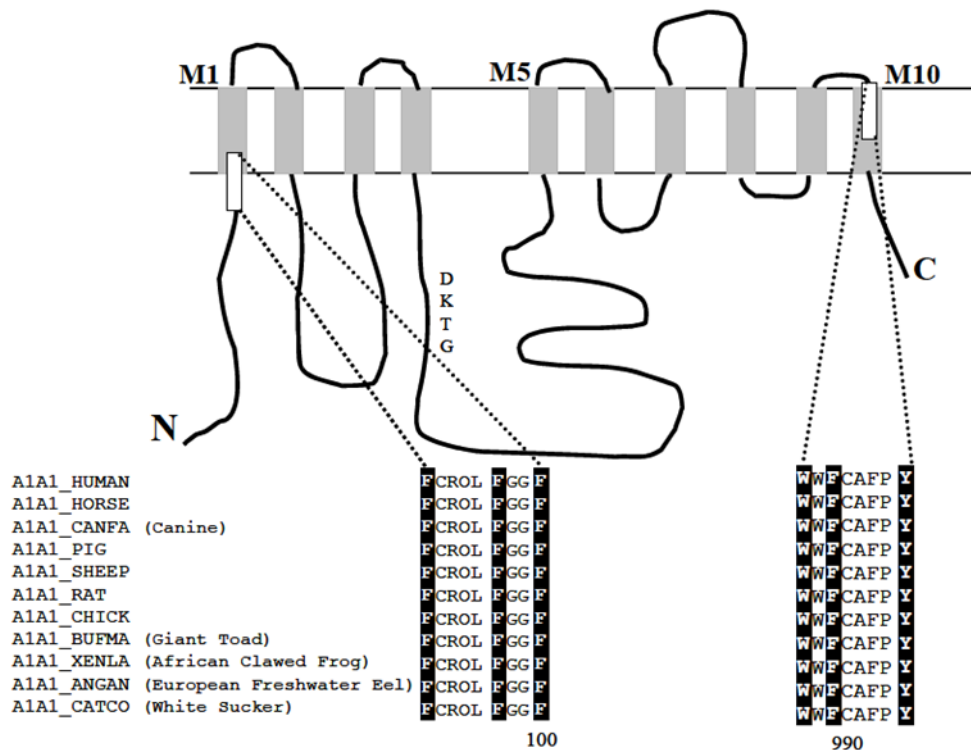
Figure 5. Schematic of α1 NKA conserved caveolin binding motifs.
The N-terminus CBM is on the intracellular side and conserved across different species. Wang et al. 2004. (H. Wang et al., 2004)

The direct interaction of NKA and Cav1 is supported by several lines of evidence. First, these two proteins can be co-immunoprecipitated from cell or tissue lysates. Further, GST-pull down assays shows a direct interaction between Cav1 through the Cav-scaffolding domain and α1 NKA (H. Wang et al., 2004). Additionally, sucrose gradient fractionation studies indicated that α1 NKA and Src are highly enriched in caveolar fractions (H. Wang et al., 2004). Moreover, Fluorescence Resonance Energy Transfer (FRET) analyses showed that α1 NKA and Cav1 are co-localized and interact. This interaction is abolished by either knockdown of α1 NKA or mutation of the N-terminal CBM (F97A and F100A) on α1 NKA (Cai et al., 2008).

The interaction between α1 NKA and Cav1 is regulated by Src-dependent cellular signal transduction. Indeed, ouabain-induced Src activation facilitates Cav1 binding to the α1 NKA. In

addition, ouabain stimulates Y14 phosphorylation of Cav1 and increases Cav1 mobility via α1 NKA-associated Src (H. Wang et al., 2004). The trafficking of Cav1 from the Golgi apparatus to the plasma membrane also appears to be regulated by α1 NKA. Knockdown of α1 NKA in LLC-PK1 cells resulted in the redistribution of Cav1 from the plasma membrane to cytosolic vesicles. This redistribution is rescued by both wild-type and pump-null exogenous α1 NKA, but not the N-terminal CBM mutant (F97A and F100A) α1 NKA (Cai et al., 2008). This suggests that the non-ion pumping property of α1 NKA is critical for the regulation of Cav1 trafficking and membrane distribution. Interestingly, α1 NKA not only regulates Cav1 behavior through CBM-mediated interaction but also regulates Cav1 mobility via Y-14 phosphorylation by regulation of Src activity. This is consistent with the established role of Src in the control of Cav1 trafficking (Gottlieb-Abraham et al., 2013; Labrecque et al., 2004).

Given that the C-terminal CBM resides on the extracellular side of NKA (Morth et al., 2007), the N-terminal CBM is thought to be key to NKA/Cav1 interaction. To further characterize the biological property of the CBM on α1 NKA, Wang X et al. introduced a CBM F97A and F100A double mutant rat α1 NKA (mCBM) in the α1 NKA knockdown LLC-PK1 cell. This mutant disrupted the NKA/Src signalosome, eliminated CTS-induced signal transduction, without affecting the ion pumping activity of NKA (X. Wang et al., 2020). The mCBM cells showed dramatically reduced cell proliferation capacity (X. Wang et al., 2020).

Furthermore, to study the non-ion pumping function of NKA in animal physiology, the α1 NKA CBM F97A and F100A double mutant knock-in mouse line was generated using the strategy developed in the Lingrel laboratory (Dostanic, Schultz Jel, Lorenz, & Lingrel, 2004). Unlike the viable mouse lines with the knockout of Cav1, IP3R, or Src (M. Hayashi et al., 1999; Razani et al., 2001; Soriano, Montgomery, Geske, & Bradley, 1991), the homozygous CBM mutation of α1

NKA in mouse is embryonic lethal (X. Wang et al., 2020). The mCBM does not block blastocyst formation and gastrulation but arrests the organogenesis at embryonic day 8.0 and onward, including the development of the brain, heart, limbs, and spinal cord. The overall size of embryos at embryonic day 9.5 was ~20% reduced in mCBM heterozygous and ~75% reduced in mCBM homozygous in comparison to the wild type. No homozygous embryos were found after embryonic day 12.5 (X. Wang et al., 2020). The CBM on NKA is evolutionarily conserved. The consensus sequence of FCxxxFGGF on NKA is present in all multicellular organisms within the animal kingdom (X. Wang et al., 2020). Similar to the mouse, mCBM on NKA of C. elegans also resulted in the arrest of organogenesis (X. Wang et al., 2020). Taken together, these data demonstrated the critical role of NKA CBM and the non-ion pumping functions of NKA in organogenesis during embryonic development, and this property of NKA is conserved among different species.

To further assess the molecular mechanism and human relevance of NKA CBM mediated regulation of tissue development, the same CBM mutation was introduced on NKA α1 in human induced pluripotent stem cells (iPSCs) using CRISPR-Cas9 gene editing (X. Wang et al., 2020). The expression of mCBM abolished the colony formation of human iPSCs, which was accompanied by a dramatic reduction in the expression of stemness marker genes (X. Wang et al., 2020). This suggested that the differentiation status of iPSCs was altered by mCBM.

Mechanistically, the canonical Wnt/β-catenin signaling pathway, which is critical in animal organogenesis (Chenn, 2008; Nusse, 2005), is found to be altered in mCBM cells. First, the cellular distribution of β-catenin in mCBM cells is shifted from the plasma membrane to cytosolic vesicles, suggesting the disassembly of the Wnt/β-catenin signaling complex. Secondly, TOPFlash luciferase activity assays show that mCBM reduced Wnt pathway activity by ~90%, indicating that the mCBM cells failed to respond to Wnt ligands or Wnt pathway agonist stimulation.

Moreover, Wnt3a failed to induce the expression of its downstream marker genes in mCBM cells (X. Wang et al., 2020). At last, global changes of gene expression in the Wnt signaling pathway indicated by RNA-seq and pathway analysis confirmed the defect of Wnt/β-catenin signaling in homozygous mCBM embryos. This was further confirmed by the downregulation of neurogenesis essential genes in homozygous mCBM embryos, which is regulated by Wnt/β-catenin signaling during embryonic development. Consistently, developmental defects in neural closure are observed in histological sections of homozygous embryos at embryonic day 9.5. (X. Wang et al., 2020).

Altogether, these suggest that the mCBM on NKA is critical in the regulation of stem cell differentiation and mouse embryonic development, possibly due to both the scaffolding function of NKA/Cav1 interaction and signal transduction mediated by NKA signalosome. The role of NKA CBM in stem cell differentiation in the context of adipogenesis, which is the focus of this research, is further considered in the following chapters.

VI.   Classic and Novel roles of NKA in the Adipose Tissue: the case for a role in adipogenesis

Overview of Adipogenesis

The adipose tissue is derived from the mesoderm during embryonic development. The differentiation of stem cells into adipocytes is termed adipogenesis. The process of adipogenesis consists of multiple phases, which are characterized by chronological changes in the expression of early, intermediate, and late marker genes and lipid accumulation (Fig. 6). (Cristancho & Lazar, 2011; Gregoire, Smas, & Sul, 1998; Lee, Schmidt, Lai, & Ge, 2019).
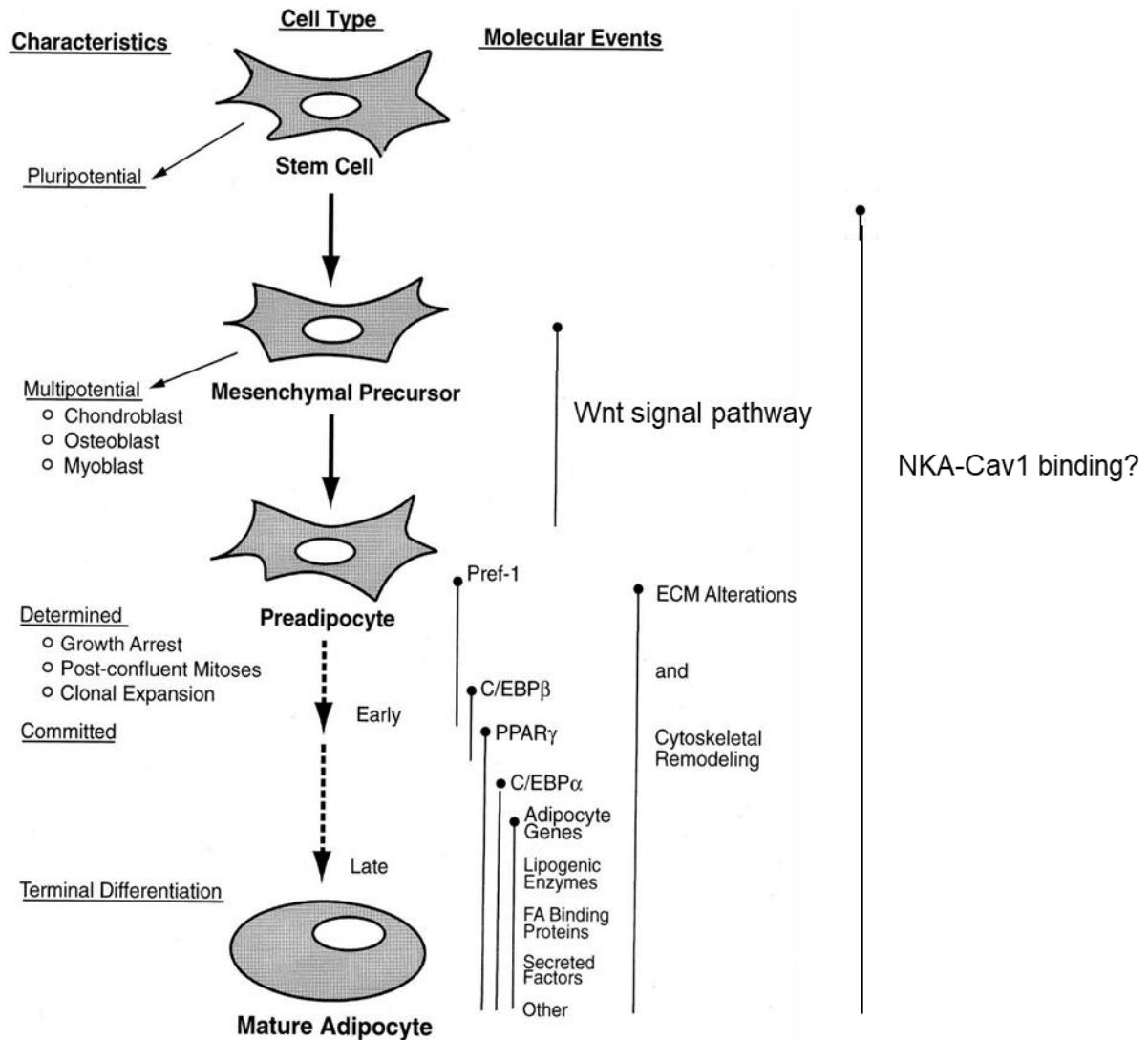
Figure 6. Overview of the stages in adipocyte differentiation.
In the commitment stage, the pluripotent stem cells differentiate into mesenchymal precursors, preadipocytes, and eventually into adipocytes. This cell fate determination is regulated by transcriptional signal networks, including multiple Wnt signaling pathways. The maturation stage is initiated by the expression of PPARγ and its downstream target genes encoding functional proteins that are critical in lipid metabolism. The mature adipocyte is characterized by large lipid droplets in the cytoplasm. Adapted from Gregoire. et al. 1998 (Gregoire et al., 1998).

From Mesenchymal Stem Cell (MSC) to Preadipocyte: role of Wnt Signaling and

Extracellular Matrix

The commitment of mesenchymal stem cells (MSCs) to preadipocytes results in the loss

of the potential to differentiate into other types of cells such as chondrocytes, myocytes, and

osteoblasts (Gregoire et al., 1998). This stem cell lineage determination is regulated by crosstalk between signaling cascades, including the Wnt signaling pathway and TGF-β signaling, as well as modifiers of extracellular matrix (ECM) structure (Cristancho & Lazar, 2011; Lee et al., 2019). For example, the canonical Wnt signaling through Wnt10b promotes osteogenesis and inhibits adipogenesis in MSCs (Steger et al., 2010). Non-canonical Wnt ligands signal through β-catenin-independent pathways. The non-canonical Wnt5B also facilitates osteogenesis and inhibits adipogenesis (Fretz et al., 2010), whereas another non-canonical Wnt5A promotes adipogenesis by inhibiting canonical Wnt (Seo et al., 2009). TGF-β expression inhibits *in vitro* adipogenesis through activation of Smad-3 and increasing synthesis of ECM components (Hiraike et al., 2017; Zamani & Brown, 2011). In contrast, several TGF-β superfamily bone morphogenetic proteins (BMPs) were reported to promote adipogenesis through the p38 kinase pathway (H. Huang et al., 2009).

The composition and stiffness of the ECM also regulate lineage commitment of mesenchymal stem cells. Low stiffness of ECM promotes adipogenesis *in vitro* (Engler, Sen, Sweeney, & Discher, 2006; Rowlands, George, & Cooper-White, 2008; Winer, Janmey, McCormick, & Funaki, 2009). In contrast, a stiffer ECM with a higher concentration of collagen I attenuate adipogenesis (Chun et al., 2006). ECM stiffness causes persistent tissue tension, which leads to enhanced actin and myosin fiber formation and cell stretching, eventually shifting the cell fate toward MSCs (Akimoto et al., 2005; Jakkaraju, Zhe, Pan, Choudhury, & Schuger, 2005). Exposure to mechanical strain activates Wnt/β-catenin and inhibits adipogenesis in MSCs (B. Sen et al., 2008). Matrix metalloproteinases (MMPs) can cleave ECM components and thereby regulate the stiffness and composition of ECM (Visse & Nagase, 2003). MMP14 is essential for adipose tissue development (Chun et al., 2006). Complete inhibition of MMP

25

activity by inhibitors of MMPs impairs adipose tissue development *in vivo* (Chavey et al., 2003;

Croissandeau, Chretien, & Mbikay, 2002; Lijnen et al., 2002; Maquoi, Munaut, Colige, Collen,

& Lijnen, 2002). Cell-cell contact and cell shape also influence adipogenesis via regulation of

RHO GTPase–RHO-associated kinase (ROCK) signaling (Dike & Farmer, 1988; Kilian,

Bugarija, Lahn, & Mrksich, 2010; McBeath, Pirone, Nelson, Bhadriraju, & Chen, 2004). ROCK

signaling inhibits adipogenesis. Confluent or rounded human MSC have inactive ROCK due to

inhibition of the dissociation of RHO-GDP, thereby promoting adipogenesis. Conversely, RHO-

GTP in spread cells has activated ROCK, which inhibits adipogenesis and promotes

myogenesis/osteogenesis through anti-adipogenic Wnts (Dike & Farmer, 1988; Kilian et al.,

2010; McBeath et al., 2004). Moreover, p190-B RHOGAP, a factor that controls RHO activity,

has also been found to be critical in MSC lineage commitment. Mice lacking p190-B RHOGAP

show decreased adiposity with decreased adipogenic capacity and increased myogenic capacity

of mouse embryonic fibroblasts (MEFs) (Sordella, Jiang, Chen, Curto, & Settleman, 2003).

From Preadipocyte to Adipocyte: major role of PPARγ and C/EBPα

Following MSC lineage commitment, the preadipocyte is further committed to adipocyte

during adipogenesis. Growth arrest is required for adipocyte commitment. Two transcription

factors — CCAAT enhancer binding protein (C/EBP-α) and proliferator-activated receptor-γ

(PPAR-γ) — appear to be involved in this process. Both are activated by adipogenic stimuli

(Cristancho & Lazar, 2011; Gregoire et al., 1998). C/EBP proteins are the early markers for

adipocyte commitment. C/EBPβ expression is extensively increased by the induction of

adipogenic stimuli such as cAMP agonists (Yeh, Cao, Classon, & McKnight, 1995). C/EBPδ

expression is also induced rapidly by glucocorticoids upon the addition of adipogenic stimuli

(Yeh et al., 1995). Subsequently, the expression of C/EBPα and PPARγ is further induced by

C/EBPβ (Cristancho & Lazar, 2011; Q. Q. Tang, Zhang, & Daniel Lane, 2004). PPARγ is the dominant regulator of adipogenesis. It belongs to the type II nuclear hormone receptor family and forms heterodimers with the retinoid X receptors (RXR) (Gregoire et al., 1998; Juge-Aubry et al., 1995). The PPARs are activated by numerous ligands, including the thiazolidinedione (TZD) class of antidiabetic drugs (Gregoire et al., 1998). PPARγ is the most adipose-specific member of the PPARs, and the expression of PPAR-γ is sufficient to induce adipogenesis in fibroblast cell lines, demonstrating its significant role in the regulation of adipogenesis (Hu, Tontonoz, & Spiegelman, 1995; Tontonoz, Hu, & Spiegelman, 1995).

Upon expression of PPARγ, the adipocyte becomes mature with increasing lipid accumulation. During the adipocyte maturation, PPARγ and C/EBPα induce the expression of multiple adipocyte genes, including genes encoding insulin signaling pathway components, lipogenic enzymes, fatty-acid-binding proteins, and adipose cytokines (Gregoire et al., 1998). Moreover, PPARγ and C/EBPα regulate each other in a positive feedback circuit to maintain the gene expression in mature adipocyte, whereas the expression of C/EBPβ and C/EBPδ is reduced (Cristancho & Lazar, 2011; Wu et al., 1999).

Glucose Handling and Lipogenesis in the Mature Adipocyte

During the maturation of adipocytes, glucose uptake is mediated by the insulin-sensitive glucose transporter (GLUT4) in response to insulin stimulation. The glucose is then converted into pyruvate via glycolysis, converted into acetyl CoA, and enters the mitochondrial TCA cycle (Sethi & Vidal-Puig, 2007). Additionally, free fatty acids (FFA) are generated from triglycerides hydrolysis by the lipoprotein lipase (LPL) on the adipocyte cell membrane, and then transported across the membrane (Peterson et al., 1990). The FFA then binds to adipocyte protein 2 (aP2) and converts into acetyl CoA to enter the mitochondrial TCA cycle (Sethi & Vidal-Puig, 2007).

27

The citrate produced by the TCA cycle is utilized to synthesize FFA via fatty acid synthase (FASN). The FFA are then subjected to *de novo* synthesis of triglyceride, and the triglycerides are stored in the lipid droplets of mature adipocytes (Sethi & Vidal-Puig, 2007).

In the development of obesity, excess lipid accumulation leads to adipocyte hypertrophy, which is characterized by enlarged cell size, disorganized cortical actin, and impaired GLUT4 translocation (Choe, Huh, Hwang, Kim, & Kim, 2016). The hypertrophic remodeling of the obese adipose tissue results in local adipose tissue hypoxia, which further activates the hypoxia-inducible factor (HIF) 1α and disturbs the homeostasis of adipose tissue macrophage, increases the secretion of inflammatory cytokines like MCP-1, TNFα, and IL-6 (Choe et al., 2016). Eventually, this remodeling accelerates adipose tissue fibrosis, chronic inflammation, and results in insulin resistance in the adipose tissue (Choe et al., 2016; Sun, Tordjman, Clement, & Scherer, 2013).

The NKA of the Adipose Tissue

The adipose tissue specializes in storing energy as fat, generating heat, and secreting cytokines. The adipocyte is the primary cell type in adipose tissue, which is derived from adipose tissue fibroblast. A series of studies of NKA in adipose tissue were published in the 1980s. The number of Na pump sites, ATP turn over, and efficiency was initially quantitated in rat adipose cells (Table. 2.)(Resh, 1982b). Following the discovery of the new NKA α-isoform in the brain (Sweadner, 1979), two different NKA α-isoforms were identified in the rat adipose tissue as α (25%) and α+ (75%), which were later termed as α1 and α2 (Lytton et al., 1985).

Rat adipocyte (Na⁺,K⁺)-ATPase		
	Cells	Plasma membranes
Na⁺ pump sites[a]	6×10^5/cell	6×10^{12}/mg
(Na⁺,K⁺)-ATPase activity[b]	1×10^9/cell/min	8.4×10^{16}/mg/min
Turnover number for ATP[c]	1.7×10^3/site/min	1.4×10^4/site/min
Efficiency[d]	12%	100%

Table 2. NKA properties in rat adipose tissue. Resh MD (Resh, 1982b).

A series of studies in adipocyte differentiation of cultured mouse fibroblast 3T3-L1 cells indicated that an NKA isoform-switch from α1 to α2 occurs during adipocyte differentiation (Resh, 1982b; Russo, Manuli, Ismail-Beigi, Sweadner, & Edelman, 1990). Either increase of intracellular sodium or stimulation by insulin activates NKA in adipocytes. (Brodsky, 1990; Lytton, 1985). Although the sodium affinity and insulin sensitivity of NKA α1 and α2 isoforms are different, isoform-specific modulation of their ion-pumping function is an unlikely explanation for the requirement of both isoforms in adipocytes. Indeed, it has been estimated that only 12% of the maximal total NKA activity is required in living cells (Brodsky, 1990; Resh, 1982b). The isoform-specific signaling function of NKA α1 and α2 (J. Xie et al., 2015) may imply a regulatory role of NKA in signaling events in adipose tissue that has not been explored yet.

Novel Functions of NKA: importance in the Adipose Tissue

Although not explicitly tested to date, some of the isoform-specific properties of the signaling NKA, combined with recent pharmacological investigations, support a significant role in adipocyte differentiation and specific functions. For example, a metabolic switch from oxidative respiration to aerobic glycolysis has been observed in α2-expressing cells without α1-specific signaling function, suggesting a role for α1 NKA signaling in energy metabolism

(Banerjee et al., 2018; Kutz et al., 2021). Consistent with a physiological role, the α1 NKA signaling is also critical for the development and metabolism of the skeletal muscle, one of the few organs expressing both α1 and α2 NKA (Kutz et al., 2021; Kutz et al., 2018).

Pharmacological approaches *in vivo* and *in vitro* also support the existence of an underappreciated role of NKA signaling in adipose tissue. Indeed, in a series of studies by Dr. Sodhi and her colleagues, the NKA α1-mimetic peptide pNaKtide mediated the inhibition of adipogenesis *in vitro*, prevented high-fat diet-induced obesity, and reduced multiple obesity-related complications in mice via normalization of NKA α1/Src and subsequent attenuation of reactive oxidative species (ROS) generation (J. Liu et al., 2016; Pratt et al., 2019; Sodhi et al., 2015; Sodhi et al., 2018; Sodhi et al., 2017; Sodhi et al., 2020). Mechanistically, ROS are chemical modifiers of the NKA that can regulate and amplify the signal transduction mediated by NKA (Z. Xie, 2003; Z. Xie & Cai, 2003; Yan et al., 2013).

Finally, the NKA scaffolding function and its effect on caveolar integrity may also influence adipose physiology. Indeed, the membrane caveolar structure is associated with adipocyte lipid trafficking (Pilch & Liu, 2011; Pilch, Meshulam, Ding, & Liu, 2011). Besides the lipid metabolic defects in Cav1 null mice (Razani, Combs, et al., 2002), cavin-1 null mice and Cav-3 null mice, which lack caveolae in all tissues, developed insulin resistance at an early age (Capozza et al., 2005) presumably due to a defect in insulin signaling and/or glucose uptake (L. Liu et al., 2008). Moreover, although the mechanism is not fully understood, CAV1 (gene encodes Cav1 protein) genetic variants have been linked to familial lipodystrophies (Garg & Agarwal, 2008; Garg et al., 2015; Schrauwen et al., 2015).

In this study, we used a genetic approach in mice and in human induced pluripotent stem cells (iPSC) to investigate the role of NKA α1 and its association with Cav1/caveolae in adipocyte biology.

CHAPTER 2

The Na/K-ATPase α1 Caveolin Binding Motif is Required for Adipogenesis

A manuscript in preparation.

Minqi Huang[1], Liquan Cai[1], Xiaoliang Wang[1,2], Yiliang Chen[3,4], Jue Zhang[3,4], Joseph I. Shapiro[2], Zijian Xie[1, †], Sandrine V. Pierre[1, *]

[1]Marshall Institute for Interdisciplinary Research, Marshall University, Huntington, WV 25703, USA.

[2]Joan C. Edwards School of Medicine, Marshall University, Huntington, WV 25701, USA.

[3]Blood Research Institute, Versiti, Blood Center of Wisconsin, Milwaukee, WI 53226, USA.

[4]Medical College of Wisconsin, Department of Medicine, Wauwatosa, WI 53226, USA.

*Corresponding author. Email: pierres@marshall.edu

†Deceased prior to the submission.

Abstract

Deficiencies in mice and humans have brought to the fore the importance of the caveolar network in key aspects of adipocyte biology. The conserved N-terminal caveolin binding motif (CBM) of the ubiquitous Na/K-ATPase (NKA) α1 isoform, which allows NKA/Cav1 interaction, influences NKA signaling, caveolar distribution, and embryonic development of the mouse. However, its role in postnatal adipogenesis is not known.

This was examined in CBM null mutant (mCBM) heterozygous mice as well as in human induced pluripotent stem cells (iPSCs) obtained through CRISPR/Cas9 genome editing. Heterozygous mCBM mice had altered adiposity and adipose fibrosis. Mutant mCBM iPSC were able to differentiate into adipocytes but histological, qPCR, western blotting and functional analyses using Seahorse metabolic flux analysis revealed profound defects. Specifically, mCBM cells had a significantly reduced lipid content, mitochondrial and caveolar anomalies, and extracellular matrix (ECM) remodeling,

Mechanistically, total Na/K-ATPase activity was unchanged in mCBM cells. A TGF-β-dependent increase of cellular redox, ECM remodeling markers, and reduction of lipid storage occurred in mCBM cells and was prevented by lentiviral expression of a wild-type mouse NKA α1 with intact CBM. Pharmacological normalization of mitochondrial using MitoTempo ameliorated lipid storage in mCBM cells but did not substantially affect ECM remodeling. Consequently, it is concluded that the CBM on NKA α1 is critical for the maintenance of low ECM stiffness and fibrosis via a TGF-β-dependent mechanism. This in turn favors metabolic homeostasis and adequate lipid storage in the adipocyte.

Beyond the new function of CBM, this result is another evidence of the importance of ECM and fibrosis for adipose structure and function, which has been increasingly recognized in obesity and related disorders.

One Sentence Summary: Na/K-ATPase α1 regulates extracellular matrix remodeling and adipogenesis via its conserved N-terminal caveolin binding motif.

Introduction

The initial report of significant adipose defects in caveolin-1 (Cav1) null mice, which lack caveolae, brought about the importance of the caveolar network in adipose structure and function (Cohen, Combs, Scherer, & Lisanti, 2003; Cohen, Schubert, Brasaemle, Scherer, & Lisanti, 2005; Razani, Combs, et al., 2002). Indeed, Cav1 null mice have smaller fat pads, a defective lipid metabolism, and do not develop high fat diet-induced obesity (Cohen, Razani, et al., 2003). At the molecular level, studies have shown the role of the caveolar network in key physiological functions of the adipocyte, such as the regulation of membrane vesicle trafficking, lipid homeostasis, and signal transduction (Cohen, Combs, et al., 2003; Pilch & Liu, 2011). As clinical reports continue to document the role of Cav1 and other key structural components of caveolae in lipodystrophies (Garg & Agarwal, 2008; Schrauwen et al., 2015), understanding the complex dynamics that govern caveolae structure and functions in the adipocyte has also become a translational aspiration.

Both α1 and α2-containing isoenzymes of Na/K-ATPase (NKA) are expressed in the mammalian adipocyte. While it has long been established that isoenzymes function as ion-pumping machinery that ensures the transport of Na^+ and K^+ across the cell membrane (Morth et al., 2011; Skou, 1957; Skou & Esmann, 1992), there are clear isoform-specific distinctions in their ability to carry on non-ion-pumping functions of NKA (Kutz et al., 2021; J. Xie et al.,

2015). The conserved N-terminal Cav-binding motifs (CBM) on NKA α1 allows NKA to interact with Cav1, regulate Cav1 trafficking and cell membrane caveolae number, and influence cell membrane cholesterol distribution (Y. Chen et al., 2009; H. Wang et al., 2004). The loss of CBM function in the NKA α1 subunit, which we have obtained through F97A/F100A double mutagenesis, disrupts its ability to act as a scaffold and a signaling receptor (Cai et al., 2008; X. Wang et al., 2020), but does not interfere with its role as a Na^+/K^+ pump (Cai et al., 2008; H. Wang et al., 2004; X. Wang et al., 2020).

To our knowledge, the physiological role and impact of the Cav1/NKA α1 interaction in the adipocyte are unknown. However, previous studies suggesting that pharmacological inhibition of NKA-mediated signal transduction influence adipose-related mechanisms such as adipogenesis of 3T3-L1 cells or high-fat diet-induced obesity and related complications in mice (J. Liu et al., 2016; Pratt et al., 2019; Sodhi et al., 2015; Sodhi et al., 2018; Sodhi et al., 2017; Yan et al., 2019) prompted us to hypothesize that Cav1/NKA α1 has a key role in the regulation of adipose function.

This was tested using a genetic approach in mice and in human induced pluripotent stem cells exposed to a protocol of adipocyte differentiation in vitro. Collectively, the contrasting results obtained in wild-type (WT) vs F97A/F100A CBM mutant (mCBM) mice and iPSC are consistent with a regulatory role of NKA α1 CBM in adipogenesis that is related to control of TGFβ signaling and extracellular matrix remodeling. This impacts cell caveolar and mitochondrial networks, redox status, and ultimately cell metabolism, insulin sensitivity, and lipid storage. Although distinct, similarities noted between the phenotypic defect of adipose structure in Cav1 genetic and NKA CBM mouse models suggest that NKA scaffolding/signaling

35

function may be relevant in the setting of familial lipodystrophies associated with caveolar gene polymorphisms.

Results

Reduced fat mass, inflammation, and fibrotic remodeling in the mCBM mouse

Using a LoxP targeting strategy, we have developed a mutant mouse carrying the double F97A; F100A substitution in Atp1a1, which encodes NKA α1 (X. Wang et al., 2020). The CBM mutation of Atp1a1 was embryonic lethal for homozygotes, but heterozygote mCBM mice survived to adulthood without overt phenotypic abnormality under basal laboratory conditions (X. Wang et al., 2020). Given the importance of NKA signaling and caveolar integrity in metabolic diseases (Sodhi et al., 2015; Sodhi et al., 2017), the adipose tissue of heterozygous mCBM mice (henceforth referred to as mCBM mouse) was further examined.

The weight of WT and mCBM male mice, recorded weekly between the age of 6 and 23 weeks, did not reveal any significant difference in growth between the two genotypes (Fig. 15A). However, Echo MRI analyses did reveal a significant reduction of over 30% of total fat mass in mCBM mice, which was compensated by an increase in lean mass (Fig. 7A). This was not related to an apparent change of food intake (Fig. 15C), and direct measurement of visceral and subcutaneous fat mass (Fig. 15B) further indicated that the reduction was uniformly distributed among fat depots. Histological analysis of the epididymal white adipose tissue (WAT) following Hematoxylin & Eosin (H&E) staining indicated that the reduced fat content in mCBM mice was associated with reduced size of their adipocytes (Fig 7B&C). Crown-like structures (CLS), a hallmark of proinflammatory activation in the adipose tissue formed by recruitment of macrophages around dead or dying adipocytes (Cinti et al., 2005; Murano et al., 2008), were essentially absent from WT preparations but detected in a high number in the mCBM adipose

36

tissue (Fig. 7B &C). Chronic inflammation in mCBM WAT was further indicated by

macrophage marker F4/80 staining (Fig. 7B&C), and increased gene expression of

proinflammatory cytokines TNF-α and IL-6 (Tnfα and Il6) in WAT from mCBM mice (Fig. 7D).

This suggested macrophage infiltration/recruitment, accompanying inflammation in fat tissue.

Masson's Trichrome staining revealed an increased collagen deposition, suggestive of fibrotic

remodeling (Fig. 7B). Consistently, type 1 collagen and fibronectin 1 gene expressions (Col1a1

and Fn1, respectively) were elevated in mCBM WAT (Fig. 7D). Accordingly, we concluded

from this set of experiments that adipose tissue remodeling occurred in the mCBM mouse. As

observed in pig epithelial cells expressing the CBM mutant NKA (X. Wang et al., 2020), an

alteration of the caveolar network (Fig. 8A&B) and redistribution of NKA and Cav1 away from

the caveolar fractions (Fig. 8C&D) were detected in mCBM WAT. This was accompanied by a

reduction of NKA α1 protein with an apparent compensatory increase of NKA α2 and Cav1 total

protein expression (Fig 8E&F). Given these structural changes and the importance of caveolae

function in adipose biology, perturbation of the cellular NKA/caveolae axis in the adipocyte

itself likely contributes to adipose tissue remodeling in the mCBM mouse. To test this explicitly,

we submitted WT and mCBM human pluripotent stem cells iPSC to an adipocyte differentiation

protocol *in vitro*.
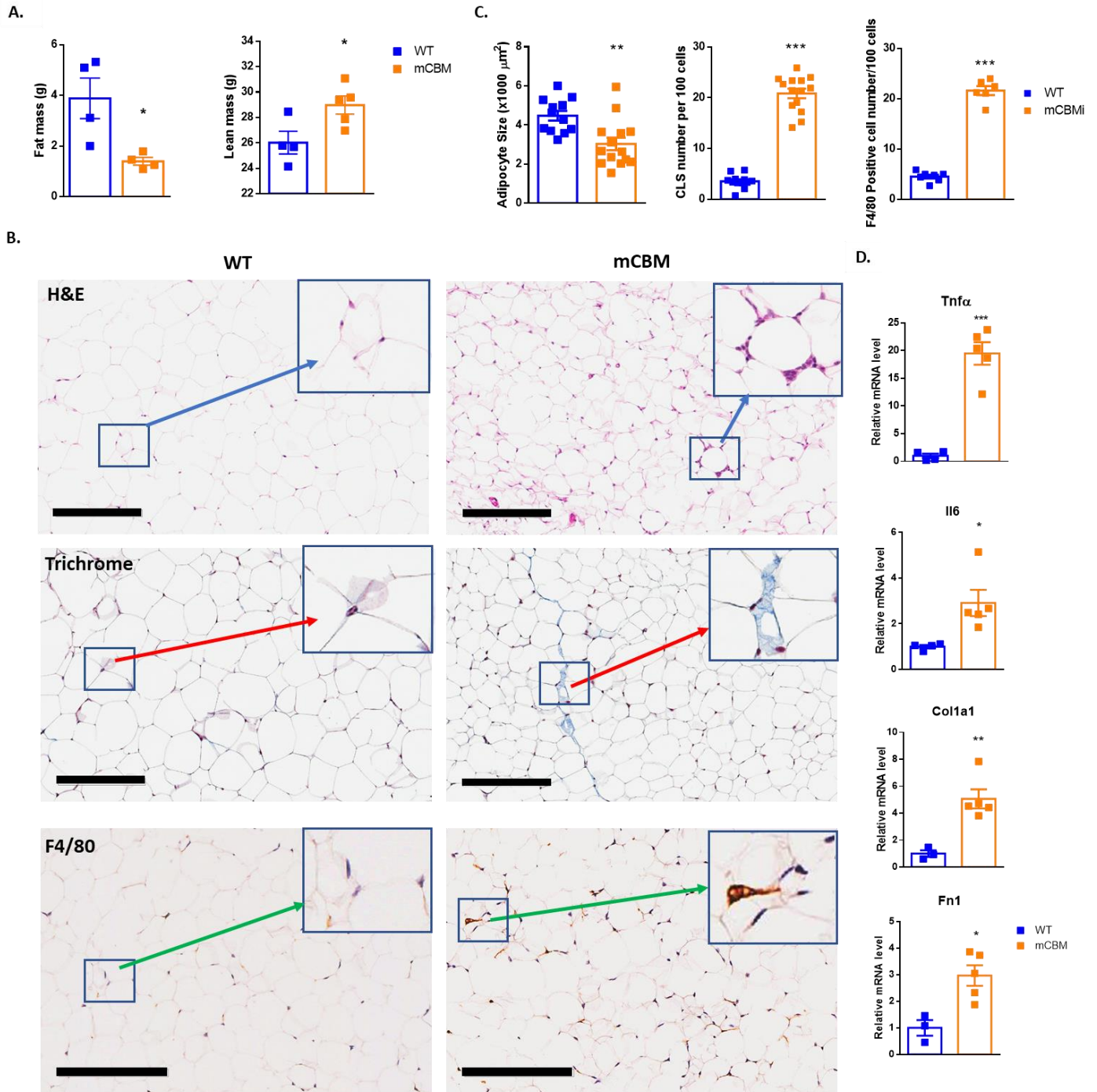
Figure 7. Fat remodeling in mCBM heterozygous mice.
A) Body composition of mCBM heterozygous and WT mice at age of 6-month, n=4. B)
Representative H&E staining, Masson's trichrome staining, and F4/80 staining of epididymal fat
from WT or mCBM heterozygous mice. Representative pictures are selected from n=4-6 mice in
each group, scale bar = 200μm. C) Quantitation of average cell size, crown-like structure
number, and F4/80 positive cells in panel A. D) The mRNA levels of Tnfα, Il6, Col1a1, and Fn1

in WAT by RT-qPCR, n=3-5. Data reported as mean ± SE. *, P < 0.05; **, P < 0.01; ***, P < 0.001 (Unpaired t-test with Welch's correction)
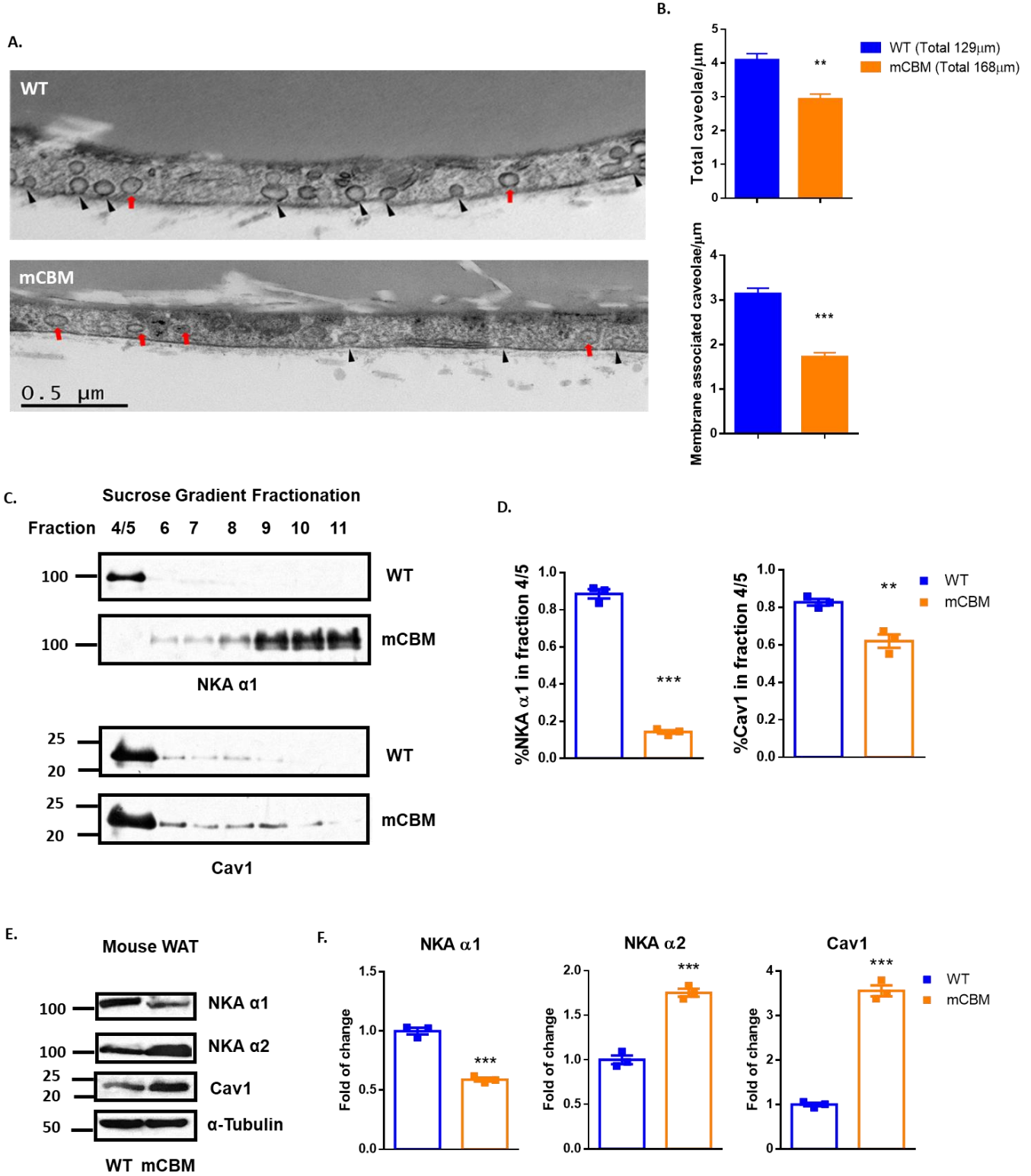
Figure 8. Reduced caveolae in adipocytes isolated from mCBM heterozygous mice.

A) Electronic microscope images showing caveolae structure in the adipocyte plasma membrane of mCBM heterozygous mice. Black arrows: membrane-associated caveolae; Red arrows: membrane-dissociated caveolae, and B) quantitation of membrane-associated caveolae and total caveolae numbers per μm. Representative pictures were selected from n=4 mice. C) Protein distribution in WT and mCBM heterozygous mice epididymal WAT and D) Quantitation of NKA α1 and Cav1 in fraction 4/5, n=3. E) Western blot of NKA α1, NKA α2, and Cav1 in epididymal WAT of WT and mCBM mice and F) Western blot quantitation, n=3. Data reported as mean ± SE. *, $P < 0.05$; **, $P < 0.01$; ***, $P < 0.001$ (Unpaired t-test with Welch's correction)

Structural remodeling in human iPSC-derived mCBM adipocytes.

The generation of NKA CBM mutant iPSC has been reported previously (X. Wang et al., 2020). Wild-type (WT) and mCBM iPSC were subjected to a well-characterized adipogenesis protocol, consisting of two sequential differentiation steps (iPSC-to-MSC, followed by MSC-to-adipocyte) as summarized in Fig. 16A (Hafner & Dani, 2014; W. Tang et al., 2008). Marker gene expression was measured by RT-qPCR before and after the first 2 weeks of mesenchymal differentiation. The loss of stemness in mCBM iPSC, which has been previously reported (X. Wang et al., 2020), was confirmed by altered expression of the stem cell marker gene SOX2 (Fig. 16B). However, the expression of adipocyte progenitor marker genes PDGFRA and PDGFRB was detected in mCBM cells (Fig. 16B), suggesting that mCBM parental iPSCs have already moved from the original pluripotent state into a more differentiated state but may still have the potential to differentiate into adipocytes. After a total of five weeks of adipocyte differentiation, a robust expression of the dominant adipogenesis marker gene PPARγ and the gene encoding the key de novo lipogenesis enzyme fatty acid synthase (FASN) was detected in both WT and mCBM cells. Elevated levels of adipocyte-specific genes ADIPOQ (which encodes Adiponectin) and FABP4 (which encodes Fatty Acid Binding Protein 4) were also measured in mCBM cells (Fig. 9C). This indicated that both WT and CBM mutant iPSCs successfully committed to the adipocyte lineage. However, Oil Red O staining indicated a drastic reduction of

40

lipid accumulation in mCBM iPSC-derived adipocytes 3 weeks after adipogenesis induction (Fig. 9A&B). This was confirmed by electron microscopy, revealing a 75% reduction of the number of lipid droplets (LD) per cell (Fig. 9D&E).

To probe the molecular mechanisms behind the defective adipogenesis in mCBM cells, we used RNA-seq analysis as an unbiased approach. Among a total of 48163 scanned genes, over 5000 genes were differentially expressed (volcano plot, Fig. 17A). KEGG enrichment indicated a global up-regulation of genes in pathways associated with ECM fibrotic remodeling, including genes related to glycosaminoglycans biosynthesis and focal adhesion (Fig. 17B). Consistently, fibrotic remodeling was observed by fluorescence imaging, with a marked increase in type I collagen deposition in mCBM adipocyte cultures (Fig. 9F). This was corroborated by increased expression of fibrosis marker genes COL1A1 (collagen type I, α1) and FN1 (fibronectin) (Fig. 9G). Importantly, as observed in the fat tissue of mCBM mice, mCBM adipocytes had a reduced expression of NKA α1 with upregulation of NKA α2 (Fig. 10A&B), without change of Na/K-ATPase-dependent enzymatic activity compared to WT adipocytes (Fig. 10C). Moreover, consistent with the previous observation that mCBM does not affect the enzymatic function of NKA (X. Wang et al., 2020), Na/K-ATPase activity was not changed in mCBM iPSC or derived adipocytes (Fig. 10C). As in mCBM fat, increased expression of Cav1 was detected in mCBM adipocytes (Fig. 10A). Hence, the anomalies observed in mouse mCBM fat were phenocopied with a high level of similarity in human IPSC-derived mCBM adipocyte cultures, indicative of a profound role of caveolar NKA signaling in adipose physiology. Consistently, lentiviral-mediated expression of WT mouse NKA α1 in mCBM iPSC prior to exposure to the adipogenesis protocol significantly rescued lipid accumulation (Fig. 10D&E),

reduced collagen deposition (Fig 10F), and decreased fibrosis marker genes expression (Fig 10G), indicative of a causal role of NKA α1 in the observed functional defects.
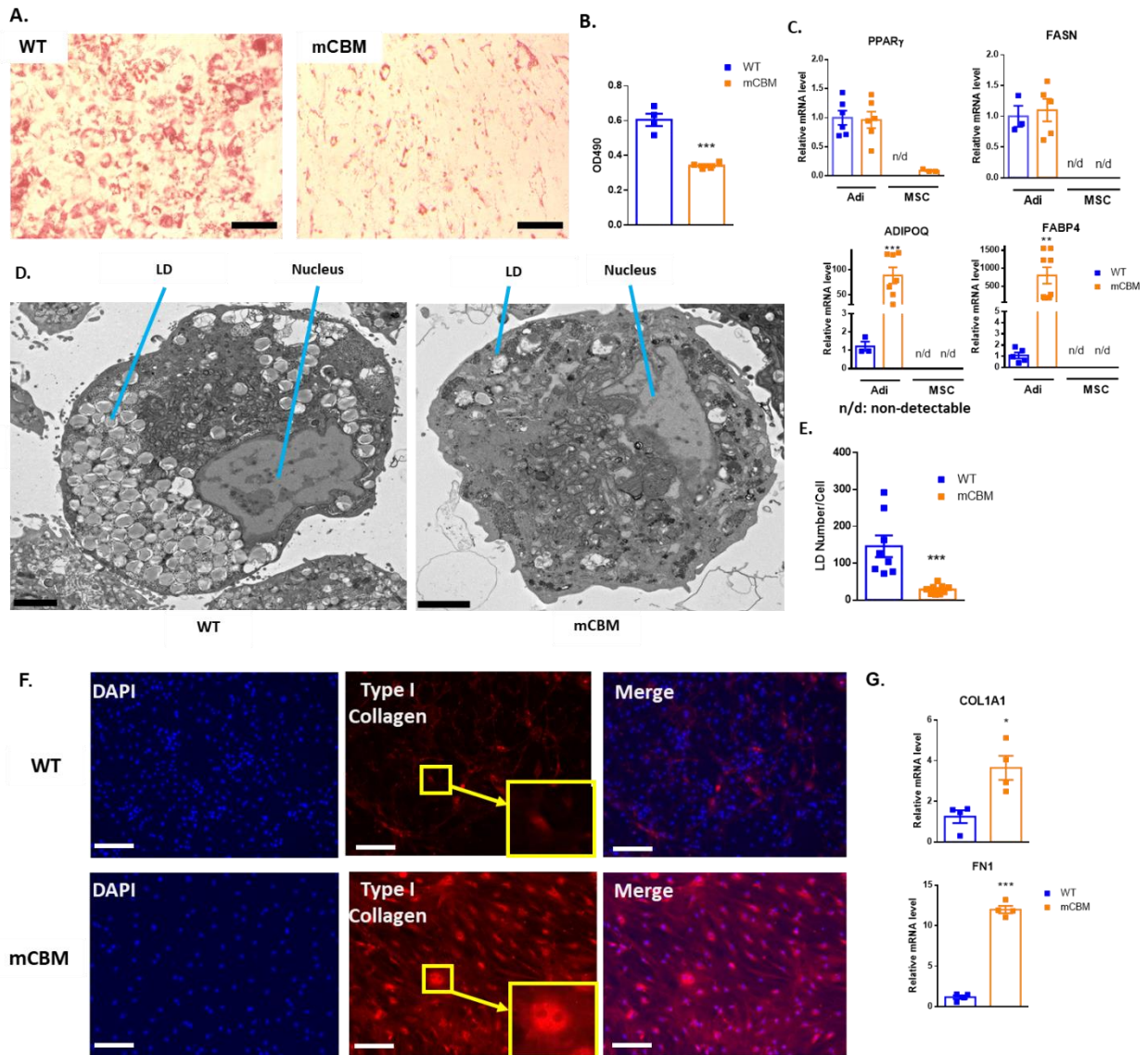
Figure 9. Adipogenesis impairment in mCBM human induced pluripotent stem cell (iPSC) derived adipocytes.

A) Oil Red O staining of iPSC-derived adipocytes, representative pictures are selected from n=4 independent repeats. Scale bar=500μm B) Quantification of Oil Red O Staining C) Expression of adipogenesis marker genes before (MSC) and after (Adi) 3 weeks of adipogenesis by RT-qPCR, n=3-6. D) Electron Microscopy (EM) images of WT and mCBM iPSC-derived adipocytes, and E) quantitation of lipid droplet (LD) per cell, n=8. Representative pictures are selected from 3 independent repeats. Scale bar=2μm F) Collagen deposition in WT and mCBM iPSC-derived adipocytes. Blue: DAPI staining for nuclear, Red: Immunostaining of type I collagen. Representative pictures are selected from n=3 independent repeats. Scale bar = 500 μm. F) mRNA levels of COL1A1 and FN1 genes in WT and mCBM iPSC-derived adipocytes measured

by RT-qPCR, n=4. Data reported as mean ± SE. *, P < 0.05; **, P < 0.01; ***, P < 0.001 (Unpaired t-test with Welch's correction)
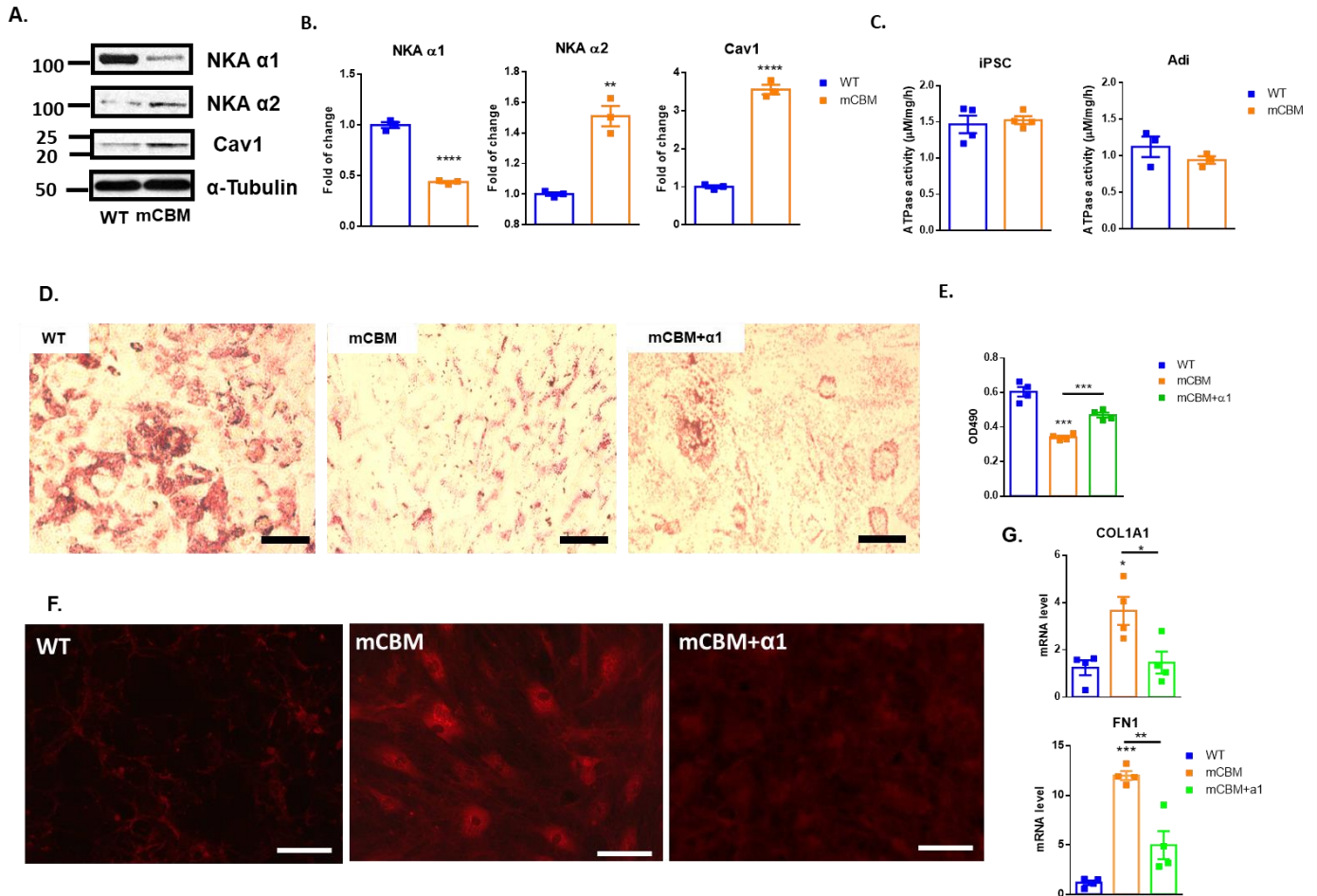
Figure 10. NKA in iPSC-derived Adipocytes.
A) Western blot of NKA α1, NKA α2, and Cav1 in WT and mCBM iPSC-derived adipocytes and B) Western blot quantitation, n=3. C) Ouabain sensitive ATPase activity in WT and mCBM iPSCs and iPSC-derived adipocytes, n=4. D) Oil Red O staining of iPSC-derived adipocytes, representative pictures are selected from n=4 independent repeats. Scale bar=200μm and E) Quantitation of Oil Red O staining. Mouse α1 was introduced into mCBM iPSC via lentivirus vector. F) Collagen deposition in iPSC-derived adipocytes. Red fluorescence indicates type I collagen. Representative pictures are selected from n=3 independent repeats. Scale bar = 200μm. G) The mRNA levels of COL1A1 and FN1 gene in iPSC-derived adipocytes measured by RT-qPCR, n=4. Data reported as mean ± SE. *, P < 0.05; **, P < 0.01; ***, P < 0.001 (Unpaired t-test with Welch's correction and one-way ANOVA with Tukey post hoc test)

Impaired metabolism, mitochondrial function, and redox state in the mCBM adipocyte.

In addition to an upregulation of genes in pathways related to ECM remodeling, our KEGG enrichment analysis indicated a significant down-regulation of metabolic genes, including those related to insulin signaling and tricarboxylic acid cycle (TCA) cycle, in mCBM adipocytes (Fig. 17B). This was explored functionally by evaluating cellular glycolysis and mitochondrial respiration using Seahorse metabolic flux analysis. Baseline extracellular acidification rate (ECAR) monitoring indicated a reduction of both basal glycolysis rate (measured in the presence of glucose) and maximum glycolytic capacity (measured in the presence of glucose and oligomycin to inhibit mitochondrial respiration) in mCBM adipocytes (Fig. 11A&B). Hence, mCBM adipocytes were able to metabolize glucose in the conditions of our Seahorse assay, but glycolysis was defective. However, this did not exclude a possible defect in insulin signaling. The RNA-seq KEGG enrichment analysis (Fig. 17B) pointed to such defect, which was corroborated at the mRNA and protein level by decreased expression of insulin receptor (IR), insulin receptor substrate (IRS), and glucose transporter 4 (GLUT 4) (Fig. 11C-E). Functionally, an alteration of the cell membrane distribution of GLUT 4 (Fig. 11F, yellow arrow) and a reduction of acute stimulation of glucose uptake (Fig. 11G) in response to insulin confirmed altered insulin signaling in mCBM adipocytes. Since long-term insulin exposure is key to the maintenance of glycolytic capacity in adipocytes (Klip, McGraw, & James, 2019), this impaired insulin signaling pathway likely contributes to the overall reduction of glycolytic capacity in mCBM adipocytes. Consistent with this notion, intracellular GLUT4-enriched vesicles (Fig. 11F, red arrow), which typically form upon long-term insulin stimulation, were not observed in the mCBM iPSCs-derived adipocytes. Of note, the reduction of basal and maximal glycolytic capacity in mature mCBM adipocytes maintained in insulin-containing media was

44

also present in the absence of insulin (Fig. 18A&B). Because the increase in glycolytic enzyme expression that normally occurs with consistent insulin stimulation during adipogenesis is likely blunted in the insulin-resistant mCBM adipocyte, a persistently decreased glycolytic capacity was not unexpected. The reduced gene expression of phosphofructokinase (PFKM), a key insulin-induced glycolytic enzyme, in mCBM adipocytes is consistent with this hypothesis (Fig. 11C).

The maximum respiratory capacity measured by Seahorse analysis was preserved in mCBM adipocytes. However, the ATP-synthesis coupled respiration rate was significantly reduced, associated with reduced ATP5A1 gene expression (Fig. 12G), without change of maximum respiratory capacity or spare capacity (Fig. 12A&B). These indicate a defect of mitochondrial respiration and ATP production in mCBM adipocytes likely to contribute to the metabolic defect. Electron microscopy revealed mitochondrial enlargement (Fig. 12C&D), a phenotype reminiscent of the Cav1-/- mouse adipose tissue that has been associated with mitochondrial dysfunction (Cohen et al., 2005). These mitochondrial abnormalities occurred with an increase of about 70% in mitochondrial ROS production in mCBM adipocytes, as indicated by mitoNeoD staining. Taken together, these observations were consistent with a profound mitochondrial dysfunction with increased mitochondrial and extramitochondrial ROS generation in mCBM adipocytes. Such perturbations of the cellular redox status have been associated with profound alterations of adipose physiology and could be key to the mCBM mouse fat phenotype (Fig. 7). Indeed, elevated oxidative stress has been shown to lead to adipose tissue fibrosis, and tissue fibrosis itself has been shown to further enhance oxidative stress (Sun et al., 2013). This positive feedback loop has been shown to eventually result in chronic inflammation, insulin resistance, and metabolic dysfunction of the adipose tissue (Sun et al.,

2013). Activation of HIF-1α and increased downstream inflammatory cytokines (IL6, encode Interleukin 6, and CCL2, encode monocyte chemoattractant protein-1) mRNA further indicated a stressed intracellular environment in mCBM adipocytes compatible with this model (Fig 12F&G). To further clarify the role of mitochondrial ROS in the mCBM adipocyte, we pre-treated mCBM MSC with the mitochondrial ROS scavenger MitoTEMPO for 72 h before initiation of the adipogenesis phase of the differentiation protocol (Fig. 16A). The MitoTEMPO treatment dose-dependently improved lipogenesis in mCBM cells (Fig. 12H) but did not prevent ECM collagen deposition (Fig. 12I&J). Taken together, these data suggested that ECM remodeling preceded mitochondrial redox imbalance and defective lipogenesis during mCBM adipocyte differentiation. Consistent with this, collagen staining and fibrosis markers gene expression (COL1A1 and FN1) indicated an early onset of ECM remodeling in precursor mCBM iPSCs (Fig. 19A&B) and MSCs (Fig. 20A&B), which was rescued upon lentiviral-mediated expression of WT mouse NKA α1 (Fig. 19A&B). Moreover, the increased NADPH/NADP ratio confirms the hypoxia condition and change of redox state in mCBM iPSCs, and this change is restored by exogenous WT NKA α1 (Fig. 19C).
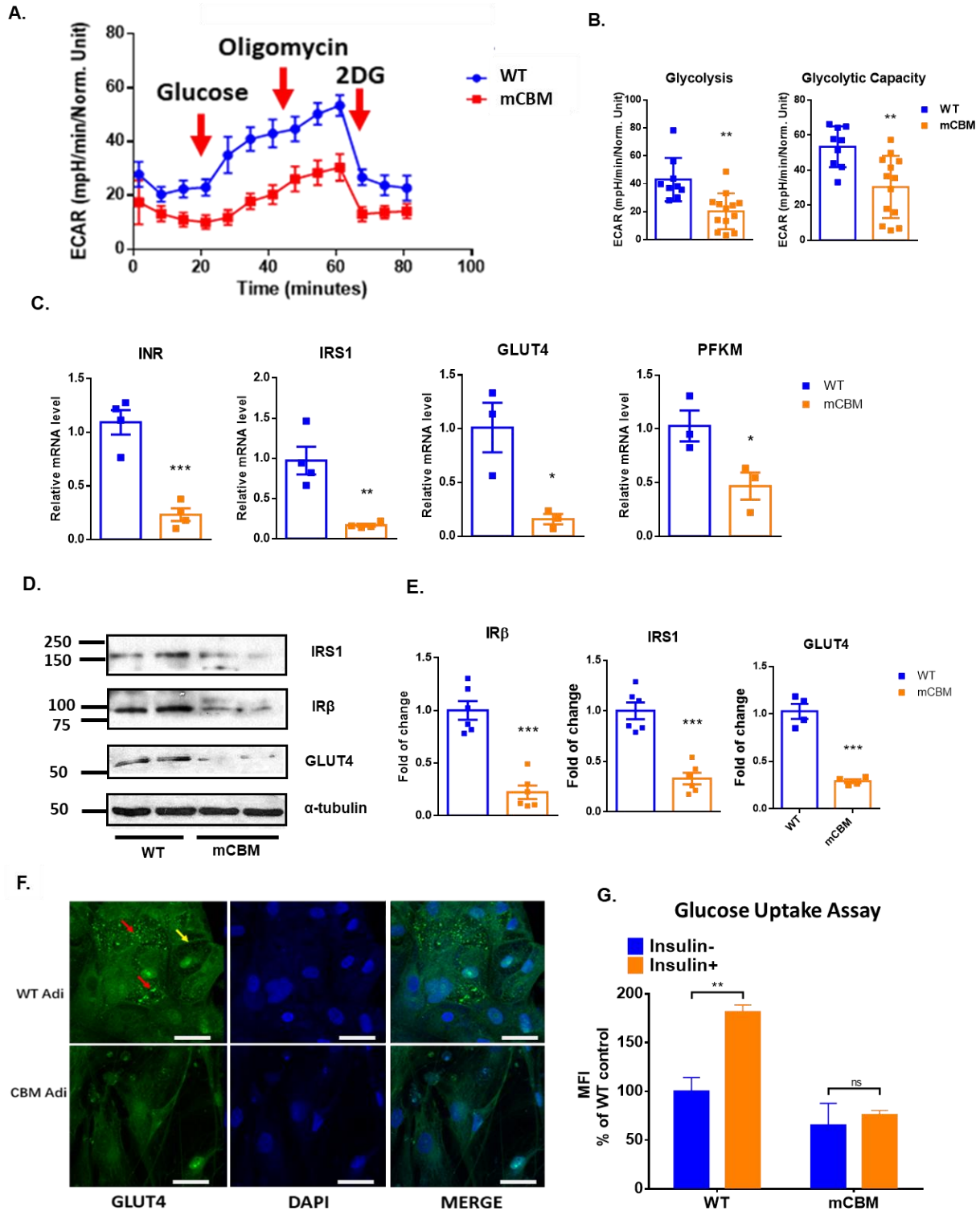
Figure 11. **Glycolysis Defect and Insulin Resistance in mCBM Adipocytes.**
A) Seahorse XF Cell Glycolysis Test in WT and mCBM iPSC-derived adipocytes, in the presence of insulin. Respectively, glucose, Oligomycin, and 2-DG were added to the cells after the basal ECAR was established (as indicated by arrow). The data are normalized by protein amount as mpH/min/Norm. Unit. B) Quantitation of panel A, n=9. C) mRNA levels of insulin

receptor (INR), insulin receptor substrate (IRS), GLUT4, and PFKM genes measured by RT-qPCR, n=3-4. D) Western blot of the protein expression level of insulin receptor substrate 1 (IRS1), insulin receptor β subunit (IRβ), and GLUT4 in mCBM adipocytes, E) Quantitative analyses of IRβ, IRS, and GLUT4 expression by WB. Data are normalized by α-tubulin level and % of WT control. n=4-6. F) Immunostaining pictures of mCBM and WT iPSC-derived adipocytes in adipogenesis medium containing 0.1% human insulin. Green: immunostaining of GLUT4; Blue: DAPI staining for cell nuclei; Red arrow: GLUT4 packed in vesicles; Yellow arrow: GLUT4 on the cell membrane. Representative pictures were selected from n=3 repeats. G) Mean fluorescence intensity (MFI) of Glucose Uptake Assay in WT and mCBM adipocytes by 10 μM 2-NBDG with 0.1% insulin in the serum-free DMEM for 3h, no insulin group as empty control. n=4/group. **P < 0.01 vs untreated. Data reported as mean ± SE. *P < 0.05, **P < 0.01, ***P < 0.001 (Unpaired t-test with Welch's correction)
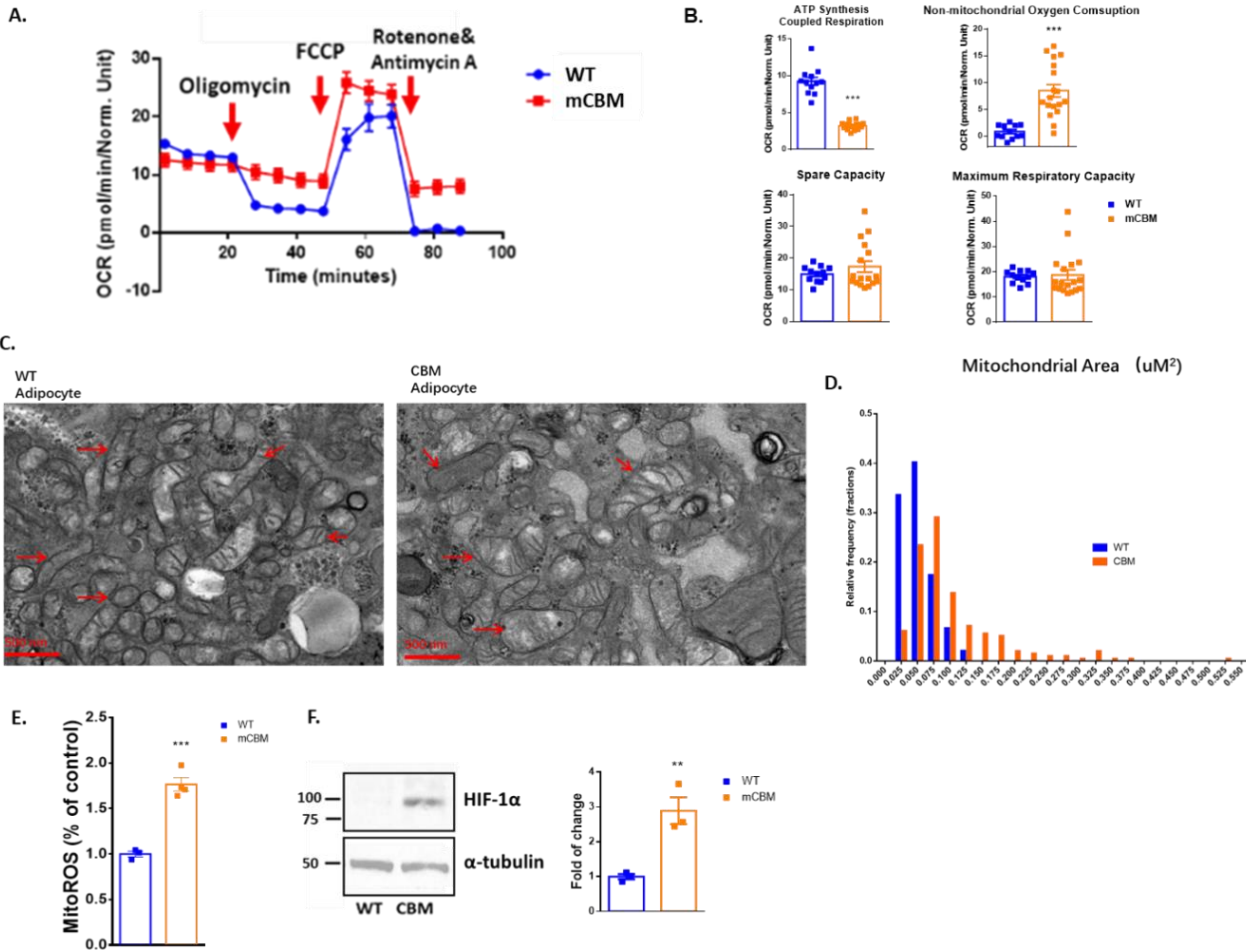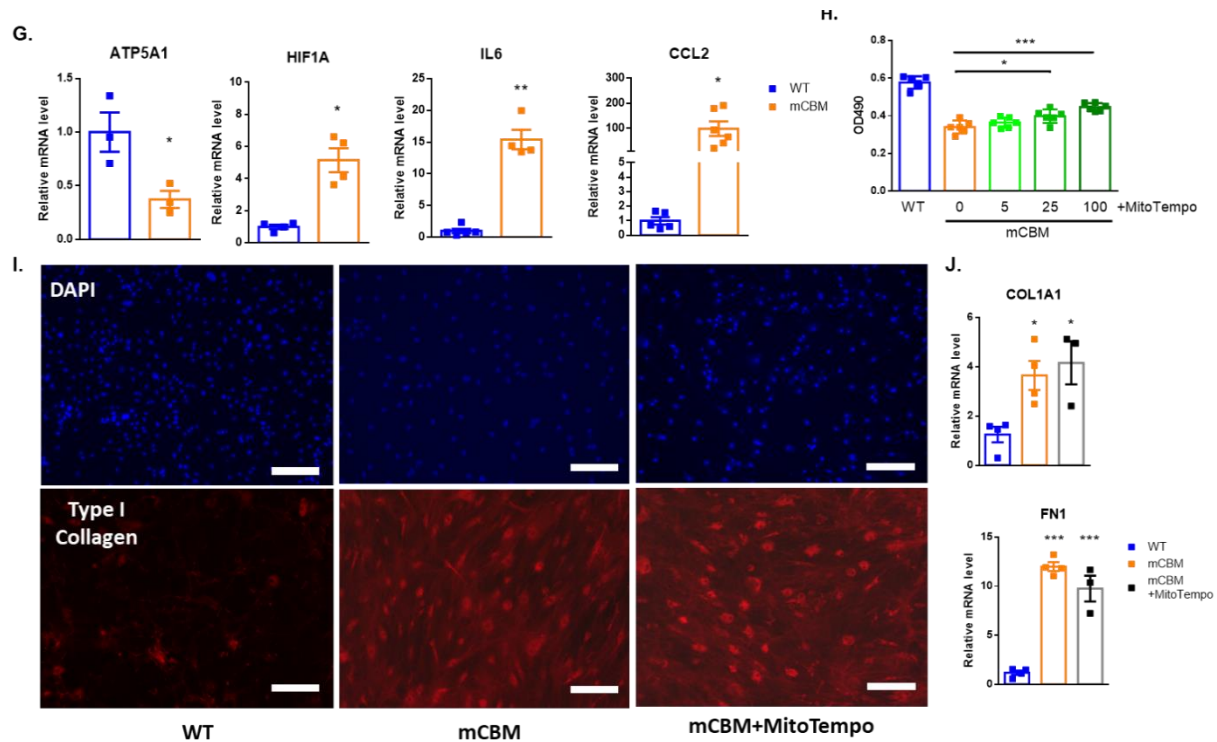
Figure 12. Metabolic dysfunction in mCBM adipocytes.
A) Seahorse XF Mito Stress Test in WT and mCBM iPSC-derived adipocytes. Respectively, Oligomycin, FCCP, and RA were added to the cells after the basal OCR was established (as indicated by arrows). The data are normalized by protein amount as pmol/min/Norm. Unit. B) Quantitation of Panel A, n=12-18. C) Mitochondrial EM images of WT and mCBM iPSC-derived adipocytes. Representative pictures are selected from n=3 independent repeats. Scale bar= 500 nm. D) Mitochondrial area relative frequency of WT and mCBM iPSC-derived adipocytes. Data are quantified from EM images in panel B. E) Mitochondrial ROS generation in WT and mCBM iPSC-derived adipocytes are detected by mitochondria-targeted superoxide probe MitoNeoD. Data show signal intensity measured with fluorescence-activated cell sorting (FACS) and were normalized by WT control, n=3. F) Western blot band of HIF-1α and α tubulin as loading control in WT and mCBM iPSC-derived adipocytes and quantification of western blot bands, n=3. G) mRNA levels of ATP5A1, HIF-1α, IL6, and MCP-1 genes in WT and mCBM iPSC-derived adipocytes measured by RT-qPCR, n=3-6. H) Quantification of Oil Red O staining of lipid on mCBM iPSC-derived adipocytes pre-treated with 0, 5, 25, 100 nM MitoTEMPO, n=4. I) Collagen deposition in iPSC-derived adipocytes. Red: Immunostaining of type I collagen, Blue: DAPI. Representative pictures are selected from n=3 independent repeats. Scale bar = 500 μm. J) mRNA levels of COL1A1 and FN1 genes in iPSC-derived adipocytes measured by RT-qPCR, n=3-4. The data were reported as mean ± SE. Data reported as mean ± SE. *, $P < 0.05$; **, $P < 0.01$; ***, $P < 0.001$ (Unpaired t-test with Welch's correction and one-way ANOVA with Tukey post hoc test)

ECM remodeling alters lipogenesis in mCBM adipocytes.

NKA-mediated signaling is well known as a potent regulator of collagen synthesis, ECM remodeling, and tissue fibrosis in cardiac and renal diseases (Fan, Xie, & Tian, 2017; Quintas et al., 2010). The above studies in mice and human iPSC-derived adipocytes suggest that disassembly of the caveolar NKA signaling complex upon mutation of the NKA's CBM led to unchecked ECM remodeling, increased oxidative stress, inflammation, and metabolic abnormalities that ultimately altered lipogenesis. During mesenchymal differentiation, adipogenesis and fibrogenesis counteract each other (Sun et al., 2013). Indeed, ECM stiffness is critical for MSC lineage commitment (Engler et al., 2006; Rowlands et al., 2008). Mesenchymal ECM must adopt a flexible structure with a remarkable reduction of fibrotic collagen type I to allow expansion of the adipocyte (Chun et al., 2006; Sun et al., 2013; Winer et al., 2009), while activation of potent profibrotic cytokines such as TGF-β induces expression of fibrosis marker genes in mesenchymal progenitor cells, increases the amount of collagen type-I-producing cells, and inhibits adipogenesis (Bortell, Owen, Ignotz, Stein, & Stein, 1994; Carthy, 2018; Choy, Skillington, & Derynck, 2000). Such fibrotic ECM also creates hypoxic conditions that further activate the HIF1-α signaling pathway, and inhibits metabolic functions of adipocytes (Sun et al., 2013), as observed in the mCBM adipocytes. Consistent with this model, TGF-β gene expression was increased in mCBM iPSC and repressed upon lentiviral delivery of WT NKA α1 (Fig. 19B). Crosstalk between TGF-β signaling and Na/K-ATPase has been reported in various experimental studies (Grigorova et al., 2018; Kennedy et al., 2018; La et al., 2016). To functionally evaluate the role of this crosstalk in the adipogenesis defect of mCBM cells, we tested whether inhibition of TGF-β signaling attenuates ECM remodeling/fibrosis in mCBM cells, thereby rescuing adipogenesis. Accordingly, WT and mCBM iPSCs were first treated with 100 μM TGF-β

50

inhibitor SB431542 for 24 h. As shown in Fig. 21A, SB431542 treatment reduced ECM stiffness

in iPSCs, significantly decreased fibrosis marker gene expression (Fig. 21B). Importantly,

SB431542 treatment also reduced the elevated NADPH/NADP ratio in mCBM iPSC (Fig. 21C),

suggesting that hypoxia and altered redox state in mCBM iPSCs is secondary to TGF-β

dependent ECM remodeling. To further test the effect of SB431542 on adipogenesis of mCBM

cells, 10 μM of SB431542 were added to the adipogenesis cocktail during the three weeks of the

adipogenesis protocol (Fig. 16A). Significantly, lipid accumulation was increased in mCBM

adipocytes exposed to the SB431542 treatment (Fig 13A&B). Additionally, SB431542 decreased

ECM stiffness, fibrosis marker gene expression (COL1A1 and FN1), and the expression of

HIF1A in mCBM adipocytes (Fig 13C&D).
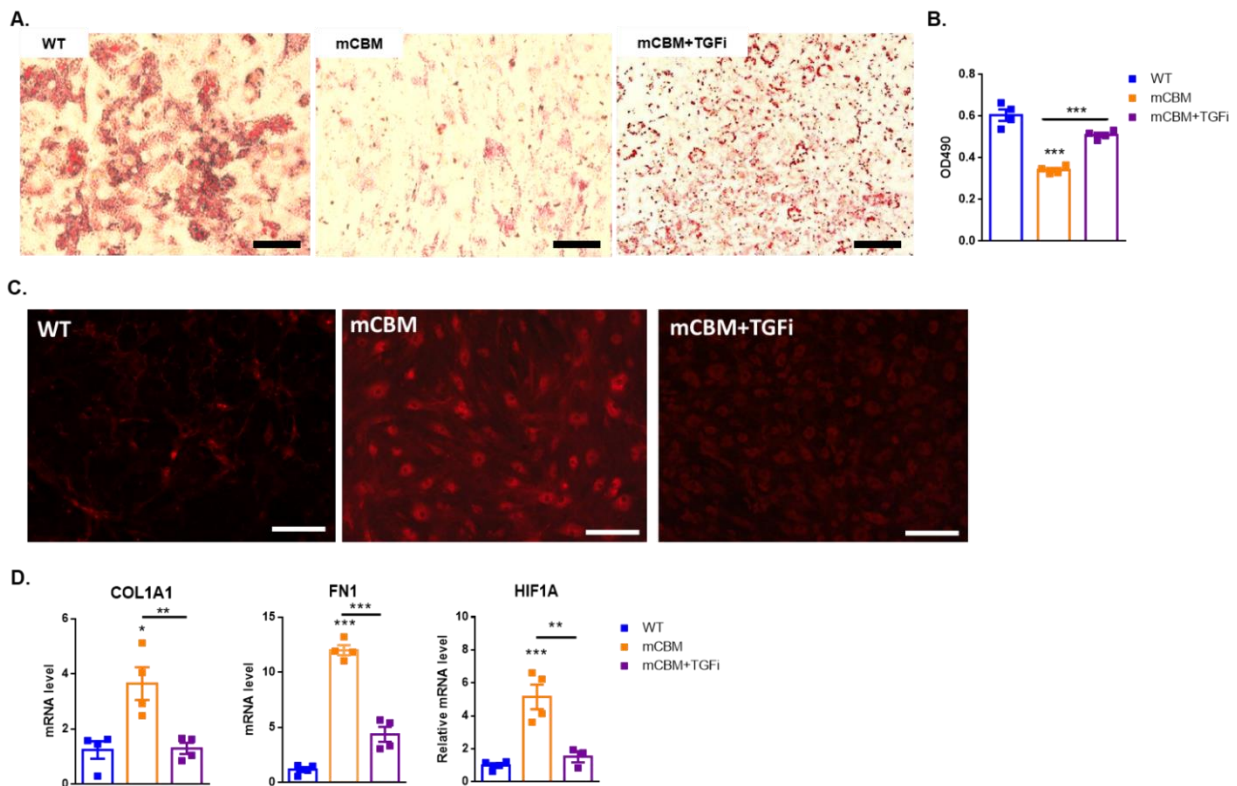
Figure 13. TGF-β inhibitor (TGFi) SB431542 rescues adipogenesis in mCBM cells.
A) Oil Red O staining of iPSC-derived adipocytes, representative pictures are selected from n=4 independent repeats. Scale bar=200μm and B) quantitation of panel A, n=4. C) Collagen deposition in iPSC-derived adipocytes. Red: Immunostaining of Type I collagen. Representative pictures are selected from n=4 independent repeats. Scale bar = 500 μm. D) mRNA levels of

COL1A1 and FN1 genes in iPSC-derived adipocytes measured by RT-qPCR, n=4. Data reported as mean ± SE. *, $P < 0.05$; **, $P < 0.01$; ***, $P < 0.001$ (One-way ANOVA with Tukey post hoc test)

Collectively, these studies provide the first genetic evidence of a critical role of caveolar NKA signaling in adipose biology. Mechanistically, this role does not appear to be related to a change in ATPase-driven ion-transport function. Rather, the adipogenesis defect secondary to the loss of CBM appears to be a consequence of the dysregulation of a TGF-β-dependent control of ECM stiffness, redox status, and inflammation, which ultimately leads to inadequate metabolic function during adipogenesis (Fig. 14).
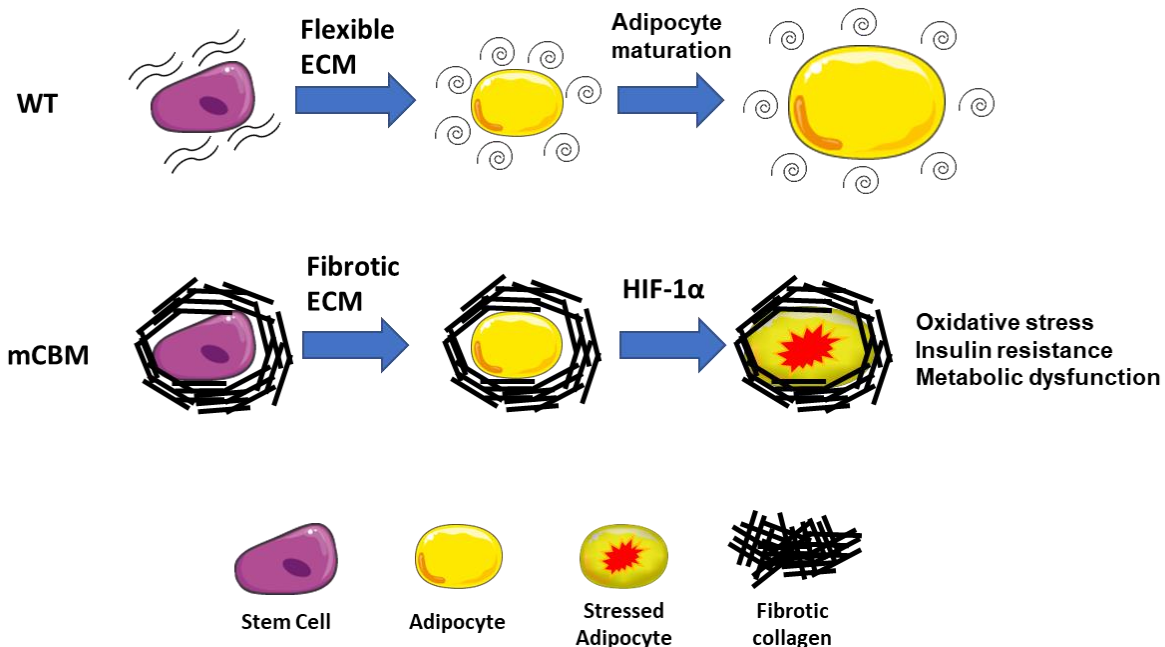
Figure 14. Role of NKA-Cav1 binding in adipogenesis.
NKA-Cav1 binding is essential for maintaining the ECM stiffness in stem cells. Loss of NKA-Cav1 binding increases ECM stiffness. The fibrotic ECM further activates HIF-1α and eventually results in metabolic dysfunction during adipogenesis.

Discussion

NKA is one of the most critical housekeeping genes in mammals. Besides its traditional role as an ion pump, accumulating evidence has shown the non-ion pumping function of the α1

NKA subunit is also essential in cell physiology. Here, we report that the conserved NKA-Cav1 interaction is a critical regulator of adipogenesis. The NKA/Cav1 interaction, which has been shown to allow the formation of an NKA/Cav1/Src signal complex and its integration with other proteins in epithelial cells, was studied in the context of adipogenesis. Our results suggest that NKA/Cav1 interaction is important for collagen production, mitochondrial function, ROS generation, and further ensures regular adipogenesis and adipocyte metabolism. Specifically, our studies in CBM mutant adipocytes indicate that increased ECM stiffness activates HIF-1α and its downstream pathway, results in elevated oxidative stress, insulin resistance, and metabolic dysfunction. These defects eventually cause impaired adipogenesis (Fig. 14). This is the first genetic evidence of NKA-mediated regulation of adipogenesis.

NKA/Cav1-binding regulates Cav1 trafficking and caveolae formation. The cell membrane-associated caveolae in the adipocyte are critical for adipocyte function and the development of lipodystrophy (Garg & Agarwal, 2008; Garg et al., 2015). Both the number of total caveolae and the number of membrane-associated caveolae were reduced in adipocytes from mCBM (Fig.16A&B), which is similar to the adipose tissue phenotype of lipodystrophy patients (Garg et al., 2015). Lipodystrophies include genetic disorders characterized by reduced fat mass and adipose metabolic dysfunction (Brown et al., 2016). They can be caused by genetic defects leading to altered adipogenesis, and patients also exhibit metabolic defects in cell respiration, elevated intracellular stress, and cell apoptosis (Schrauwen et al., 2015). CAV1 is known as one of the loci for genetic lipodystrophies in humans (Garg & Agarwal, 2008). Moreover, the Cav1 -/- mice also show adipose tissue dysfunction including insulin resistance, cell respiratory defects, and impaired metabolism (Cohen, Razani, et al., 2003). These findings have suggested a fundamental role of Cav1 in adipose biology, which was not fully understood.

In this study, we first time reported the mechanistic role of NKA CBM in the regulation of adipogenesis, this fulfills the puzzle of how the loss of Cav1 function associate with adipogenesis defect. However, none of the NKA mutations were reported to cause genetic lipodystrophy, possibly due to the more essential role of NKA in survival. While the NKA CBM homozygous mutation is embryonic lethal, the Cav1 -/- mouse can survive to adulthood (Cohen, Razani, et al., 2003; X. Wang et al., 2020). In addition, although both Cav1 knockout and NKA CBM mutant caused adipose insulin resistance, the Cav1 knockout shows defect in insulin signal transduction without change of protein expression in the insulin signaling pathway (Cohen, Razani, et al., 2003), and the NKA CBM mutant adipocytes exhibited a decrease in total gene and protein expression in the insulin signaling pathway. Moreover, a previous study on NKA α1 +/- mouse shows no difference in fat mass, which indicates the altered adiposity is a consequence of CBM mutation rather than decreased NKA α1 expression (Kutz et al., 2018). This implied a manner-dependent regulation of NKA/Cav1 distribution is more critical than the expression of Cav1 or NKA in organogenesis and adipose function.

Although we have identified the mechanistic role of NKA CBM in the regulation of adipogenesis through manipulation of ECM remodeling and metabolic function, the molecular details remain a blur. Adipose tissue fibrosis was recently recognized to contribute to the dysfunctional adipose tissue in obesity and related disorders (Bielczyk-Maczynska, 2019; Sun et al., 2013). The cardiotonic steroids-induced tissue fibrosis through NKA/Src-mediated signaling was well documented in the cardiac and renal model, but not yet in the adipose tissue (Elkareh et al., 2007; Elkareh et al., 2009; L. V. Fedorova et al., 2009; Kennedy et al., 2006; Shapiro & Tian, 2011; Tian, Shidyak, et al., 2009). Whether the loss of NKA CBM induced adipose fibrosis through a similar mechanism remains unknown. The NKA/Cav1 binding is essential for the

formation of cell membrane NKA/Src complex (Cai et al., 2008; H. Wang et al., 2004), loss of

CBM may alter the dynamic regulation of NKA-mediated signal transduction in adipocyte.

Besides, loss of CBM also alters the cellular distribution of NKA and Cav1 (Cai et al., 2008).

The scaffolding function of Cav1 is critical for both ECM remodeling (Castello-Cros et al., 2011;

Del Galdo et al., 2008; Drab et al., 2001; Razani et al., 2001; X. M. Wang et al., 2006) and lipid

metabolism (Lockwich et al., 2000; Ostermeyer et al., 2004; Pilch & Liu, 2011; Pilch et al.,

2011), which could be disturbed by the loss of CBM induced Cav1 redistribution and

independent of Src. Pharmaceutical inhibition of the NKA/Src/ERK axis can reduce the adipose

tissue oxidative stress in obese mice, and therefore benefits metabolic symptoms (Sodhi et al.,

2015; Sodhi et al., 2017). The manipulation of intracellular ROS via NKA/Src/ERK signaling

was thought to be critical for this therapeutic effect (Pratt et al., 2019). However, mitochondrial

ROS scavenger failed to rescue the adipogenesis defects in mCBM. Our data has shown the

NKA CBM regulates adipogenesis through ECM remodeling over ROS generation. This implies

the Src-independent function of NKA CBM. Evolutionarily, the gain of the caveolin binding site

on NKA occurred at the same time as the acquisition of the binding sites for sodium and

potassium (X. Wang et al., 2020), which is much earlier than the NKA/Src binding. This

confirms the critical role of NKA CBM in mammal species survival. Taken together, the CBM is

more essential for the post-embryonic development of adipose tissue, and the NKA/Src/ERK

axis may be more specific in the regulation of ROS-associated signaling in adipocytes.

Materials and Methods

Reagents

bFGF, Gibco #1949360

Serum knock out replacement, Gibco #10828010

Human insulin, Sigma #I9278

Dexamethasone, Sigma #D1756

Indomethacin, Sigma #I7378

3-Isobutyl-1-methylxanthine (IBMX), Sigma #I5897

Rosiglitazone, Sigma #2408

Alamethicin, Sigma #A4665

Ouabain, Sigma #O3125

Adenosine 5-triphosphate magnesium (ATP/Mg), Sigma #A9178

mCBM Mouse

Animal protocols were approved by the Marshall University Institutional Animal Care and Use
Committee (IACUC) according to National Institutes of Health (NIH) guidelines. The mCBM
heterozygous mice were generated as previously described by Wang *et al*. (X. Wang et al.,
2020). In short, a LoxP-neomycin-LoxP cassette knockdown and rescue protocol was used to
generate a mouse line that expresses the CBM F97A and F100A mutant α1 NKA. All mCBM
heterozygous mice were backcrossed to C57BL6 for at least six generations.

Body composition

As described by Parkman JK, *et al*.(Parkman et al., 2016), the body composition of mice was
measured by quantitative magnetic resonance imaging using an EchoMRI-100 whole-body
composition analyzer (Echo Medical Systems, Houston, TX). The device was provisionally
calibrated on traditional phantoms representing fat (canola oil), and water. The quantities
measured by EchoMRI were fat, lean, free water, and total water.

Adipose tissue collection and histology staining

Mice were anesthetized with 50 mg/kg pentobarbital administered via IP injection. Epididymal adipose tissue was collected, flash-frozen in liquid nitrogen, and stored at -80° C until used for Western blot analysis, Na/K-ATPase activity, or qPCR. For histological staining, isolated tissues were fixed in 10% neutrally buffered formalin for 24 hours and stored in 70% ethanol until further processing. Transverse sections of visceral adipose tissue were subjected to H&E staining, Trichrome staining, and F4/80 immunohistochemistry staining by Wax-It, Inc. (Vancouver, Canada).

Human iPSCs

As previously described by Wang, *et al*. (X. Wang et al., 2020), human iPSCs were purchased from iXCells (catalog no. 30HU-002) and cultured with the TeSR-E8 Kit (STEMCELL Technologies Inc., catalog no. 05940). mCBM F97A and F100A mutant human iPSCs were generated by CRISPRCas9 genome editing. The DNA plasmids for Cas9–green fluorescent protein (GFP) (Addgene, no. 44719) and guide RNA (gRNA) cloning vector (Addgene, no. 41824) were from Addgene. sgDNA (single-guide DNA) and ssODN (single-stranded oligodeoxynucleotides) were designed according to the published protocol (Ran et al., 2013). The cloned Cas9-GFP vector inserted with sgDNA, along with ssODN, was transfected into human iPS cells with a 4D nucleofector device. Single-cell sorting and plating were later performed with FACS flow cytometry and the clones were selected and validated via genotyping PCR and DNA sequencing. For exogenous NKA α1 rescue, mouse Atp1a1 (NM_144900.2) was cloned into a lentiviral expression vector with the help of Vectorbuilder (Fig. 22A). The cloning strategy and DNA construct are derived from our previous product (Pratt et al., 2019). We validated transgene expression using real-time qPCR. (Fig. 22B)

Human iPSC-derived adipocytes

For adipocyte differentiation, human iPSCs were incubated with an MSC differentiation medium (DMEM+10%FBS and 2.5 ng/mL bFGF) for 7-10 days until a monolayer was formed. The mature MSCs were then transferred to collagen-coated plates at the ratio 1:3 as passage 1 and maintained with DMEM+10% FBS. MSCs within 3 passages were subjected to adipogenesis. MSCs at 100% confluence were incubated with adipogenesis medium (DMEM+15% serum knockout replacement, 0.1% human insulin, 125nM Dexamethasone, 0.2mM Indomethacin, 100μg/mL IBMX, and 5μM Rosiglitazone, see reagents section) for 3 weeks to fully differentiated into adipocytes and then were subjected to further measurements (Hafner & Dani, 2014). For the MitoTEMPO treatment, cells were treated with MitoTEMPO (Sigma # SML0737) with the final dosage of 0, 5, 25, 100nM for 3 days before induction of adipogenesis. For the TGF inhibitor treatment, SB431542 (Selleckchem #S1067) with the final concentration 10nM of is added to the adipogenesis medium during the 3 weeks differentiation.

Oil Red O Staining

Oil red O staining for adipocytes was conducted as follows: mature adipocytes after 3 weeks of adipogenesis were washed twice with ice-cold PBS, then fixed with 4% formaldehyde for 10 min at room temperature. The fixed cells were stained with 0.21% Oil Red O in 60% isopropanol for 10 min at room temperature, then washed twice with PBS before imaging. After imaging, the cells were dried out at room temperature overnight, the staining was then washed down by 100% isopropanol for 10 min at room temperature. Then the concentration of Oil Red O was measured at OD 490 nm by Spectramax 190 Microplate Reader (Molecular Devices, Inc).

Electron Microscopy (EM) imaging

Epididymal fat tissues of 6 weeks old male mice were fixed with glutaraldehyde and paraformaldehyde followed by osmium tetroxide and uranyl acetate, dehydrated in ethanol and

embedded in epoxy. Sections were cut at about 90 nm thickness, stained with lead citrate, and imaged on an FEI Techai 12 using a Gatan camera and software. Cultured cells were digested with 0.25% trypsin, washed twice with PBS, and then fixed with Karnovsky's Fixative (2% Paraformaldehyde, 2.5% Glutaraldehyde and 0.1M Sodium Phosphate Buffer. EMS Catalog #15720) and store at 4°C. For transmission EM, as described by Erin M. Zeituni *et al*. (Zeituni et al., 2016), samples were washed 3x5 min with PBS, rinsed in 0.1M cacodylate pH 7.4 embedded in agarose (cells) then 1%Osmium tetroxide for 1 h in cacodylate, followed by washes in water, cacodylate, and water again (2×10 min each) and then incubation in 0.05 m maleate, pH 6.5, for 10 min. Samples were then stained en bloc with 0.5% uranyl acetate in maleate for 1.5 h at room temperature. After 10-min washes with water, samples were dehydrated through graded ethanol dilution (35%, 2×10 min; 50%, 10 min; 75%, 10 min; 95%, 10 min; 100%, 3×10 min). Samples were then washed with propylene oxide 4 x 15min before incubation in 1:1 propylene oxide/resin for 1 h, followed by two 3 x 1h washes in 100% resin and a final embedding in 100% resin at 55 °C overnight followed by 70 °C for 3 days. Sections were made with a Reichert Ultracut-S (Leica Microsystems), mounted on naked 200 thin mesh grids, and stained with lead citrate. Images were captured by a blind investigator, with a Phillips Tecnai 12 microscope and recorded with a Gatan multiscan CCD camera using Digital Micrograph software. The mitochondrial area was quantitated from at least 8 single cell fields/group, the numbers of caveolae were quantitated from at least 40 fields from 5-6 mice. Quantitation was done by ImageJ 1.52a (Wayne Rasband, National Institute of Health).

Ouabain-sensitive Na/K-ATPase Activity

As described by Lai *et al*. (Lai et al., 2013), cells were collected and homogenized in ice-cold buffer A (150 mm sucrose, 5 mm HEPES, 4 mm EGTA, 0.8 mm dithiothreitol) and briefly

sonicated. After centrifugation (800 × g for 10 min), the post-nuclear fraction was further

centrifuged (45,000 × g for 45 min) to obtain a crude membrane preparation. The crude

membrane pellet was resuspended in buffer A, and the protein content was determined.

Resuspended crude membranes were treated with alamethicin (0.1 mg/mg of protein) for 10 min

at room temperature and then added to the buffer containing 50 mm Tris (pH 7.4), 1 mm EGTA,

1 mm $MgCl_2$, 25 mm KCl, 100 mm NaCl, 5 mm NaN_3. After 15 min of preincubation at 37 °C,

ATP/Mg was added to a final concentration of 2 mM to start the reaction. The reaction continued

for 40 min and was stopped by adding 8% ice-cold trichloroacetic acid. Phosphate generated

during the ATP hydrolysis was measured by BIOMOL GREEN Reagent (Enzo Life Science,

Cat# BML-AK111). Ouabain-sensitive Na/K-ATPase activities were calculated as the difference

between the values obtained in the presence or absence of 1 mM ouabain.

Seahorse glycolysis test and mito-stress test

As previously described by Kutz *et al* (Kutz et al., 2021), cells were plated in Seahorse XFp cell

culture miniplates (Agilent # 103025-100) and subjected to both the mitochondrial stress test kit

(Agilent #103017-100) and the glycolytic stress test kit (Agilent #103010-100). The assay was

run by an Agilent Seahorse XF analyzer. In short, MSCs were plated on a sterile XFp plate in

triplicate at 1×10^5 total cells per well before the 3-week-induction of adipogenesis. For the

mitochondrial stress test, cells were stimulated in the following sequence: (A) oligomycin; (B)

carbonyl cyanide-4-(trifluoromethoxy)phenylhydrazone (FCCP); (C) rotenone/antimycin A.

Respiratory parameters calculated included basal oxygen consumption rate (OCR), ATP

synthesis-coupled respiration, maximum respiratory capacity, spare respiratory capacity, and

non-mitochondrial respiration. The appropriate concentration of FCCP was determined by FCCP

titration as recommended by the manufacturer, and all experiments were performed with this

concentration of FCCP (0.6 nM). For the glycolysis test, cells were stimulated in the following sequence: (A) glucose; (B) oligomycin; (C) 2-Deoxy-D-glucose (2-DG). Glycolysis parameters calculated included basal Extracellular Acidification Rate (ECAR) and maximum glycolytic capacity. For insulin-induced glycolysis, 0.1% human insulin is added to the glycolysis basal medium. The ATP synthesis-coupled respiration is calculated as decrees of OCR after adding oligomycin. The maximum respiratory capacity is calculated as an increase of OCR after adding FCCP. The spare respiratory capacity is calculated as the increase of OCR with FCCP vs. basal OCR. The non-mitochondrial respiration is calculated as the OCR after adding rotenone/antimycin A. The basal glycolysis is calculated as an increase of ECAR after adding glucose. The maximum glycolytic capacity is calculated as the ECAR after adding oligomycin.

Flow Cytometry Assays

As previously described in Chen Y, et al. (Y. Chen et al., 2019). For glucose uptake assay, mature adipocytes after 3 weeks of differentiation were incubated in serum-free DMEM media with 10μM 2-NBDG (Invitrogen, Cat#N13195) and 0.1% human insulin (Sigma, Cat#I-034) for 3h at 37°C. Cells were then lifted by scraping and suspended in 200μl buffer (PBS with 5% FBS and 0.1% sodium azide) for flow cytometry. Intracellular fluorescence was quantified using the FITC.

For measurement of mitochondrial ROS, mature adipocytes after 3 weeks differentiation incubated in dMEM with10% FBS in the presence of 5μM MitoNeoD (Shchepinova et al., 2017) for 15min at 37°C. At the end of incubation, cells were lifted by scraping and suspended in 200μl buffer and immediately subjected to flow cytometry analysis. MitoNeoD fluorescence was detected with the PE channel.

NADP/NADPH Ratio Quantitation

The NADP/NADPH ratio was measured by NADP/NADPH Quantitation Kit (Sigma #MAK038) according to the technical bulletin. In short, about 3×10^5 human iPSCs for each sample were pelleted in a microcentrifuge tube and extracted with 600 µL of NADP/NADPH Extraction Buffer, then placed on ice for 10min. Samples were centrifuged at 10,000g for 10 min, and supernatants were transferred into another tube. For detection of total NADP, 50 µL of extracted samples were added into 96-well plates in triplicate. To detect NADPH, 200 µL of extracted samples were aliquoted into microcentrifuge tubes and heat to 60 °C for 30 minutes in a water bath, then samples were cooled on ice. Under these conditions, all NADP will be decomposed leaving NADPH only. 50 µL of NADPH (NADP decomposed) samples were transferred into labeled 96-well plates in triplicate. 100 µL of the Master Reaction Mix (2 µL NADP Cycling Enzyme Mix+98 µL NADP Cycling Buffer) were added to each of the standard and sample wells. After 5 minutes of incubation at room temperature to convert NADP to NADPH, 10 µL of NADPH developer were added into each well. Plates were incubated at room temperature for 1.5 hours. NADPH concentration was measured as the absorbance at 450 nm, the NADP/NADPH ratio = (NADPtotal – NADPH)/ NADPH

Immunostaining

Adipocytes were differentiated on coverslips for 3 weeks and then fixed with Fixation/Permeabilization Solution Kit (BD Cytofix/Cytoperm™). For immunostaining, the fixed cells were blocked with 3% horse serum and incubated with primary antibody overnight at 4°C, followed by incubation with Alexa Fluor–conjugated antibody. The stained cells on coverslips were washed, mounted, and then visualized using a Leica confocal SP5 microscope (Leica Microscopes, Wetzlar, Germany). The images were processed with the Leica (LAS/AF) suite (Wetzlar, Germany).

Sucrose Gradient Fractionation

The membrane fraction was obtained by sucrose gradient fractionation as described previously (H. Wang et al., 2004). In brief, Epidemdemal adipose tissue was washed with ice-cold PBS and homogenized by polytron tissue grinder in 2ml 500 mM sodium carbonate (pH 11.0). Then the lysate was sonicated for 3x40s, wait for 30s between two sonication operations. 2ml of each sample was added to a tube for ultra-centrifugation, then add 2 ml of 90% sucrose in MBS {25mM MES (2-(N-morpholino)ethanesulfonic acid) saline, 150mM NaCl, 2mM EDTA, pH 6.5} and mix by pipetting to reach final sucrose concentration of 45%. 4 ml of 35% sucrose (in MBS, pH 6.5, with 250 mM sodium carbonate) were gently added, then gently add 4 ml of 5% sucrose (in MBS, pH 6.5, with 250 mM sodium carbonate), centrifuge for 39K rpm for 17 hours in an SW41 rotor (Beckman Coulter). Cell fractions were collected from top to bottom, 1 ml for each fraction. Combine fractions 4&5, this is the caveolae enriched fraction. Eleven gradient fractions of 1 ml were collected from the top to the bottom of the centrifuge tube. Fractions 4 and 5 were transferred and combined into a new ultra-centrifuge tube, 4 ml MBS was added with 250mM sodium carbonate, then centrifuge at 40K rpm in type 65 rotor for 1 hour. Supernatants were removed, Pellets were resuspended in 250 ul MBS with 250 mM sodium carbonate, this suspension is considered as the caveolae enriched membrane fraction. Equal volumes of each fraction were analyzed by Western blot.

SDS-PAGE western blot analysis

Mature adipocytes were washed twice with ice-cold PBS and then solubilized in modified radioimmunoprecipitation assay (RIPA) buffer containing 0.25% sodium deoxycholate, 1% NP-40, 1 mM EDTA, 1 mM phenylmethylsulfonyl fluoride, 1 mM sodium orthovanadate, 1 mM NaF, aprotinin (10 μg/ml), leupeptin (10 μg/ml), 150 mM NaCl, and 50 mM Tris-HCl (pH 7.4).

Cell lysates were centrifuged at 14,000 rpm for 15 min; supernatants were collected. After determining protein concentration by the Lowry method (Lowry, Rosebrough, Farr, & Randall, 1951), equal amounts of protein were loaded in each lane of freshly prepared SDS–polyacrylamide gel electrophoresis gel. Separated proteins were transferred onto nitrocellulose membranes, blocked with milk or bovine serum albumin solution in a mixture of TBST (tris-buffered saline and Tween 20) for 1 hour, and then incubated with the primary antibody in blocking solution overnight. Membranes were washed three times with TBS-T, incubated with secondary antibody in blocking solution for 1 hour, and washed again. Proteins were visualized with enhanced chemiluminescence reagent (Thermo Fisher Scientific) and autoradiography films. The intensity of bands was quantified with ImageJ 1.52a (Wayne Rasband, National Institute of Health). The antibodies are listed in Table 3.

RT-qPCR

Total RNA was extracted from cell lysates using Trizol (Invitrogen #15596-018) and reverse-transcribed into cDNA with the SuperScript III First-Strand Synthesis SuperMix (Thermo Fisher # 18080400). The cDNA from each sample was then amplified in LightCycler 480 Instrument II (Roche Life Science, Inc) through (LightCycler 480 SYBR Green I Master, Roche #04887352001). All primers were synthesized by Integrated DNA Technologies, Inc. The primer sequences are listed in Table 4-5.

RNA-Seq and Data Analysis

RNAseq analysis was performed by Novogene Co., LTD (California, USA). Briefly, mRNA was fragmented with fragmentation buffer, and cDNAs were synthesized using them as templates. After agarose gel electrophoresis, suitable fragments were selected for PCR amplification as templates. During QC steps, Agilent BioAnalyzer 2100 and ABI StepOnePlus Real-Time PCR

System were used for quantification and qualification of the sample library. The library was sequenced using HiSeq 2000 sequencer. Bioinformatic analysis was performed by deep analysis of gene expression. Differential gene expression was established with a $\log_{10}(padj)$ threshold of -1.2 using the DESeq2 package (Love, Huber, & Anders, 2014). The KEGG pathways were specifically queried with a gmt file obtained at the KEGG website (https://www.genome.jp/kegg/pathway.html.). Results were obtained with RStudio Version 1.3.1056

Statistical analysis

All data were presented as mean ± S.E.M. Statistical analysis was performed using the Student's t-test to compare two groups. When more than two groups were compared, one-way ANOVA was performed before post-hoc comparison of individual groups using Dunnet's multiple comparison test. Significance was accepted at $P < 0.05$. Statistical analyses were performed using GraphPad Prism version 6.01 for Windows, GraphPad Software. La Jolla, CA.

Author contributions

Conceptualization: MH, LC, SVP, ZX. Investigation: MH, LC, XW, YC, JZ. Methodology: MH, LC, SVP, ZX. Project administration: SVP, ZX. Funding acquisition: YC, SVP, ZX. Resources: YC, SVP, ZX. Supervision: JIS, SVP, ZX. Validation: LC, JIS, SVP, ZX. Visualization: MH, LC, XW. Writing – original draft: MH, LC, SVP, ZX. Writing – review & editing: MH, LC, YC, JIS, SVP, ZX.

Competing interests

Authors declare that they have no competing interests

Supplementary Materials

Primary Antibody	Source	Dilution
NKA α1	Millipore #a6f	1000x
NKA α2	Millipore #07-674	1000x
α-Tubulin	Sigma #T5168	1000x
Cav1	Cell Signaling #3267	1000x
IRβ	Santa Cruz #6093	1000x
IRS1	Sigma I7153	200x
GLUT4	Sigma #G4048	1000x
HIF-1α	Cell Signaling #36169S	1000x
Type I collagen	SounthernBiotech #1310-01	200x
Secondary Antibody	Source	Dilution
HRP-conjugated anti-mouse IgG	Santa Cruz #C1120	1000x
HRP-conjugated anti-rabbit IgG	R&D systems #HAF008	1000x
Alexa Fluor 594 donkey anti-goat	Invitrogen #A-11058	200x
Alexa Fluor 488 goat anti-rabbit	Invitrogen #A-32731	200x

Table 3. **List of antibodies**

Gene	Sequences	
SOX2	Forward	GCTACAGCATGATGCAGGACCA
	Reverse	TCTGCGAGCTGGTCATGGAGTT
SOX17	Forward	TCATGGTGTGGGCTAAGGAC
	Reverse	CACGACTTGCCCAGCATCT
PDGFRA	Forward	GGGCACGCTCTTTACTCCAT
	Reverse	GCTCTGGGAAACTTCTCCTCC
PDGFRB	Forward	GGAGAGGGCAGTAAGGAGGA
	Reverse	ATGGTGTCCTTGCTGCTGAT
PPARγ	Forward	GATACACTGTCTGCAAACATATCACAA
	Reverse	CCACGGAGCTGATCCCAA
FASN	Forward	TCGTGGGCTACAGCATGGT
	Reverse	GCCCTCTGAAGTCGAAGAAGAA
ADIPOQ	Forward	TCTGCCTTCCGCAGTGTAGG
	Reverse	GGTGTGGCTTGGGGATACGA
FABP42	Forward	GCTTTGCCACCAGGAAAGTG
	Reverse	ATGGACGCATTCCACCACCA
COL1A1	Forward	GATTCCCTGGACCTAAAGGTGC
	Reverse	AGCCTCTCCATCTTTGCCAGCA
TGFB1	Forward	CCCAGCATCTGCAAAGCTC
	Reverse	GTCAATGTACAGCTGCCGCA
FN1	Forward	AATGTTGGTGAATCGCAGGT
	Reverse	GGAAAGTGTCCCTATCTCTGATACC
INR	Forward	GCTGGTGTCTGAGCTTCAG
	Reverse	CTCGCACCCTTGAGAAGAACC
IRS1	Forward	GTTTCCAGAAGCAGCCAGAG
	Reverse	ACTCTCTCCACCCAACGTGA
GLUT4	Forward	GCCGGACGTTTGACCAGAT
	Reverse	TGGGTTTCACCTCCTGCTCTA
PFKM	Forward	GGCTGTGGTTCGAGTTGGTA
	Reverse	CCAGGTGGCTTCCTTGATGT
ATP5A1	Forward	AAGACACGCCCAGTTTCTTC
	Reverse	TTTGGGTTCATCTTTCATTGC
HIF1A	Forward	CATAAAGTCTGCAACATGGAAGGT
	Reverse	ATTTGATGGGTGAGGAATGGGTT
IL6	Forward	AGCCCTGAGAAAGGAGACATGTA
	Reverse	TCTGCCAGTGCCTCTTTGCT
CCL2	Forward	CCCCAGTCACCTGCTGTTAT
	Reverse	TGGAATCCTGAACCCACTTC
HPRT1	Forward	TGGACAGGACTGAACGTCTT
	Reverse	TCCAGCAGGTCAGCAAAGAA

Table 4. **List of human primers sequences**

Gene	Sequences	
Tnfa	Forward	GCCTCTTCTCATTCCTGCTTG
	Reverse	CTGATGAGAGGGAGGCCATT
Il6	Forward	CTTCCATCCAGTTGCCTTCTTG
	Reverse	AATTAAGCCTCCGACTTGTGAAG
Col1a1	Forward	CCTCAGGGTATTGCTGGACAAC
	Reverse	CAGAAGGACCTTGTTTGCCAGG
Fn1	Forward	GATGTCCGAACAGCTATTTACCA
	Reverse	CCTTGCGACTTCAGCCACT
18s	Forward	CGAAAGCATTTGCCAAGAAT
	Reverse	AGTCGGCATCGTTTATGGTC

Table 5. **List of mouse primers sequences**
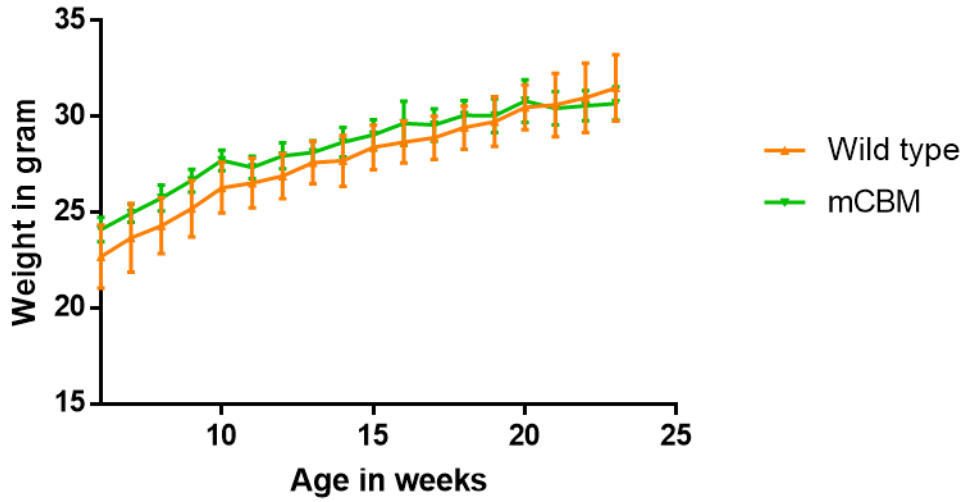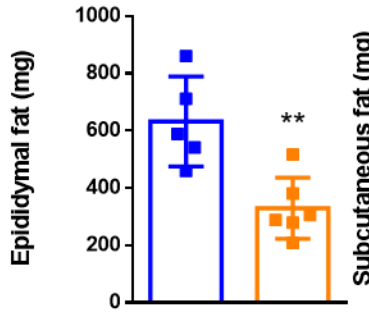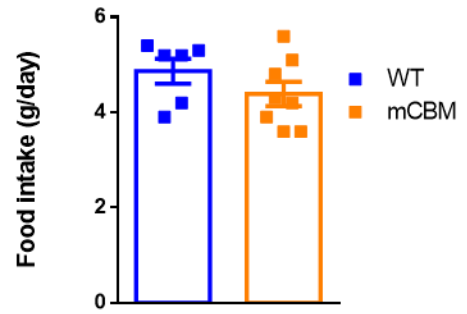
Figure 15. Growth curve of mCBM mice.
A) mCBM heterozygous mice body weight-age growth curve, n=4. B) Organ weight of epididymal/subcutaneous fat and C) daily food intake, n=5-6. Data reported as mean ± SE. *, $P < 0.05$; **, $P < 0.01$ (Unpaired t-test with Welch's correction)
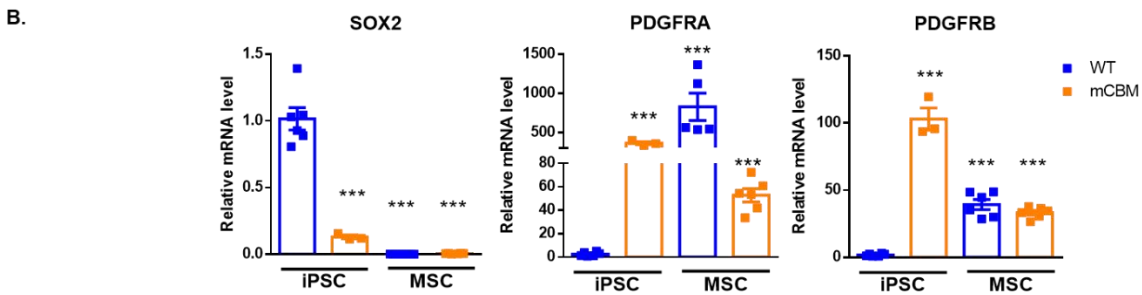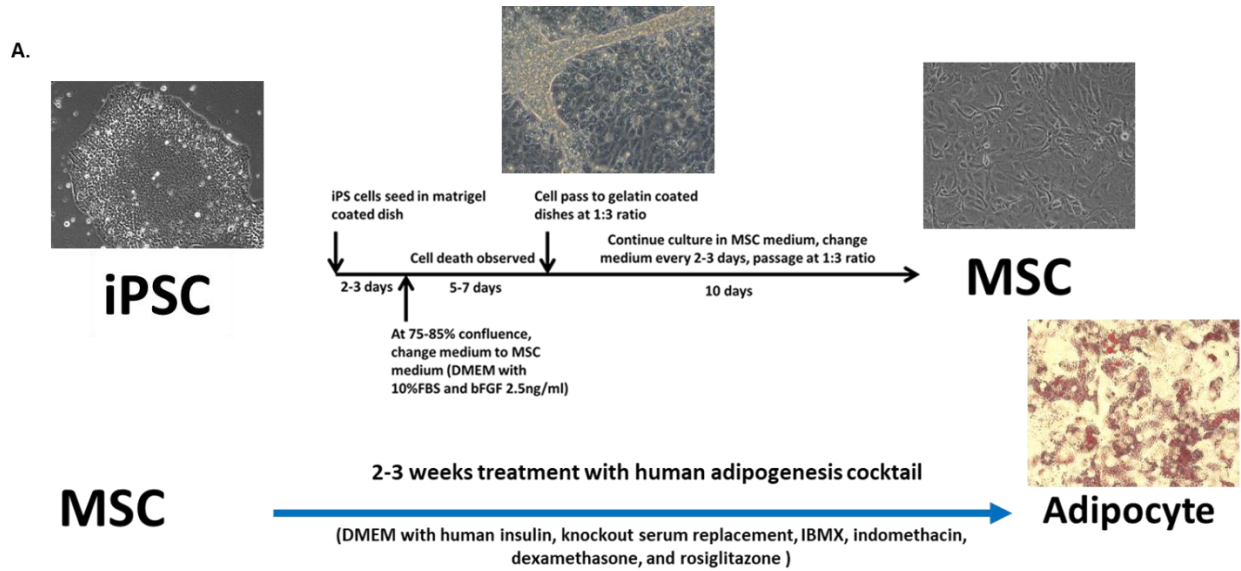
Figure 16. In vitro iPSC-derived Adipogenesis model.
A) in vitro differentiation from human iPSC to adipocyte, MSC: mesenchymal stem cell. B) mRNA levels of SOX2, PDGFRα and, PDGFRβ genes in iPSC-derived MSCs, n=3-6. Data reported as mean ± SE. *, P < 0.05; **, P < 0.01; ***, P < 0.001 (One-way ANOVA with Tukey post hoc test)

A.   RNA sequencing DE genes
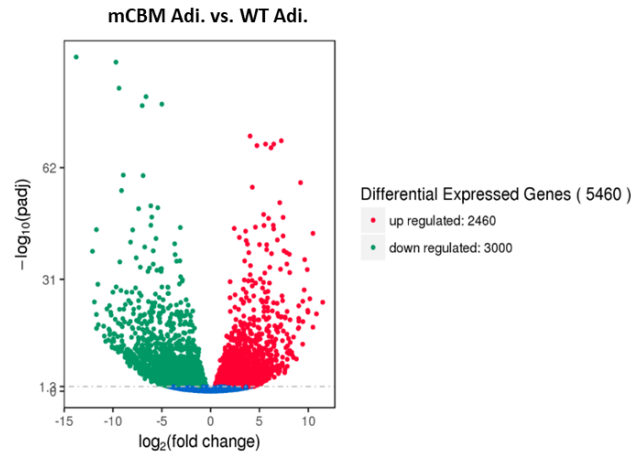
B.

KEGG Pathway Analysis
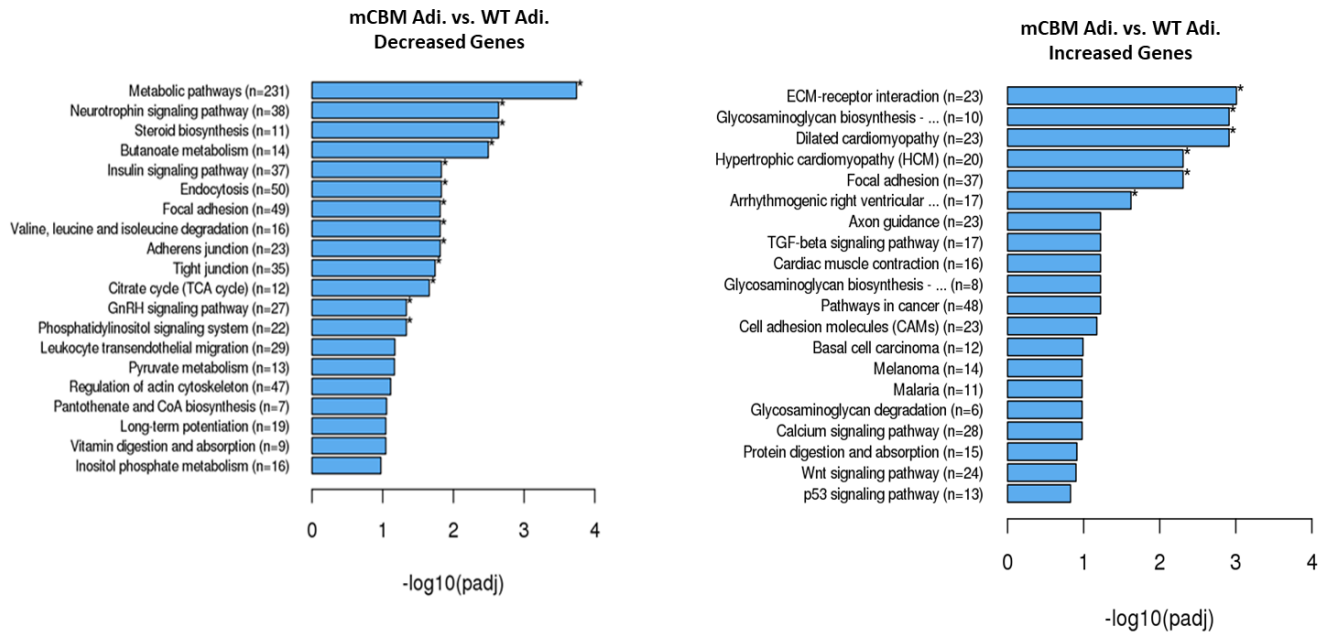
Figure 17. **RNA sequencing and enrichment analysis in iPSC-derived adipocytes.**
A) Comparison of RNA sequencing data of WT and mCBM adipocytes, n=3. Differentially expressed genes were determined using DESeq2 and presented as fold change plotted against adjusted p-value. B) Enriched KEGG pathways of decreased and increased genes. log10 (padj) < 1.2 considered nominally significant

A.

Seahorse XF Cell Glycolysis Test

B.

Glycolysis

Glycolytic Capacity
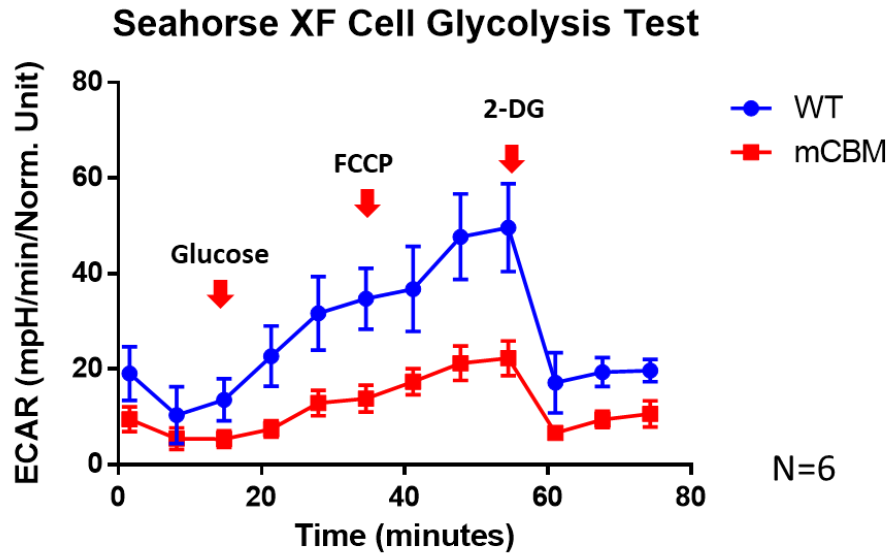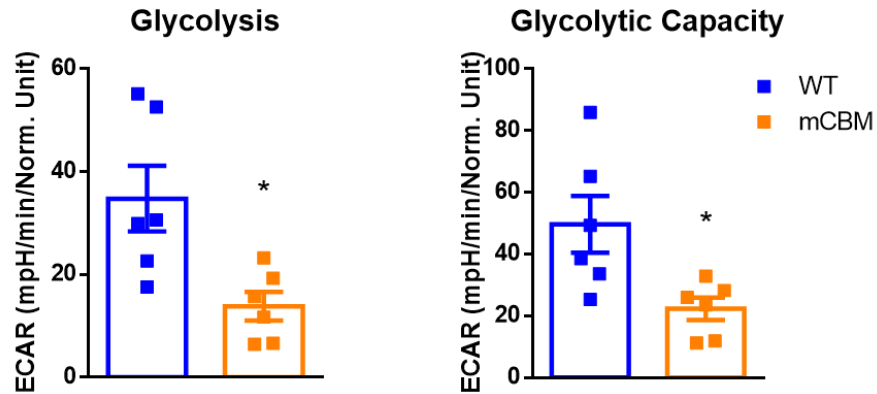
Figure 18. Basal Glycolysis on mCBM adipocytes.
A) Seahorse XF Cell Glycolysis Test in WT and mCBM iPSC-derived adipocytes, insulin was removed from the medium 1 h before the test and was absent during the test. Respectively Glucose, Oligomycin, and 2-DG were added to the cells after the basal ECAR was established (as indicated by arrow). The data are normalized by protein amount as mpH/min/Norm. Unit. B) Quantitation of basal glycolysis and glycolytic capacity of WT and mCBM iPSC-derived adipocytes, calculated from data in Panel A, n=6. Data reported as mean ± SE. *, $P < 0.05$; **, $P < 0.01$; ***, $P < 0.001$ (Unpaired t-test with Welch's correction)
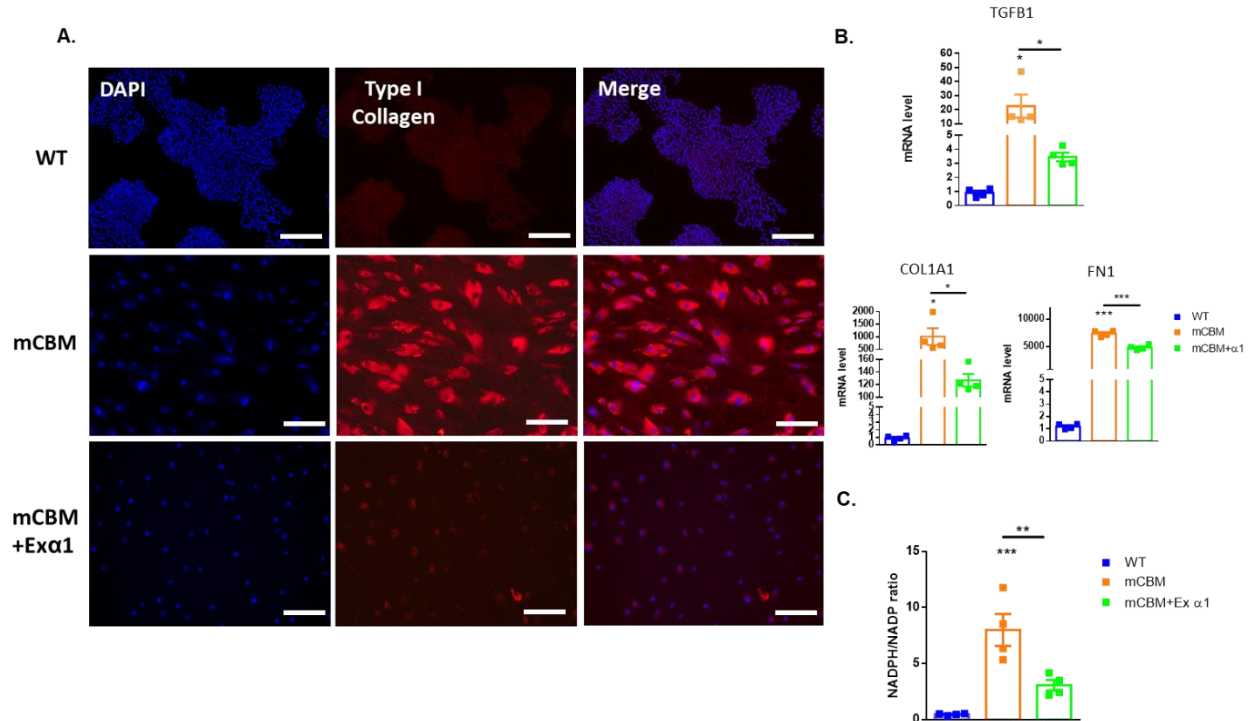
Figure 19. ECM remodeling in mCBM iPSCs.
A) Collagen deposition in WT, mCBM, and mCBM + exogenous mouse α1 (mCBM+Exα1) human iPSCs, representative pictures from n=3 repeats. Scale bar = 500 μm. B) mRNA levels of TGFB1, COL1A1, and FN1 genes in WT, mCBM, and mCBM+Exα1 iPSCs measured by RT-qPCR, n=4. C) NADPH/NADP ratio in iPSCs, n=4. The data were reported as mean ± SE. Data reported as mean ± SE. *, $P < 0.05$; **, $P < 0.01$; ***, $P < 0.001$ (Unpaired t-test with Welch's correction and one-way ANOVA with Tukey post hoc test)
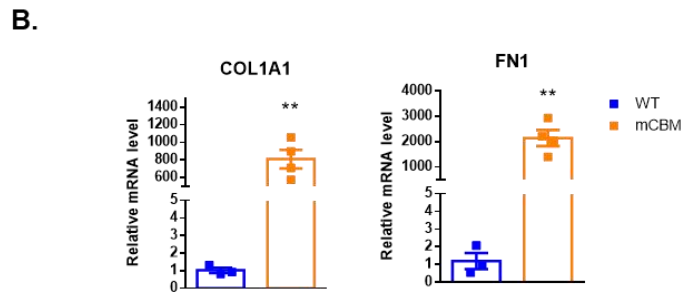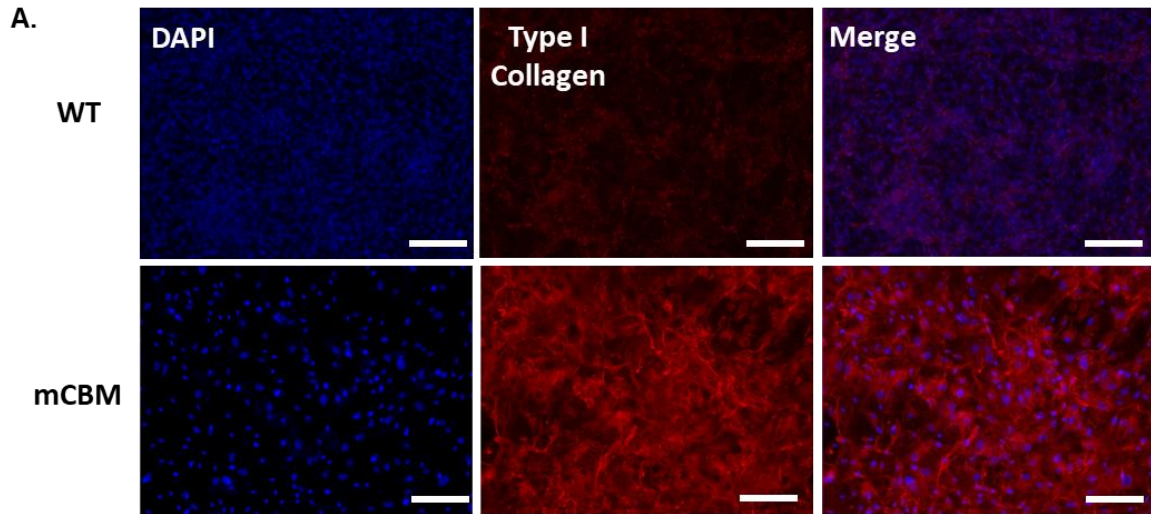
Figure 20. ECM remodeling in mCBM MSCs.
A) Collagen deposition in WT and mCBM MSCs, representative pictures from n=3 repeats.
Scale bar = 500 μm. B) mRNA levels of COL1A1 and FN1 genes in WT and mCBM MSCs
measured by RT-qPCR, n=4. The data were reported as mean ± SE. Data reported as mean ± SE.
*, P < 0.05; **, P < 0.01; ***, P < 0.001 (Unpaired t-test with Welch's correction)
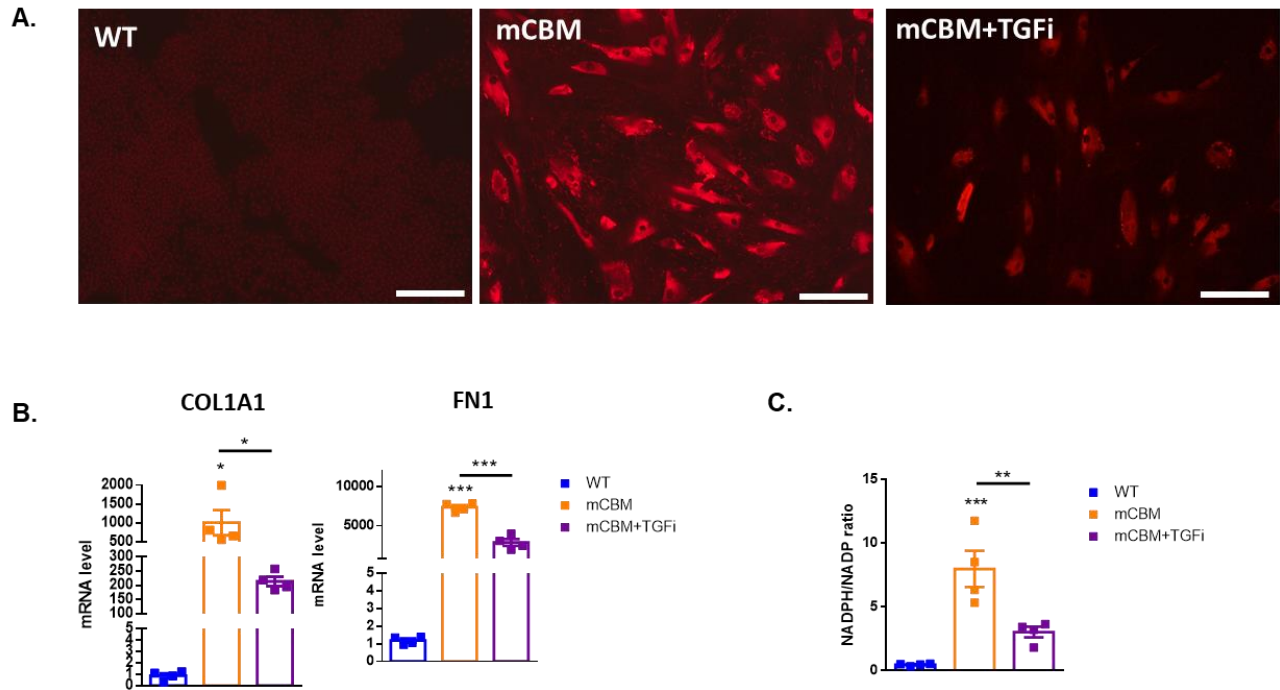
Figure 21. **TGF-β inhibitor (TGFi) SB431542 decreased ECM stiffness and hypoxia in mCBM iPSCs.**
A) WT and mCBM iPSCs were stained with type I collagen (red). Representative pictures are selected from n=4 independent repeats. Scale bar = 500 μm. B) mRNA expression for COL1A1, FN1, and HIF1A genes in WT and mCBM iPSCs measured by RT-qPCR, n=4. C) NADPH/NADP ratio in iPSCs measured by NADPH/NADP quantitation assay, n=4. Data reported as mean ± SE. *, P < 0.05; **, P < 0.01; ***, P < 0.001 (One-way ANOVA with Tukey post hoc test)
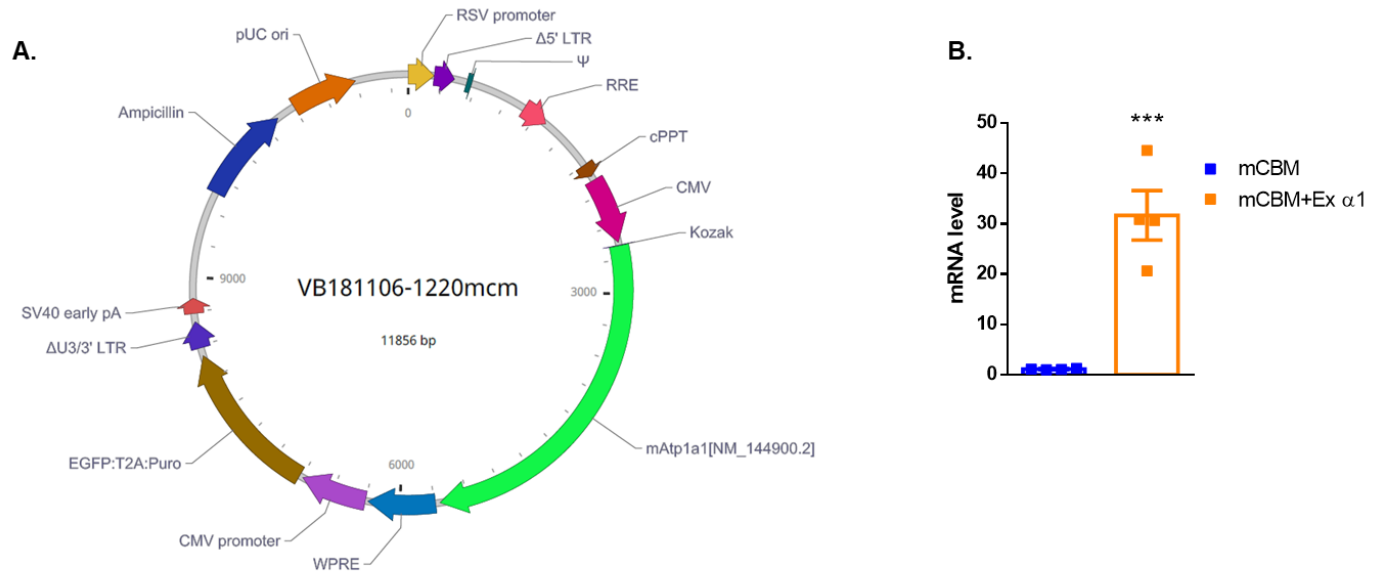
Figure 22. Exogenous mouse NKA α1 rescue of mCBM stem cells.
A) Vector map of the lentivirus expression vector containing a mouse Atp1a1 cDNA. B) mRNA expression of the exogenous mouse Atp1a1 transgene (Ex α1) in iPSCs was measured by RT-qPCR, n=4. The data were reported as mean ± SE. Data reported as mean ± SE. *, $P < 0.05$; **, $P < 0.01$; ***, $P < 0.001$ (Unpaired t-test with Welch's correction)

CHAPTER 3

DISCUSSION AND CONCLUSIONS

CBM is a tool to discriminate the ion transporting and signaling functions of NKA

isoforms.

NKA assembles signalosomes with other signaling partners. Series of studies have shown

that α1 NKA forms a signaling complex with Src, Cav1, EGFR, PI3R, PLC, and PKC (Cai et al.,

2008; Y. Chen et al., 2008; Haas et al., 2000; Z. Li & Xie, 2009; Liang et al., 2006; Mohammadi,

Kometiani, Xie, & Askari, 2001; H. Wang et al., 2004; Yuan et al., 2005). There are also reports

suggesting that α1 NKA is associated with other receptors, such as CD36, TLR4, angiotensin

receptor, and the TGF-β receptor (Y. Chen et al., 2017; Kennedy et al., 2013; Ketchem et al.,

2016; La et al., 2016). In addition to NKA α1 receptor interactions, the α2 NKA may form a

calcium signaling complex with NCX (Golovina, Song, James, Lingrel, & Blaustein, 2003). The

α3 and α4 isoform NKA can also mediate ouabain-induced signal transduction, but the

mechanism is not clear yet (Madan et al., 2017; Pierre et al., 2008). It has been difficult to

distinguish the signaling function and ion-pumping function of NKA using pharmacological

approaches or gene deletion. The conserved N-terminal CBM on NKA was first identified and

studied by Wang et al and Cai et al (Cai et al., 2008; H. Wang et al., 2004). The mCBM cell

shows disrupted NKA/Cav1/Src complex and blunted NKA-mediated signal transduction,

without an effect on the enzymatic function of NKA (Cai et al., 2008; X. Wang et al., 2020).

This mutant that maintains its pumping function but lacks signaling capacity provided an

excellent genetic model to further study the non-ion pumping properties of NKA. Interestingly,

unlike the α1 NKA specific Src binding sites, the CBM is also found in other sequences of NKA

α-isoforms (Lingrel, Van Huysse, O'Brien, Jewell-Motz, & Schultheis, 1994). This may imply

that CBM is important for non-ion pumping properties of other NKA α-isoforms, such as α2 NKA crosstalk with NCX (Blaustein & Hamlyn, 2020), or other signaling partners.

Modulation of NKA α1 and α2 isoform expression during adipogenesis: a metabolic signaling hypothesis.

The first study of mCBM in physiological processes by Wang et al. indicated the essential role of NKA-Cav1 binding in embryonic development (X. Wang et al., 2020). This provided the first line of genetic evidence that the non-ion pumping property of NKA is as critical as its ion pumping function. The present study is the first to provide genetic evidence supporting the role of the non-ion pumping property of α1 NKA in the regulation of adipogenesis. This regulation is independent of a total change in allele NKA enzymatic capacity in both iPSCs and adipocytes (Figure 10). However, in contrast to mCBM models in epithelial cells, the mCBM adipocytes have reduced α1 NKA expression and increased expression of α2 NKA. The increase in α2 NKA may provide compensation for the change of α1, explaining why the total enzymatic activity is constant. It should be noted that in the conditions of this study, we cannot exclude a change of intracellular ion homeostasis of mCBM cells under physiological conditions. Indeed, NKA-mediated signal transduction is critical for NKA internalization as well as in the trafficking of other membrane ion transporters, such as NHE3 (J. Liu et al., 2004; J. Liu et al., 2005; J. Liu & Shapiro, 2007; Yan et al., 2012). A redistribution of NKA is observed in mCBM model cells, mCBM iPSCs, and mCBM adipose tissue (Figure 8) (Cai et al., 2008; X. Wang et al., 2020). Hence, there may be an association between the signaling of NKA and the modulation of cell membrane ion transport that is independent of the loss of total cellular Na/K-ATPase activity.

Skeletal muscle and adipose tissue are the two major organs in whole-body energy metabolism. Interestingly, the major NKA isoform in both of these organs is α2, which is different from most other cells with ubiquitous α1 NKA as their major isoform. The isoform switch from α1 to α2 happens during the adipogenesis and the myogenesis processes (Brodsky, 1990; Orlowski & Lingrel, 1988). During the same period, the cell gains insulin sensitivity through increased expression of insulin signaling pathway components. During the development of these two organs, the reason why α1 NKA needs to be replaced by α2 NKA has long been unknown. An isoform-specific role of α1 Na/K-ATPase signaling is in the regulation of energy metabolism was recently discovered in specifically manipulated cells and mice (Kutz et al., 2021). In addition, we found that the disruption of α1 NKA signaling by mCBM impaired the insulin signaling pathway and reduced the expression of the insulin signaling pathway components (Figure 11). It is, therefore, possible that the NKA isoform-switch is associated with an altered NKA-mediated signaling background (increase in basal levels of pERK, ROS…), which is essential for the gain of insulin sensitivity during adipogenesis and myogenesis.

CBM-dependent scaffolding function during adipogenesis: role of Wnt/β-catenin and Src-mediated signal transduction during adipogenesis

Several studies have documented the specific NKA-Src binding sites in α1 NKA (Banerjee et al., 2018; Lai et al., 2013; Z. Li et al., 2009; Yu et al., 2018). The NKA/Src/ROS axis is the most studied downstream cascade of NKA-mediated signaling and is altered by the mCBM mutation (Cai et al., 2008; X. Wang et al., 2020). Sodhi et al. have shown that inhibition of NKA/Src/ROS signaling by pNaKtide attenuates adipogenesis, possibly due to the inhibition of ROS signaling (Sodhi et al., 2015). Our data show that the ROS scavenger MitoTEMPO failed to rescue the ECM fibrotic remodeling, but partially restored adipogenesis in mCBM iPSC-

derived adipocytes (Figure 12). On the other hand, expression of an exogenous NKA α1 with

intact CBM or TGF-β inhibition did restore ECM, redox homeostasis, and lipid storage in

mCBM iPSCs (Figure 13 and 20). This suggests that the scaffolding function of NKA CBM

regulates redox homeostasis through an ECM/ROS axis during adipogenesis via a mechanism

that is, at least in part, independent from the NKA/Src/ROS mechanism. Similarly, the mCBM-

induced defects in mouse embryogenesis observed in the recent study by Wang et al (X. Wang et

al., 2020) did not appear to be caused by the disruption of NKA/Src. Rather, Wang et al showed

that the disruption of NKA CBM-dependent control of Wnt/β-catenin played a critical role.

Consistent with a CBM-dependent mechanism that is not functionally mediated by Src, we have

obtained preliminary indications that pNaKtide treatment does not restore lipid storage in the

mCBM iPSC-derived adipocytes (unpublished observations).

Given the reported role of the NKA CBM/Wnt/β-catenin axis during embryonic

development, the possible impact of the Wnt signaling pathway (which is dominant in the

regulation of stem cell linage commitment) should also be considered in the context of the

present study. Indeed, the canonical Wnt signaling through the Wnt/β-catenin complex inhibits

adipogenesis in MSCs (Steger et al., 2010). Non-canonical Wnt ligands signal through β-catenin-

independent pathways and can promote adipogenesis by inhibiting canonical Wnt (Seo et al.,

2009). The study by Wang et al. (X. Wang et al., 2020) showed that the disrupted Wnt/β-catenin

complex in mCBM cells leads to dramatically reduced canonical Wnt signaling pathway activity.

Hence, inhibition of canonical Wnt signaling upon CBM loss of function may have facilitated

cell linage commitment towards adipocyte. This is consistent with the increase in adipocyte

progenitor marker gene expression (PDGFRA and PDGFRB) that we observed in mCBM iPSC

(Figure 16). Importantly, beyond cell linage commitment, mesenchymal adipogenesis is

independent of the Wnt/β-catenin signal pathway, and therefore unlikely to explain the defect in lipid storage. On the other hand, the TGF-β signaling pathway regulates the balance of fibroblasts and adipocytes in adipose tissue (Clouthier, Comerford, & Hammer, 1997; Song et al., 2000; Sun et al., 2013; W. Wang et al., 2019). Increased fibrogenesis results in adipose tissue remodeling, impaired adipogenesis, and adipose metabolic dysfunction, which is observed in obesity development (Choe et al., 2016; Sun et al., 2013).

Taken together, these support a model whereby the loss of CBM in iPSC may disrupt Wnt, TGF-β, and Src-dependent non-ion pumping NKA functions, which regulate different phases of adipogenesis through downstream signaling pathways. Although this remains to be explicitly tested, it supports the role of NKA as an important signal integrator in adipogenesis and suggests a therapeutic potential.

α1 NKA as a novel target for developing therapeutics of obesity and related metabolic disorders.

MAPK pathway and ROS have been reported to regulate energy metabolism in adipocytes (Bost, Aouadi, Caron, & Binetruy, 2005; de Villiers et al., 2018). Liu, J et al. and Yan, Y et al. have shown that increased ROS results in NKA oxidation, which inhibits its activity and further promotes NKA degradation through endosomal/lysosomal proteolytic pathways (J. Liu, Kennedy, Yan, & Shapiro, 2012; Yan et al., 2013). Decreases in functional NKA α1 have been reported in adipose tissue biopsies from obese patients (Srikanthan, Feyh, Visweshwar, Shapiro, & Sodhi, 2016), which may be due to the elevated oxidative stress caused by excessive energy accumulation. Reduced functional NKA α1 may lead to dysregulation of the NKA/Src/ROS amplification loop, further increasing oxidative stress, and ultimately facilitating adipose dysfunction during obesity development. Consistent with this hypothesis, a series of

81

studies from Sodhi, K have indicated the therapeutic effect of pNaKtide in obesity and related complications (J. Liu et al., 2016; Sodhi et al., 2015; Sodhi et al., 2017). This validated α1 NKA, and the downstream NKA/Src/ROS amplification loop, as a potential therapeutic target of obesity. However, the downregulation of NKA during obesity development may also impair its scaffolding function as a signal integrator, which is critical for adipose tissue remodeling and metabolic function (Figure 14). During obesity development, adipose tissue fibrosis contributes to chronic inflammation and metabolic dysfunction (Choe et al., 2016; Sun et al., 2013). Both NKA/Src/ ROS and NKA/TGF-β/ECM/ROS axis may therefore be involved in this process. Interestingly, the loss of progenitor cell stemness is another symptom in obese patients and results in obesity-related complications in multiple organs (Rodrigues et al., 2015). The great potential of MSC-based therapy in treating diabetic complications has been reported (Basmaeil et al., 2020; Davey, Patil, O'Loughlin, & O'Brien, 2014; Khan et al., 2013). However, the adipose-derived MSCs from obese patients show reduced stem cell function and differentiation ability (Pachon-Pena et al., 2016). Treatment with ROS scavenger in obese stem cells improved differentiation ability and therapeutic effect (Gu et al., 2015), suggesting that redox homeostasis is key to restoring the function of obese stem cells.

REFERENCES

Akimoto, T., Ushida, T., Miyaki, S., Akaogi, H., Tsuchiya, K., Yan, Z., . . . Tateishi, T. (2005). Mechanical stretch inhibits myoblast-to-adipocyte differentiation through Wnt signaling. *Biochem Biophys Res Commun, 329*(1), 381-385. doi: 10.1016/j.bbrc.2005.01.136

Albers, R. W., Koval, G. J., & Siegel. (1968). Studies on the interaction of ouabain and other cardio-active steroids with sodium-potassium-activated adenosine triphosphatase. *Mol Pharmacol, 4*(4), 324-336.

Anderson, R. G. (1998). The caveolae membrane system. *Annu Rev Biochem, 67*, 199-225. doi: 10.1146/annurev.biochem.67.1.199

Aoki, S., Thomas, A., Decaffmeyer, M., Brasseur, R., & Epand, R. M. (2010). The role of proline in the membrane re-entrant helix of Cav1. *J Biol Chem, 285*(43), 33371-33380. doi: 10.1074/jbc.M110.153569

Bagrov, A. Y., Roukoyatkina, N. I., Pinaev, A. G., Dmitrieva, R. I., & Fedorova, O. V. (1995). Effects of two endogenous Na+,K(+)-ATPase inhibitors, marinobufagenin and ouabain, on isolated rat aorta. *Eur J Pharmacol, 274*(1-3), 151-158. doi: 10.1016/0014-2999(94)00735-p

Bagrov, A. Y., Shapiro, J. I., & Fedorova, O. V. (2009). Endogenous cardiotonic steroids: physiology, pharmacology, and novel therapeutic targets. *Pharmacol Rev, 61*(1), 9-38. doi: 10.1124/pr.108.000711

Baker, P. F., Blaustein, M. P., Hodgkin, A. L., & Steinhardt, R. A. (1969). The influence of calcium on sodium efflux in squid axons. *J Physiol, 200*(2), 431-458. doi: 10.1113/jphysiol.1969.sp008702

Banerjee, M., Cui, X., Li, Z., Yu, H., Cai, L., Jia, X., . . . Xie, Z. (2018). Na/K-ATPase Y260 Phosphorylation-mediated Src Regulation in Control of Aerobic Glycolysis and Tumor Growth. *Sci Rep, 8*(1), 12322. doi: 10.1038/s41598-018-29995-2

Banerjee, M., Duan, Q., & Xie, Z. (2015). SH2 Ligand-Like Effects of Second Cytosolic Domain of Na/K-ATPase alpha1 Subunit on Src Kinase. *PLoS One, 10*(11), e0142119. doi: 10.1371/journal.pone.0142119

Basmaeil, Y., Rashid, M. A., Khatlani, T., AlShabibi, M., Bahattab, E., Abdullah, M. L., . . . Abumaree, M. (2020). Preconditioning of Human Decidua Basalis Mesenchymal

83

Stem/Stromal Cells with Glucose Increased Their Engraftment and Anti-diabetic Properties. *Tissue Eng Regen Med, 17*(2), 209-222. doi: 10.1007/s13770-020-00239-7

Bielawski, K., Winnicka, K., & Bielawska, A. (2006). Inhibition of DNA topoisomerases I and II, and growth inhibition of breast cancer MCF-7 cells by ouabain, digoxin and proscillaridin A. *Biol Pharm Bull, 29*(7), 1493-1497. doi: 10.1248/bpb.29.1493

Bielczyk-Maczynska, E. (2019). White Adipocyte Plasticity in Physiology and Disease. *Cells, 8*(12). doi: 10.3390/cells8121507

Blanco, G., Melton, R. J., Sanchez, G., & Mercer, R. W. (1999). Functional characterization of a testes-specific alpha-subunit isoform of the sodium/potassium adenosinetriphosphatase. *Biochemistry, 38*(41), 13661-13669. doi: 10.1021/bi991207b

Blanco, G., & Mercer, R. W. (1998). Isozymes of the Na-K-ATPase: heterogeneity in structure, diversity in function. *Am J Physiol, 275*(5), F633-650. doi: 10.1152/ajprenal.1998.275.5.F633

Blaustein, M. P. (2018). The pump, the exchanger, and the holy spirit: origins and 40-year evolution of ideas about the ouabain-Na(+) pump endocrine system. *Am J Physiol Cell Physiol, 314*(1), C3-C26. doi: 10.1152/ajpcell.00196.2017

Blaustein, M. P., & Hamlyn, J. M. (2020). Ouabain, endogenous ouabain and ouabain-like factors: The Na(+) pump/ouabain receptor, its linkage to NCX, and its myriad functions. *Cell Calcium, 86*, 102159. doi: 10.1016/j.ceca.2020.102159

Bortell, R., Owen, T. A., Ignotz, R., Stein, G. S., & Stein, J. L. (1994). TGF beta 1 prevents the down-regulation of type I procollagen, fibronectin, and TGF beta 1 gene expression associated with 3T3-L1 pre-adipocyte differentiation. *J Cell Biochem, 54*(2), 256-263. doi: 10.1002/jcb.240540214

Bost, F., Aouadi, M., Caron, L., & Binetruy, B. (2005). The role of MAPKs in adipocyte differentiation and obesity. *Biochimie, 87*(1), 51-56. doi: 10.1016/j.biochi.2004.10.018

Briones, A. M., Xavier, F. E., Arribas, S. M., Gonzalez, M. C., Rossoni, L. V., Alonso, M. J., & Salaices, M. (2006). Alterations in structure and mechanics of resistance arteries from ouabain-induced hypertensive rats. *Am J Physiol Heart Circ Physiol, 291*(1), H193-201. doi: 10.1152/ajpheart.00802.2005

Brodsky, J. L. (1990). Characterization of the (Na+ (+) K+)-ATPase from 3T3-F442A fibroblasts and adipocytes. Isozymes and insulin sensitivity. *J Biol Chem, 265*(18), 10458-10465.

Brown, R. J., Araujo-Vilar, D., Cheung, P. T., Dunger, D., Garg, A., Jack, M., . . . Yorifuji, T. (2016). The Diagnosis and Management of Lipodystrophy Syndromes: A Multi-Society Practice Guideline. *J Clin Endocrinol Metab, 101*(12), 4500-4511. doi: 10.1210/jc.2016-2466

Burns, E. L., Nicholas, R. A., & Price, E. M. (1996). Random mutagenesis of the sheep Na,K-ATPase alpha1 subunit generating the ouabain-resistant mutant L793P. *J Biol Chem, 271*(27), 15879-15883. doi: 10.1074/jbc.271.27.15879

Cai, T., Wang, H., Chen, Y., Liu, L., Gunning, W. T., Quintas, L. E., & Xie, Z. J. (2008). Regulation of Cav1 membrane trafficking by the Na/K-ATPase. *J Cell Biol, 182*(6), 1153-1169. doi: 10.1083/jcb.200712022

Capozza, F., Combs, T. P., Cohen, A. W., Cho, Y. R., Park, S. Y., Schubert, W., . . . Lisanti, M. P. (2005). Cav-3 knockout mice show increased adiposity and whole body insulin resistance, with ligand-induced insulin receptor instability in skeletal muscle. *Am J Physiol Cell Physiol, 288*(6), C1317-1331. doi: 10.1152/ajpcell.00489.2004

Carthy, J. M. (2018). TGFbeta signaling and the control of myofibroblast differentiation: Implications for chronic inflammatory disorders. *J Cell Physiol, 233*(1), 98-106. doi: 10.1002/jcp.25879

Castello-Cros, R., Whitaker-Menezes, D., Molchansky, A., Purkins, G., Soslowsky, L. J., Beason, D. P., . . . Lisanti, M. P. (2011). Scleroderma-like properties of skin from Cav1-deficient mice: implications for new treatment strategies in patients with fibrosis and systemic sclerosis. *Cell Cycle, 10*(13), 2140-2150. doi: 10.4161/cc.10.13.16227

Catalan, V., Gomez-Ambrosi, J., Rodriguez, A., Silva, C., Rotellar, F., Gil, M. J., . . . Fruhbeck, G. (2008). Expression of Cav1 in human adipose tissue is upregulated in obesity and obesity-associated type 2 diabetes mellitus and related to inflammation. *Clin Endocrinol (Oxf), 68*(2), 213-219. doi: 10.1111/j.1365-2265.2007.03021.x

Chavey, C., Mari, B., Monthouel, M. N., Bonnafous, S., Anglard, P., Van Obberghen, E., & Tartare-Deckert, S. (2003). Matrix metalloproteinases are differentially expressed in adipose tissue during obesity and modulate adipocyte differentiation. *J Biol Chem, 278*(14), 11888-11896. doi: 10.1074/jbc.M209196200

85

Chen, K. K., & Kovarikova, A. (1967). Pharmacology and toxicology of toad venom. *J Pharm Sci, 56*(12), 1535-1541. doi: 10.1002/jps.2600561202

Chen, Y., Cai, T., Wang, H., Li, Z., Loreaux, E., Lingrel, J. B., & Xie, Z. (2009). Regulation of intracellular cholesterol distribution by Na/K-ATPase. *J Biol Chem, 284*(22), 14881-14890. doi: 10.1074/jbc.M109.003574

Chen, Y., Cai, T., Yang, C., Turner, D. A., Giovannucci, D. R., & Xie, Z. (2008). Regulation of inositol 1,4,5-trisphosphate receptor-mediated calcium release by the Na/K-ATPase in cultured renal epithelial cells. *J Biol Chem, 283*(2), 1128-1136. doi: 10.1074/jbc.M708025200

Chen, Y., Huang, W., Yang, M., Xin, G., Cui, W., Xie, Z., & Silverstein, R. L. (2017). Cardiotonic Steroids Stimulate Macrophage Inflammatory Responses Through a Pathway Involving CD36, TLR4, and Na/K-ATPase. *Arterioscler Thromb Vasc Biol, 37*(8), 1462-1469. doi: 10.1161/ATVBAHA.117.309444

Chen, Y., Yang, M., Huang, W., Chen, W., Zhao, Y., Schulte, M. L., . . . Silverstein, R. L. (2019). Mitochondrial Metabolic Reprogramming by CD36 Signaling Drives Macrophage Inflammatory Responses. *Circ Res, 125*(12), 1087-1102. doi: 10.1161/CIRCRESAHA.119.315833

Chenn, A. (2008). Wnt/beta-catenin signaling in cerebral cortical development. *Organogenesis, 4*(2), 76-80. doi: 10.4161/org.4.2.5852

Choe, S. S., Huh, J. Y., Hwang, I. J., Kim, J. I., & Kim, J. B. (2016). Adipose Tissue Remodeling: Its Role in Energy Metabolism and Metabolic Disorders. *Front Endocrinol (Lausanne), 7*, 30. doi: 10.3389/fendo.2016.00030

Chow, D. C., & Forte, J. G. (1995). Functional significance of the beta-subunit for heterodimeric P-type ATPases. *J Exp Biol, 198*(Pt 1), 1-17.

Choy, L., Skillington, J., & Derynck, R. (2000). Roles of autocrine TGF-beta receptor and Smad signaling in adipocyte differentiation. *J Cell Biol, 149*(3), 667-682. doi: 10.1083/jcb.149.3.667

Chun, T. H., Hotary, K. B., Sabeh, F., Saltiel, A. R., Allen, E. D., & Weiss, S. J. (2006). A pericellular collagenase directs the 3-dimensional development of white adipose tissue. *Cell, 125*(3), 577-591. doi: 10.1016/j.cell.2006.02.050

Cinti, S., Mitchell, G., Barbatelli, G., Murano, I., Ceresi, E., Faloia, E., . . . Obin, M. S. (2005). Adipocyte death defines macrophage localization and function in adipose tissue of obese mice and humans. *J Lipid Res, 46*(11), 2347-2355. doi: 10.1194/jlr.M500294-JLR200

Clarkson, E. M., & Maizels, M. (1954). Respiration, glycolysis and sodium transport in chicken erythrocytes. *J Physiol, 124*(2), 19-20P.

Clouthier, D. E., Comerford, S. A., & Hammer, R. E. (1997). Hepatic fibrosis, glomerulosclerosis, and a lipodystrophy-like syndrome in PEPCK-TGF-beta1 transgenic mice. *J Clin Invest, 100*(11), 2697-2713. doi: 10.1172/JCI119815

Cohen, A. W., Combs, T. P., Scherer, P. E., & Lisanti, M. P. (2003). Role of caveolin and caveolae in insulin signaling and diabetes. *Am J Physiol Endocrinol Metab, 285*(6), E1151-1160. doi: 10.1152/ajpendo.00324.2003

Cohen, A. W., Razani, B., Wang, X. B., Combs, T. P., Williams, T. M., Scherer, P. E., & Lisanti, M. P. (2003). Cav1-deficient mice show insulin resistance and defective insulin receptor protein expression in adipose tissue. *Am J Physiol Cell Physiol, 285*(1), C222-235. doi: 10.1152/ajpcell.00006.2003

Cohen, A. W., Schubert, W., Brasaemle, D. L., Scherer, P. E., & Lisanti, M. P. (2005). Cav1 expression is essential for proper nonshivering thermogenesis in brown adipose tissue. *Diabetes, 54*(3), 679-686. doi: 10.2337/diabetes.54.3.679

Cornelius, F., & Skou, J. C. (1988). The sided action of Na+ on reconstituted shark Na+/K+-ATPase engaged in Na+-Na+ exchange accompanied by ATP hydrolysis. II. Transmembrane allosteric effects on Na+ affinity. *Biochim Biophys Acta, 944*(2), 223-232. doi: 10.1016/0005-2736(88)90435-x

Cristancho, A. G., & Lazar, M. A. (2011). Forming functional fat: a growing understanding of adipocyte differentiation. *Nat Rev Mol Cell Biol, 12*(11), 722-734. doi: 10.1038/nrm3198

Croissandeau, G., Chretien, M., & Mbikay, M. (2002). Involvement of matrix metalloproteinases in the adipose conversion of 3T3-L1 preadipocytes. *Biochem J, 364*(Pt 3), 739-746. doi: 10.1042/BJ20011158

Croyle, M. L., Woo, A. L., & Lingrel, J. B. (1997). Extensive random mutagenesis analysis of the Na+/K+-ATPase alpha subunit identifies known and previously unidentified amino acid residues that alter ouabain sensitivity--implications for ouabain binding. *Eur J Biochem, 248*(2), 488-495. doi: 10.1111/j.1432-1033.1997.00488.x

Cuff, J. M., & Lichtman, M. A. (1975). The effects of ouabain on the cell mitotic cycle of mouse lymphoblasts. *J Cell Physiol, 85*(2 Pt 1), 227-234. doi: 10.1002/jcp.1040850209

Daly, S. E., Lane, L. K., & Blostein, R. (1996). Structure/function analysis of the amino-terminal region of the 1 and 2 subunits of Na,K-ATPase. *J Biol Chem, 271*(39), 23683-23689. doi: 10.1074/jbc.271.39.23683

Davey, G. C., Patil, S. B., O'Loughlin, A., & O'Brien, T. (2014). Mesenchymal stem cell-based treatment for microvascular and secondary complications of diabetes mellitus. *Front Endocrinol (Lausanne), 5*, 86. doi: 10.3389/fendo.2014.00086

de Villiers, D., Potgieter, M., Ambele, M. A., Adam, L., Durandt, C., & Pepper, M. S. (2018). The Role of Reactive Oxygen Species in Adipogenic Differentiation. *Adv Exp Med Biol, 1083*, 125-144. doi: 10.1007/5584_2017_119

De Wardener, H. E., Mills, I. H., Clapham, W. F., & Hayter, C. J. (1961). Studies on the efferent mechanism of the sodium diuresis which follows the administration of intravenous saline in the dog. *Clin Sci, 21*, 249-258.

Dean, R. B. 1941. Theories of Electrolyte Equilibrium in Muscle. *Biol. Symposia, 3*, 331–348

Del Galdo, F., Sotgia, F., de Almeida, C. J., Jasmin, J. F., Musick, M., Lisanti, M. P., & Jimenez, S. A. (2008). Decreased expression of caveolin 1 in patients with systemic sclerosis: crucial role in the pathogenesis of tissue fibrosis. *Arthritis Rheum, 58*(9), 2854-2865. doi: 10.1002/art.23791

Dike, L. E., & Farmer, S. R. (1988). Cell adhesion induces expression of growth-associated genes in suspension-arrested fibroblasts. *Proc Natl Acad Sci U S A, 85*(18), 6792-6796. doi: 10.1073/pnas.85.18.6792

Dmitrieva, R. I., Bagrov, A. Y., Lalli, E., Sassone-Corsi, P., Stocco, D. M., & Doris, P. A. (2000). Mammalian bufadienolide is synthesized from cholesterol in the adrenal cortex by a pathway that Is independent of cholesterol side-chain cleavage. *Hypertension, 36*(3), 442-448. doi: 10.1161/01.hyp.36.3.442

Dmitrieva, R. I., & Doris, P. A. (2003). Ouabain is a potent promoter of growth and activator of ERK1/2 in ouabain-resistant rat renal epithelial cells. *J Biol Chem, 278*(30), 28160-28166. doi: 10.1074/jbc.M303768200

Dmitrieva, R. I., Lalli, E., & Doris, P. A. (2005). Regulation of adrenocortical cardiotonic steroid production by dopamine and PKA signaling. *Front Biosci, 10*, 2489-2495. doi: 10.2741/1713

Dostanic, I., Schultz Jel, J., Lorenz, J. N., & Lingrel, J. B. (2004). The alpha 1 isoform of Na,K-ATPase regulates cardiac contractility and functionally interacts and co-localizes with the Na/Ca exchanger in heart. *J Biol Chem, 279*(52), 54053-54061. doi: 10.1074/jbc.M410737200

Drab, M., Verkade, P., Elger, M., Kasper, M., Lohn, M., Lauterbach, B., . . . Kurzchalia, T. V. (2001). Loss of caveolae, vascular dysfunction, and pulmonary defects in Cav1 gene-disrupted mice. *Science, 293*(5539), 2449-2452. doi: 10.1126/science.1062688

El-Okdi, N., Smaili, S., Raju, V., Shidyak, A., Gupta, S., Fedorova, L., . . . Shapiro, J. I. (2008). Effects of cardiotonic steroids on dermal collagen synthesis and wound healing. *J Appl Physiol (1985), 105*(1), 30-36. doi: 10.1152/japplphysiol.00119.2008

Elkareh, J., Kennedy, D. J., Yashaswi, B., Vetteth, S., Shidyak, A., Kim, E. G., . . . Shapiro, J. I. (2007). Marinobufagenin stimulates fibroblast collagen production and causes fibrosis in experimental uremic cardiomyopathy. *Hypertension, 49*(1), 215-224. doi: 10.1161/01.HYP.0000252409.36927.05

Elkareh, J., Periyasamy, S. M., Shidyak, A., Vetteth, S., Schroeder, J., Raju, V., . . . Shapiro, J. I. (2009). Marinobufagenin induces increases in procollagen expression in a process involving protein kinase C and Fli-1: implications for uremic cardiomyopathy. *Am J Physiol Renal Physiol, 296*(5), F1219-1226. doi: 10.1152/ajprenal.90710.2008

Engler, A. J., Sen, S., Sweeney, H. L., & Discher, D. E. (2006). Matrix elasticity directs stem cell lineage specification. *Cell, 126*(4), 677-689. doi: 10.1016/j.cell.2006.06.044

Fan, X., Xie, J., & Tian, J. (2017). Reducing Cardiac Fibrosis: Na/K-ATPase Signaling Complex as a Novel Target. *Cardiovasc Pharm Open Access, 6*(1). doi: 10.4172/2329-6607.1000204

Fedorova, L. V., Raju, V., El-Okdi, N., Shidyak, A., Kennedy, D. J., Vetteth, S., . . . Malhotra, D. (2009). The cardiotonic steroid hormone marinobufagenin induces renal fibrosis: implication of epithelial-to-mesenchymal transition. *Am J Physiol Renal Physiol, 296*(4), F922-934. doi: 10.1152/ajprenal.90605.2008

Fedorova, O. V., Kolodkin, N. I., Agalakova, N. I., Lakatta, E. G., & Bagrov, A. Y. (2001). Marinobufagenin, an endogenous alpha-1 sodium pump ligand, in hypertensive Dahl salt-sensitive rats. *Hypertension, 37*(2 Pt 2), 462-466. doi: 10.1161/01.hyp.37.2.462

Fedorova, O. V., Lakatta, E. G., & Bagrov, A. Y. (2000). Endogenous Na,K pump ligands are differentially regulated during acute NaCl loading of Dahl rats. *Circulation, 102*(24), 3009-3014. doi: 10.1161/01.cir.102.24.3009

Ferrandi, M., Molinari, I., Barassi, P., Minotti, E., Bianchi, G., & Ferrari, P. (2004). Organ hypertrophic signaling within caveolae membrane subdomains triggered by ouabain and antagonized by PST 2238. *J Biol Chem, 279*(32), 33306-33314. doi: 10.1074/jbc.M402187200

Fra, A. M., Williamson, E., Simons, K., & Parton, R. G. (1995). De novo formation of caveolae in lymphocytes by expression of VIP21-caveolin. *Proc Natl Acad Sci U S A, 92*(19), 8655-8659. doi: 10.1073/pnas.92.19.8655

Fretz, J. A., Nelson, T., Xi, Y., Adams, D. J., Rosen, C. J., & Horowitz, M. C. (2010). Altered metabolism and lipodystrophy in the early B-cell factor 1-deficient mouse. *Endocrinology, 151*(4), 1611-1621. doi: 10.1210/en.2009-0987

Fujimoto, T., Miyawaki, A., & Mikoshiba, K. (1995). Inositol 1,4,5-trisphosphate receptor-like protein in plasmalemmal caveolae is linked to actin filaments. *J Cell Sci, 108 (Pt 1)*, 7-15.

Gadsby, D. C., Bezanilla, F., Rakowski, R. F., De Weer, P., & Holmgren, M. (2012). The dynamic relationships between the three events that release individual Na(+) ions from the Na(+)/K(+)-ATPase. *Nat Commun, 3*, 669. doi: 10.1038/ncomms1673

Galbiati, F., Razani, B., & Lisanti, M. P. (2001). Caveolae and Cav-3 in muscular dystrophy. *Trends Mol Med, 7*(10), 435-441. doi: 10.1016/s1471-4914(01)02105-0

Gardos, G. (1954). [Accumulation of potassium ions by human blood corpuscles]. *Acta Physiol Acad Sci Hung, 6*(2-3), 191-199.

Garg, A., & Agarwal, A. K. (2008). Cav1: a new locus for human lipodystrophy. *J Clin Endocrinol Metab, 93*(4), 1183-1185. doi: 10.1210/jc.2008-0426

Garg, A., Kircher, M., Del Campo, M., Amato, R. S., Agarwal, A. K., & University of Washington Center for Mendelian, G. (2015). Whole exome sequencing identifies de novo heterozygous CAV1 mutations associated with a novel neonatal onset lipodystrophy syndrome. *Am J Med Genet A, 167A*(8), 1796-1806. doi: 10.1002/ajmg.a.37115

Geering, K. (2005). Function of FXYD proteins, regulators of Na, K-ATPase. *J Bioenerg Biomembr, 37*(6), 387-392. doi: 10.1007/s10863-005-9476-x

Golden, W. C., & Martin, L. J. (2006). Low-dose ouabain protects against excitotoxic apoptosis and up-regulates nuclear Bcl-2 in vivo. *Neuroscience, 137*(1), 133-144. doi: 10.1016/j.neuroscience.2005.10.004

Golovina, V. A., Song, H., James, P. F., Lingrel, J. B., & Blaustein, M. P. (2003). Na+ pump alpha 2-subunit expression modulates Ca2+ signaling. *Am J Physiol Cell Physiol, 284*(2), C475-486. doi: 10.1152/ajpcell.00383.2002

Gottlieb-Abraham, E., Shvartsman, D. E., Donaldson, J. C., Ehrlich, M., Gutman, O., Martin, G. S., & Henis, Y. I. (2013). Src-mediated Cav1 phosphorylation affects the targeting of active Src to specific membrane sites. *Mol Biol Cell, 24*(24), 3881-3895. doi: 10.1091/mbc.E13-03-0163

Gregoire, F. M., Smas, C. M., & Sul, H. S. (1998). Understanding adipocyte differentiation. *Physiol Rev, 78*(3), 783-809. doi: 10.1152/physrev.1998.78.3.783

Grigorova, Y. N., Wei, W., Petrashevskaya, N., Zernetkina, V., Juhasz, O., Fenner, R., . . . Fedorova, O. V. (2018). Dietary Sodium Restriction Reduces Arterial Stiffness, Vascular TGF-beta-Dependent Fibrosis and Marinobufagenin in Young Normotensive Rats. *Int J Mol Sci, 19*(10). doi: 10.3390/ijms19103168

Gruber, K. A., Whitaker, J. M., & Buckalew, V. M., Jr. (1980). Endogenous digitalis-like substance in plasma of volume-expanded dogs. *Nature, 287*(5784), 743-745. doi: 10.1038/287743a0

Gu, M., Mordwinkin, N. M., Kooreman, N. G., Lee, J., Wu, H., Hu, S., . . . Wu, J. C. (2015). Pravastatin reverses obesity-induced dysfunction of induced pluripotent stem cell-derived endothelial cells via a nitric oxide-dependent mechanism. *Eur Heart J, 36*(13), 806-816. doi: 10.1093/eurheartj/ehu411

91

Haas, M., Askari, A., & Xie, Z. (2000). Involvement of Src and epidermal growth factor receptor in the signal-transducing function of Na+/K+-ATPase. *J Biol Chem, 275*(36), 27832-27837. doi: 10.1074/jbc.M002951200

Haas, M., Wang, H., Tian, J., & Xie, Z. (2002). Src-mediated inter-receptor cross-talk between the Na+/K+-ATPase and the epidermal growth factor receptor relays the signal from ouabain to mitogen-activated protein kinases. *J Biol Chem, 277*(21), 18694-18702. doi: 10.1074/jbc.M111357200

Hafner, A. L., & Dani, C. (2014). Human induced pluripotent stem cells: A new source for brown and white adipocytes. *World J Stem Cells, 6*(4), 467-472. doi: 10.4252/wjsc.v6.i4.467

Hamlyn, J. M., Blaustein, M. P., Bova, S., DuCharme, D. W., Harris, D. W., Mandel, F., . . . Ludens, J. H. (1991). Identification and characterization of a ouabain-like compound from human plasma. *Proc Natl Acad Sci U S A, 88*(14), 6259-6263. doi: 10.1073/pnas.88.14.6259

Hamlyn, J. M., Ringel, R., Schaeffer, J., Levinson, P. D., Hamilton, B. P., Kowarski, A. A., & Blaustein, M. P. (1982). A circulating inhibitor of (Na+ + K+)ATPase associated with essential hypertension. *Nature, 300*(5893), 650-652. doi: 10.1038/300650a0

Hauptman, P. J., & Kelly, R. A. (1999). Digitalis. *Circulation, 99*(9), 1265-1270. doi: 10.1161/01.cir.99.9.1265

Hayashi, M., Monkawa, T., Yoshida, T., Sasamura, H., Matsumoto, M., Inoue, T., . . . Saruta, T. (1999). Intracellular calcium concentration in the inositol trisphosphate receptor type 1 knockout mouse. *J Am Soc Nephrol, 10*(10), 2094-2101.

Hayashi, Y., Mimura, K., Matsui, H., & Takagi, T. (1989). Minimum enzyme unit for Na+/K+-ATPase is the alpha beta-protomer. Determination by low-angle laser light scattering photometry coupled with high-performance gel chromatography for substantially simultaneous measurement of ATPase activity and molecular weight. *Biochim Biophys Acta, 983*(2), 217-229. doi: 10.1016/0005-2736(89)90237-x

Hilton, P. J., White, R. W., Lord, G. A., Garner, G. V., Gordon, D. B., Hilton, M. J., . . . Morden, W. E. (1996). An inhibitor of the sodium pump obtained from human placenta. *Lancet, 348*(9023), 303-305. doi: 10.1016/s0140-6736(96)02257-x

Hiraike, Y., Waki, H., Yu, J., Nakamura, M., Miyake, K., Nagano, G., . . . Kadowaki, T. (2017). NFIA co-localizes with PPARgamma and transcriptionally controls the brown fat gene program. *Nat Cell Biol, 19*(9), 1081-1092. doi: 10.1038/ncb3590

Hoffman, J. F. (1962). Cation transport and structure of the red-cell plasma membrane. *Circulation, 26*, 1202-1213. doi: 10.1161/01.cir.26.5.1201

Hu, E., Tontonoz, P., & Spiegelman, B. M. (1995). Transdifferentiation of myoblasts by the adipogenic transcription factors PPAR gamma and C/EBP alpha. *Proc Natl Acad Sci U S A, 92*(21), 9856-9860. doi: 10.1073/pnas.92.21.9856

Huang, H., Song, T. J., Li, X., Hu, L., He, Q., Liu, M., . . . Tang, Q. Q. (2009). BMP signaling pathway is required for commitment of C3H10T1/2 pluripotent stem cells to the adipocyte lineage. *Proc Natl Acad Sci U S A, 106*(31), 12670-12675. doi: 10.1073/pnas.0906266106

Huang, L., Li, H., & Xie, Z. (1997). Ouabain-induced hypertrophy in cultured cardiac myocytes is accompanied by changes in expression of several late response genes. *J Mol Cell Cardiol, 29*(2), 429-437. doi: 10.1006/jmcc.1996.0320

Hundal, H. S., Marette, A., Mitsumoto, Y., Ramlal, T., Blostein, R., & Klip, A. (1992). Insulin induces translocation of the alpha 2 and beta 1 subunits of the Na+/K(+)-ATPase from intracellular compartments to the plasma membrane in mammalian skeletal muscle. *J Biol Chem, 267*(8), 5040-5043.

Jakkaraju, S., Zhe, X., Pan, D., Choudhury, R., & Schuger, L. (2005). TIPs are tension-responsive proteins involved in myogenic versus adipogenic differentiation. *Dev Cell, 9*(1), 39-49. doi: 10.1016/j.devcel.2005.04.015

Jorgensen, C. B., Levi, H., & Zerahn, K. (1954). On active uptake of sodium and chloride ions in anurans. *Acta Physiol Scand, 30*(2-3), 178-190. doi: 10.1111/j.1748-1716.1954.tb01086.x

Jorgensen, P. L., & Andersen, J. P. (1988). Structural basis for E1-E2 conformational transitions in Na,K-pump and Ca-pump proteins. *J Membr Biol, 103*(2), 95-120. doi: 10.1007/BF01870942

Juge-Aubry, C. E., Gorla-Bajszczak, A., Pernin, A., Lemberger, T., Wahli, W., Burger, A. G., & Meier, C. A. (1995). Peroxisome proliferator-activated receptor mediates cross-talk with thyroid hormone receptor by competition for retinoid X receptor. Possible role of a

leucine zipper-like heptad repeat. *J Biol Chem, 270*(30), 18117-18122. doi: 10.1074/jbc.270.30.18117

Kaplan, J. G. (1978). Membrane cation transport and the control of proliferation of mammalian cells. *Annu Rev Physiol, 40*, 19-41. doi: 10.1146/annurev.ph.40.030178.000315

Karlish, S. J., Yates, D. W., & Glynn, I. M. (1976). Transient kinetics of (Na+ +K+)-ATPase studied with a fluorescent substrate. *Nature, 263*(5574), 251-253. doi: 10.1038/263251a0

Kennedy, D. J., Chen, Y., Huang, W., Viterna, J., Liu, J., Westfall, K., . . . Silverstein, R. L. (2013). CD36 and Na/K-ATPase-alpha1 form a proinflammatory signaling loop in kidney. *Hypertension, 61*(1), 216-224. doi: 10.1161/HYPERTENSIONAHA.112.198770

Kennedy, D. J., Khalaf, F. K., Sheehy, B., Weber, M. E., Agatisa-Boyle, B., Conic, J., . . . Tang, W. H. W. (2018). Telocinobufagin, a Novel Cardiotonic Steroid, Promotes Renal Fibrosis via Na(+)/K(+)-ATPase Profibrotic Signaling Pathways. *Int J Mol Sci, 19*(9). doi: 10.3390/ijms19092566

Kennedy, D. J., Vetteth, S., Periyasamy, S. M., Kanj, M., Fedorova, L., Khouri, S., . . . Shapiro, J. I. (2006). Central role for the cardiotonic steroid marinobufagenin in the pathogenesis of experimental uremic cardiomyopathy. *Hypertension, 47*(3), 488-495. doi: 10.1161/01.HYP.0000202594.82271.92

Kernan, R. P. (1962). Membrane potential changes during sodium transport in frog sartorius muscle. *Nature, 193*, 986-987. doi: 10.1038/193986a0

Ketchem, C. J., Conner, C. D., Murray, R. D., DuPlessis, M., Lederer, E. D., Wilkey, D., . . . Khundmiri, S. J. (2016). Low dose ouabain stimulates NaK ATPase alpha1 subunit association with angiotensin II type 1 receptor in renal proximal tubule cells. *Biochim Biophys Acta, 1863*(11), 2624-2636. doi: 10.1016/j.bbamcr.2016.07.008

Khan, M., Ali, F., Mohsin, S., Akhtar, S., Mehmood, A., Choudhery, M. S., . . . Riazuddin, S. (2013). Preconditioning diabetic mesenchymal stem cells with myogenic medium increases their ability to repair diabetic heart. *Stem Cell Res Ther, 4*(3), 58. doi: 10.1186/scrt207

Kilian, K. A., Bugarija, B., Lahn, B. T., & Mrksich, M. (2010). Geometric cues for directing the differentiation of mesenchymal stem cells. *Proc Natl Acad Sci U S A, 107*(11), 4872-4877. doi: 10.1073/pnas.0903269107

Klip, A., McGraw, T. E., & James, D. E. (2019). Thirty sweet years of GLUT4. *J Biol Chem, 294*(30), 11369-11381. doi: 10.1074/jbc.REV119.008351

Koefoed-Johnsen, V., Ussing, H. H., & Zerahn, K. (1952). The origin of the short-circuit current in the adrenaline stimulated frog skin. *Acta Physiol Scand, 27*(1), 38-48. doi: 10.1111/j.1748-1716.1953.tb00922.x

Kojima, I., Yoshihara, S., & Ogata, E. (1982). Involvement of endogenous digitalis-like substance in genesis of deoxycorticosterone-salt hypertension. *Life Sci, 30*(21), 1775-1781. doi: 10.1016/0024-3205(82)90313-7

Kometiani, P., Li, J., Gnudi, L., Kahn, B. B., Askari, A., & Xie, Z. (1998). Multiple signal transduction pathways link Na+/K+-ATPase to growth-related genes in cardiac myocytes. The roles of Ras and mitogen-activated protein kinases. *J Biol Chem, 273*(24), 15249-15256. doi: 10.1074/jbc.273.24.15249

Komiyama, Y., Nishimura, N., Munakata, M., Mori, T., Okuda, K., Nishino, N., . . . Takahashi, H. (2001). Identification of endogenous ouabain in culture supernatant of PC12 cells. *J Hypertens, 19*(2), 229-236. doi: 10.1097/00004872-200102000-00009

Kulikov, A., Eva, A., Kirch, U., Boldyrev, A., & Scheiner-Bobis, G. (2007). Ouabain activates signaling pathways associated with cell death in human neuroblastoma. *Biochim Biophys Acta, 1768*(7), 1691-1702. doi: 10.1016/j.bbamem.2007.04.012

Kurzchalia, T. V., & Parton, R. G. (1999). Membrane microdomains and caveolae. *Curr Opin Cell Biol, 11*(4), 424-431. doi: 10.1016/s0955-0674(99)80061-1

Kutz, L. C., Cui, X., Xie, J. X., Mukherji, S. T., Terrell, K. C., Huang, M., . . . Pierre, S. V. (2021). The Na/K-ATPase alpha1/Src interaction regulates metabolic reserve and Western diet intolerance. *Acta Physiol (Oxf)*, e13652. doi: 10.1111/apha.13652

Kutz, L. C., Mukherji, S. T., Wang, X., Bryant, A., Larre, I., Heiny, J. A., . . . Xie, Z. (2018). Isoform-specific role of Na/K-ATPase alpha1 in skeletal muscle. *Am J Physiol Endocrinol Metab, 314*(6), E620-E629. doi: 10.1152/ajpendo.00275.2017

La, J., Reed, E., Chan, L., Smolyaninova, L. V., Akomova, O. A., Mutlu, G. M., . . . Dulin, N. O. (2016). Downregulation of TGF-beta Receptor-2 Expression and Signaling through Inhibition of Na/K-ATPase. *PLoS One, 11*(12), e0168363. doi: 10.1371/journal.pone.0168363

Labrecque, L., Nyalendo, C., Langlois, S., Durocher, Y., Roghi, C., Murphy, G., . . . Beliveau, R. (2004). Src-mediated tyrosine phosphorylation of Cav1 induces its association with membrane type 1 matrix metalloproteinase. *J Biol Chem, 279*(50), 52132-52140. doi: 10.1074/jbc.M409617200

Lai, F., Madan, N., Ye, Q., Duan, Q., Li, Z., Wang, S., . . . Xie, Z. (2013). Identification of a mutant alpha1 Na/K-ATPase that pumps but is defective in signal transduction. *J Biol Chem, 288*(19), 13295-13304. doi: 10.1074/jbc.M113.467381

Lee, J. E., Schmidt, H., Lai, B., & Ge, K. (2019). Transcriptional and Epigenomic Regulation of Adipogenesis. *Mol Cell Biol, 39*(11). doi: 10.1128/MCB.00601-18

Levenson, R. (1994). Isoforms of the Na,K-ATPase: family members in search of function. *Rev Physiol Biochem Pharmacol, 123*, 1-45. doi: 10.1007/BFb0030902

Li, J., Zelenin, S., Aperia, A., & Aizman, O. (2006). Low doses of ouabain protect from serum deprivation-triggered apoptosis and stimulate kidney cell proliferation via activation of NF-kappaB. *J Am Soc Nephrol, 17*(7), 1848-1857. doi: 10.1681/ASN.2005080894

Li, M., Wang, Q., & Guan, L. (2007). Effects of ouabain on proliferation, intracellular free calcium and c-myc mRNA expression in vascular smooth muscle cells. *J Comp Physiol B, 177*(5), 589-595. doi: 10.1007/s00360-007-0157-4

Li, Z., Cai, T., Tian, J., Xie, J. X., Zhao, X., Liu, L., . . . Xie, Z. (2009). NaKtide, a Na/K-ATPase-derived peptide Src inhibitor, antagonizes ouabain-activated signal transduction in cultured cells. *J Biol Chem, 284*(31), 21066-21076. doi: 10.1074/jbc.M109.013821

Li, Z., & Xie, Z. (2009). The Na/K-ATPase/Src complex and cardiotonic steroid-activated protein kinase cascades. *Pflugers Arch, 457*(3), 635-644. doi: 10.1007/s00424-008-0470-0

Liang, M., Cai, T., Tian, J., Qu, W., & Xie, Z. J. (2006). Functional characterization of Src-interacting Na/K-ATPase using RNA interference assay. *J Biol Chem, 281*(28), 19709-19719. doi: 10.1074/jbc.M512240200

Liang, M., Tian, J., Liu, L., Pierre, S., Liu, J., Shapiro, J., & Xie, Z. J. (2007). Identification of a pool of non-pumping Na/K-ATPase. *J Biol Chem, 282*(14), 10585-10593. doi: 10.1074/jbc.M609181200

Lichtstein, D., Gati, I., & Ovadia, H. (1993). Digitalis-like compounds in the toad Bufo viridis: interactions with plasma proteins. *J Cardiovasc Pharmacol, 22 Suppl 2*, S102-105. doi: 10.1097/00005344-199322002-00033

Lijnen, H. R., Maquoi, E., Hansen, L. B., Van Hoef, B., Frederix, L., & Collen, D. (2002). Matrix metalloproteinase inhibition impairs adipose tissue development in mice. *Arterioscler Thromb Vasc Biol, 22*(3), 374-379. doi: 10.1161/hq0302.104522

Lingrel, J. B., & Kuntzweiler, T. (1994). Na+,K(+)-ATPase. *J Biol Chem, 269*(31), 19659-19662.

Lingrel, J. B., Van Huysse, J., O'Brien, W., Jewell-Motz, E., Askew, R., & Schultheis, P. (1994). Structure-function studies of the Na,K-ATPase. *Kidney Int Suppl, 44*, S32-39.

Lingrel, J. B., Van Huysse, J., O'Brien, W., Jewell-Motz, E., & Schultheis, P. (1994). Na,K-ATPase: structure-function studies. *Ren Physiol Biochem, 17*(3-4), 198-200. doi: 10.1159/000173818

Liu, J., Kennedy, D. J., Yan, Y., & Shapiro, J. I. (2012). Reactive Oxygen Species Modulation of Na/K-ATPase Regulates Fibrosis and Renal Proximal Tubular Sodium Handling. *Int J Nephrol, 2012*, 381320. doi: 10.1155/2012/381320

Liu, J., Kesiry, R., Periyasamy, S. M., Malhotra, D., Xie, Z., & Shapiro, J. I. (2004). Ouabain induces endocytosis of plasmalemmal Na/K-ATPase in LLC-PK1 cells by a clathrin-dependent mechanism. *Kidney Int, 66*(1), 227-241. doi: 10.1111/j.1523-1755.2004.00723.x

Liu, J., Liang, M., Liu, L., Malhotra, D., Xie, Z., & Shapiro, J. I. (2005). Ouabain-induced endocytosis of the plasmalemmal Na/K-ATPase in LLC-PK1 cells requires Cav1. *Kidney Int, 67*(5), 1844-1854. doi: 10.1111/j.1523-1755.2005.00283.x

Liu, J., & Shapiro, J. I. (2007). Regulation of sodium pump endocytosis by cardiotonic steroids: Molecular mechanisms and physiological implications. *Pathophysiology, 14*(3-4), 171-181. doi: 10.1016/j.pathophys.2007.09.008

Liu, J., Tian, J., Chaudhry, M., Maxwell, K., Yan, Y., Wang, X., . . . Shapiro, J. I. (2016). Attenuation of Na/K-ATPase Mediated Oxidant Amplification with pNaKtide Ameliorates Experimental Uremic Cardiomyopathy. *Sci Rep, 6*, 34592. doi: 10.1038/srep34592

Liu, L., Brown, D., McKee, M., Lebrasseur, N. K., Yang, D., Albrecht, K. H., . . . Pilch, P. F. (2008). Deletion of Cavin/PTRF causes global loss of caveolae, dyslipidemia, and glucose intolerance. *Cell Metab, 8*(4), 310-317. doi: 10.1016/j.cmet.2008.07.008

Lockwich, T. P., Liu, X., Singh, B. B., Jadlowiec, J., Weiland, S., & Ambudkar, I. S. (2000). Assembly of Trp1 in a signaling complex associated with Cav-scaffolding lipid raft domains. *J Biol Chem, 275*(16), 11934-11942. doi: 10.1074/jbc.275.16.11934

Lopez-Lazaro, M., Pastor, N., Azrak, S. S., Ayuso, M. J., Austin, C. A., & Cortes, F. (2005). Digitoxin inhibits the growth of cancer cell lines at concentrations commonly found in cardiac patients. *J Nat Prod, 68*(11), 1642-1645. doi: 10.1021/np050226l

Love, M. I., Huber, W., & Anders, S. (2014). Moderated estimation of fold change and dispersion for RNA-seq data with DESeq2. *Genome Biol, 15*(12), 550. doi: 10.1186/s13059-014-0550-8

Lowry, O. H., Rosebrough, N. J., Farr, A. L., & Randall, R. J. (1951). Protein measurement with the Folin phenol reagent. *J Biol Chem, 193*(1), 265-275.

Ludens, J. H., Clark, M. A., DuCharme, D. W., Harris, D. W., Lutzke, B. S., Mandel, F., . . . Hamlyn, J. M. (1991). Purification of an endogenous digitalislike factor from human plasma for structural analysis. *Hypertension, 17*(6 Pt 2), 923-929. doi: 10.1161/01.hyp.17.6.923

Lytton, J. (1985). Insulin affects the sodium affinity of the rat adipocyte (Na+,K+)-ATPase. *J Biol Chem, 260*(18), 10075-10080.

Lytton, J., Lin, J. C., & Guidotti, G. (1985). Identification of two molecular forms of (Na+,K+)-ATPase in rat adipocytes. Relation to insulin stimulation of the enzyme. *J Biol Chem, 260*(2), 1177-1184.

Madan, N., Xu, Y., Duan, Q., Banerjee, M., Larre, I., Pierre, S. V., & Xie, Z. (2017). Src-independent ERK signaling through the rat alpha3 isoform of Na/K-ATPase. *Am J Physiol Cell Physiol, 312*(3), C222-C232. doi: 10.1152/ajpcell.00199.2016

Manunta, P., Stella, P., Rivera, R., Ciurlino, D., Cusi, D., Ferrandi, M., . . . Bianchi, G. (1999). Left ventricular mass, stroke volume, and ouabain-like factor in essential hypertension. *Hypertension, 34*(3), 450-456. doi: 10.1161/01.hyp.34.3.450

Maquoi, E., Munaut, C., Colige, A., Collen, D., & Lijnen, H. R. (2002). Modulation of adipose tissue expression of murine matrix metalloproteinases and their tissue inhibitors with obesity. *Diabetes, 51*(4), 1093-1101. doi: 10.2337/diabetes.51.4.1093

Maunsbach, A. B., Skriver, E., & Hebert, H. (1991). Two-dimensional crystals and three-dimensional structure of Na,K-ATPase analyzed by electron microscopy. *Soc Gen Physiol Ser, 46*, 159-172.

McBeath, R., Pirone, D. M., Nelson, C. M., Bhadriraju, K., & Chen, C. S. (2004). Cell shape, cytoskeletal tension, and RhoA regulate stem cell lineage commitment. *Dev Cell, 6*(4), 483-495. doi: 10.1016/s1534-5807(04)00075-9

McGill, D. L., & Guidotti, G. (1991). Insulin stimulates both the alpha 1 and the alpha 2 isoforms of the rat adipocyte (Na+,K+) ATPase. Two mechanisms of stimulation. *J Biol Chem, 266*(24), 15824-15831.

Mijatovic, T., Roland, I., Van Quaquebeke, E., Nilsson, B., Mathieu, A., Van Vynckt, F., . . . Kiss, R. (2007). The alpha1 subunit of the sodium pump could represent a novel target to combat non-small cell lung cancers. *J Pathol, 212*(2), 170-179. doi: 10.1002/path.2172

Mobasheri, A., Avila, J., Cozar-Castellano, I., Brownleader, M. D., Trevan, M., Francis, M. J., . . . Martin-Vasallo, P. (2000). Na+, K+-ATPase isozyme diversity; comparative biochemistry and physiological implications of novel functional interactions. *Biosci Rep, 20*(2), 51-91. doi: 10.1023/a:1005580332144

Mohammadi, K., Kometiani, P., Xie, Z., & Askari, A. (2001). Role of protein kinase C in the signal pathways that link Na+/K+-ATPase to ERK1/2. *J Biol Chem, 276*(45), 42050-42056. doi: 10.1074/jbc.M107892200

Morth, J. P., Pedersen, B. P., Buch-Pedersen, M. J., Andersen, J. P., Vilsen, B., Palmgren, M. G., & Nissen, P. (2011). A structural overview of the plasma membrane Na+,K+-ATPase and H+-ATPase ion pumps. *Nat Rev Mol Cell Biol, 12*(1), 60-70. doi: 10.1038/nrm3031

Morth, J. P., Pedersen, B. P., Toustrup-Jensen, M. S., Sorensen, T. L., Petersen, J., Andersen, J. P., . . . Nissen, P. (2007). Crystal structure of the sodium-potassium pump. *Nature, 450*(7172), 1043-1049. doi: 10.1038/nature06419

Munzer, J. S., Daly, S. E., Jewell-Motz, E. A., Lingrel, J. B., & Blostein, R. (1994). Tissue- and isoform-specific kinetic behavior of the Na,K-ATPase. *J Biol Chem, 269*(24), 16668-16676.

99

Murano, I., Barbatelli, G., Parisani, V., Latini, C., Muzzonigro, G., Castellucci, M., & Cinti, S. (2008). Dead adipocytes, detected as crown-like structures, are prevalent in visceral fat depots of genetically obese mice. *J Lipid Res, 49*(7), 1562-1568. doi: 10.1194/jlr.M800019-JLR200

Nusse, R. (2005). Wnt signaling in disease and in development. *Cell Res, 15*(1), 28-32. doi: 10.1038/sj.cr.7290260

Ohtsubo, M., Noguchi, S., Takeda, K., Morohashi, M., & Kawamura, M. (1990). Site-directed mutagenesis of Asp-376, the catalytic phosphorylation site, and Lys-507, the putative ATP-binding site, of the alpha-subunit of Torpedo californica Na+/K(+)-ATPase. *Biochim Biophys Acta, 1021*(2), 157-160. doi: 10.1016/0005-2736(90)90028-m

Orlowski, J., & Lingrel, J. B. (1988). Differential expression of the Na,K-ATPase alpha 1 and alpha 2 subunit genes in a murine myogenic cell line. Induction of the alpha 2 isozyme during myocyte differentiation. *J Biol Chem, 263*(33), 17817-17821.

Ostermeyer, A. G., Ramcharan, L. T., Zeng, Y., Lublin, D. M., & Brown, D. A. (2004). Role of the hydrophobic domain in targeting Cav1 to lipid droplets. *J Cell Biol, 164*(1), 69-78. doi: 10.1083/jcb.200303037

Ottolenghi, P. (1979). The relipidation of delipidated Na,K-ATPase. An analysis of complex formation with dioleoylphosphatidylcholine and with dioleoylphosphatidylethanolamine. *Eur J Biochem, 99*(1), 113-131. doi: 10.1111/j.1432-1033.1979.tb13238.x

Overbeck, H. W., Pamnani, M. B., Akera, T., Brody, T. M., & Haddy, F. J. (1976). Depressed function of a ouabain-sensitive sodium-potassium pump in blood vessels from renal hypertensive dogs. *Circ Res, 38*(6 Suppl 2), 48-52. doi: 10.1161/01.res.38.6.48

Pachon-Pena, G., Serena, C., Ejarque, M., Petriz, J., Duran, X., Oliva-Olivera, W., . . . Vendrell, J. (2016). Obesity Determines the Immunophenotypic Profile and Functional Characteristics of Human Mesenchymal Stem Cells From Adipose Tissue. *Stem Cells Transl Med, 5*(4), 464-475. doi: 10.5966/sctm.2015-0161

Park, D. S., Woodman, S. E., Schubert, W., Cohen, A. W., Frank, P. G., Chandra, M., . . . Lisanti, M. P. (2002). Cav1/3 double-knockout mice are viable, but lack both muscle and non-muscle caveolae, and develop a severe cardiomyopathic phenotype. *Am J Pathol, 160*(6), 2207-2217. doi: 10.1016/S0002-9440(10)61168-6

Parkman, J. K., Mao, X., Dillon, K., Gudivada, A., Moustaid-Moussa, N., Saxton, A. M., & Kim, J. H. (2016). Genotype-dependent Metabolic Responses to Semi-Purified High-Sucrose High-Fat Diets in the TALLYHO/Jng vs. C57BL/6 Mouse during the Development of Obesity and Type 2 Diabetes. *Exp Clin Endocrinol Diabetes, 124*(10), 622-629. doi: 10.1055/s-0042-109605

Parton, R. G. (2003). Caveolae--from ultrastructure to molecular mechanisms. *Nat Rev Mol Cell Biol, 4*(2), 162-167. doi: 10.1038/nrm1017

Parton, R. G., & del Pozo, M. A. (2013). Caveolae as plasma membrane sensors, protectors and organizers. *Nat Rev Mol Cell Biol, 14*(2), 98-112. doi: 10.1038/nrm3512

Parton, R. G., Hanzal-Bayer, M., & Hancock, J. F. (2006). Biogenesis of caveolae: a structural model for Cav-induced domain formation. *J Cell Sci, 119*(Pt 5), 787-796. doi: 10.1242/jcs.02853

Parton, R. G., & Simons, K. (2007). The multiple faces of caveolae. *Nat Rev Mol Cell Biol, 8*(3), 185-194. doi: 10.1038/nrm2122

Peterson, J., Bihain, B. E., Bengtsson-Olivecrona, G., Deckelbaum, R. J., Carpentier, Y. A., & Olivecrona, T. (1990). Fatty acid control of lipoprotein lipase: a link between energy metabolism and lipid transport. *Proc Natl Acad Sci U S A, 87*(3), 909-913. doi: 10.1073/pnas.87.3.909

Petrosian, S. A., Carr, D. L., Guerrero, G., & Pressley, T. A. (1998). Mutagenesis disrupts posttranslational processing of the Na,K-ATPase catalytic subunit. *Arch Biochem Biophys, 357*(2), 249-258. doi: 10.1006/abbi.1998.0816

Pierre, S. V., Sottejeau, Y., Gourbeau, J. M., Sanchez, G., Shidyak, A., & Blanco, G. (2008). Isoform specificity of Na-K-ATPase-mediated ouabain signaling. *Am J Physiol Renal Physiol, 294*(4), F859-866. doi: 10.1152/ajprenal.00089.2007

Pilch, P. F., & Liu, L. (2011). Fat caves: caveolae, lipid trafficking and lipid metabolism in adipocytes. *Trends Endocrinol Metab, 22*(8), 318-324. doi: 10.1016/j.tem.2011.04.001

Pilch, P. F., Meshulam, T., Ding, S., & Liu, L. (2011). Caveolae and lipid trafficking in adipocytes. *Clin Lipidol, 6*(1), 49-58. doi: 10.2217/clp.10.80

Pollack, L. R., Tate, E. H., & Cook, J. S. (1981a). Na+, K+-ATPase in HeLa cells after prolonged growth in low K+ or ouabain. *J Cell Physiol, 106*(1), 85-97. doi: 10.1002/jcp.1041060110

Pollack, L. R., Tate, E. H., & Cook, J. S. (1981b). Turnover and regulation of Na-K-ATPase in HeLa cells. *Am J Physiol, 241*(5), C173-183. doi: 10.1152/ajpcell.1981.241.5.C173

Post, R. L., Kume, S., Tobin, T., Orcutt, B., & Sen, A. K. (1969). Flexibility of an active center in sodium-plus-potassium adenosine triphosphatase. *J Gen Physiol, 54*(1), 306-326. doi: 10.1085/jgp.54.1.306

Pratt, R. D., Brickman, C., Nawab, A., Cottrill, C., Snoad, B., Lakhani, H. V., . . . Sodhi, K. (2019). The Adipocyte Na/K-ATPase Oxidant Amplification Loop is the Central Regulator of Western Diet-Induced Obesity and Associated Comorbidities. *Sci Rep, 9*(1), 7927. doi: 10.1038/s41598-019-44350-9

Pressley, T. A., Duran, M. J., & Pierre, S. V. (2005). Regions conferring isoform-specific function in the catalytic subunit of the Na,K-pump. *Front Biosci, 10*, 2018-2026. doi: 10.2741/1677

Quintas, L. E., Pierre, S. V., Liu, L., Bai, Y., Liu, X., & Xie, Z. J. (2010). Alterations of Na+/K+-ATPase function in Cav1 knockout cardiac fibroblasts. *J Mol Cell Cardiol, 49*(3), 525-531. doi: 10.1016/j.yjmcc.2010.04.015

Ramirez-Ortega, M., Maldonado-Lagunas, V., Melendez-Zajgla, J., Carrillo-Hernandez, J. F., Pastelin-Hernandez, G., Picazo-Picazo, O., & Ceballos-Reyes, G. (2006). Proliferation and apoptosis of HeLa cells induced by in vitro stimulation with digitalis. *Eur J Pharmacol, 534*(1-3), 71-76. doi: 10.1016/j.ejphar.2006.01.035

Ran, F. A., Hsu, P. D., Wright, J., Agarwala, V., Scott, D. A., & Zhang, F. (2013). Genome engineering using the CRISPR-Cas9 system. *Nat Protoc, 8*(11), 2281-2308. doi: 10.1038/nprot.2013.143

Razani, B., Combs, T. P., Wang, X. B., Frank, P. G., Park, D. S., Russell, R. G., . . . Lisanti, M. P. (2002). Cav1-deficient mice are lean, resistant to diet-induced obesity, and show hypertriglyceridemia with adipocyte abnormalities. *J Biol Chem, 277*(10), 8635-8647. doi: 10.1074/jbc.M110970200

Razani, B., Engelman, J. A., Wang, X. B., Schubert, W., Zhang, X. L., Marks, C. B., . . . Lisanti, M. P. (2001). Cav1 null mice are viable but show evidence of hyperproliferative and

vascular abnormalities. *J Biol Chem, 276*(41), 38121-38138. doi: 10.1074/jbc.M105408200

Razani, B., Woodman, S. E., & Lisanti, M. P. (2002). Caveolae: from cell biology to animal physiology. *Pharmacol Rev, 54*(3), 431-467. doi: 10.1124/pr.54.3.431

Resh, M. D. (1982a). Development of insulin responsiveness of the glucose transporter and the (Na+,K+)-adenosine triphosphatase during in vitro adipocyte differentiation. *J Biol Chem, 257*(12), 6978-6986.

Resh, M. D. (1982b). Quantitation and characterization of the (Na+,K+)-adenosine triphosphatase in the rat adipocyte plasma membrane. *J Biol Chem, 257*(20), 11946-11952.

Reuter, H., Henderson, S. A., Han, T., Ross, R. S., Goldhaber, J. I., & Philipson, K. D. (2002). The Na+-Ca2+ exchanger is essential for the action of cardiac glycosides. *Circ Res, 90*(3), 305-308. doi: 10.1161/hh0302.104562

Robenek, H., Weissen-Plenz, G., & Severs, N. J. (2008). Freeze-fracture replica immunolabelling reveals Cav1 in the human cardiomyocyte plasma membrane. *J Cell Mol Med, 12*(6A), 2519-2521. doi: 10.1111/j.1582-4934.2008.00498.x

Robinson, J. D. (1969). Kinetic studies on a brain microsomal adenosine triphosphatase. II. Potassium-dependent phosphatase activity. *Biochemistry, 8*(8), 3348-3355. doi: 10.1021/bi00836a032

Robinson, J. D. (1970). Phosphatase activity stimulated by Na+ plus K+: implications for the (Na+ plus K+)-dependent adenosine triphosphatase. *Arch Biochem Biophys, 139*(1), 164-171. doi: 10.1016/0003-9861(70)90057-3

Rodrigues, M., Wong, V. W., Rennert, R. C., Davis, C. R., Longaker, M. T., & Gurtner, G. C. (2015). Progenitor cell dysfunctions underlie some diabetic complications. *Am J Pathol, 185*(10), 2607-2618. doi: 10.1016/j.ajpath.2015.05.003

Rossoni, L. V., Salaices, M., Miguel, M., Briones, A. M., Barker, L. A., Vassallo, D. V., & Alonso, M. J. (2002). Ouabain-induced hypertension is accompanied by increases in endothelial vasodilator factors. *Am J Physiol Heart Circ Physiol, 283*(5), H2110-2118. doi: 10.1152/ajpheart.00454.2002

Rothberg, K. G., Heuser, J. E., Donzell, W. C., Ying, Y. S., Glenney, J. R., & Anderson, R. G. (1992). Caveolin, a protein component of caveolae membrane coats. *Cell, 68*(4), 673-682. doi: 10.1016/0092-8674(92)90143-z

Rowlands, A. S., George, P. A., & Cooper-White, J. J. (2008). Directing osteogenic and myogenic differentiation of MSCs: interplay of stiffness and adhesive ligand presentation. *Am J Physiol Cell Physiol, 295*(4), C1037-1044. doi: 10.1152/ajpcell.67.2008

Russo, J. J., Manuli, M. A., Ismail-Beigi, F., Sweadner, K. J., & Edelman, I. S. (1990). Na(+)-K(+)-ATPase in adipocyte differentiation in culture. *Am J Physiol, 259*(6 Pt 1), C968-977. doi: 10.1152/ajpcell.1990.259.6.C968

Sargiacomo, M., Scherer, P. E., Tang, Z., Kubler, E., Song, K. S., Sanders, M. C., & Lisanti, M. P. (1995). Oligomeric structure of caveolin: implications for caveolae membrane organization. *Proc Natl Acad Sci U S A, 92*(20), 9407-9411. doi: 10.1073/pnas.92.20.9407

Schatzmann, H. J. (1953). [Cardiac glycosides as inhibitors of active potassium and sodium transport by erythrocyte membrane]. *Helv Physiol Pharmacol Acta, 11*(4), 346-354.

Schlegel, A., & Lisanti, M. P. (2001). The caveolin triad: caveolae biogenesis, cholesterol trafficking, and signal transduction. *Cytokine Growth Factor Rev, 12*(1), 41-51. doi: 10.1016/s1359-6101(00)00022-8

Schneider, R., Wray, V., Nimtz, M., Lehmann, W. D., Kirch, U., Antolovic, R., & Schoner, W. (1998). Bovine adrenals contain, in addition to ouabain, a second inhibitor of the sodium pump. *J Biol Chem, 273*(2), 784-792. doi: 10.1074/jbc.273.2.784

Schrauwen, I., Szelinger, S., Siniard, A. L., Kurdoglu, A., Corneveaux, J. J., Malenica, I., . . . Huentelman, M. J. (2015). A Frame-Shift Mutation in CAV1 Is Associated with a Severe Neonatal Progeroid and Lipodystrophy Syndrome. *PLoS One, 10*(7), e0131797. doi: 10.1371/journal.pone.0131797

Sen, A. K., & Post, R. L. (1964). Stoichiometry and Localization of Adenosine Triphosphate-Dependent Sodium and Potassium Transport in the Erythrocyte. *J Biol Chem, 239*, 345-352.

Sen, B., Xie, Z., Case, N., Ma, M., Rubin, C., & Rubin, J. (2008). Mechanical strain inhibits adipogenesis in mesenchymal stem cells by stimulating a durable beta-catenin signal. *Endocrinology, 149*(12), 6065-6075. doi: 10.1210/en.2008-0687

Seo, J., Fortuno, E. S., 3rd, Suh, J. M., Stenesen, D., Tang, W., Parks, E. J., . . . Graff, J. M. (2009). Atf4 regulates obesity, glucose homeostasis, and energy expenditure. *Diabetes, 58*(11), 2565-2573. doi: 10.2337/db09-0335

Sethi, J. K., & Vidal-Puig, A. J. (2007). Thematic review series: adipocyte biology. Adipose tissue function and plasticity orchestrate nutritional adaptation. *J Lipid Res, 48*(6), 1253-1262. doi: 10.1194/jlr.R700005-JLR200

Shapiro, J. I., & Tian, J. (2011). Signaling through the Na/K-ATPase: implications for cardiac fibrosis. *Am J Physiol Heart Circ Physiol, 300*(1), H29-30. doi: 10.1152/ajpheart.01038.2010

Shchepinova, M. M., Cairns, A. G., Prime, T. A., Logan, A., James, A. M., Hall, A. R., . . . Hartley, R. C. (2017). MitoNeoD: A Mitochondria-Targeted Superoxide Probe. *Cell Chem Biol, 24*(10), 1285-1298 e1212. doi: 10.1016/j.chembiol.2017.08.003

Shull, G. E., Schwartz, A., & Lingrel, J. B. (1985). Amino-acid sequence of the catalytic subunit of the (Na+ + K+)ATPase deduced from a complementary DNA. *Nature, 316*(6030), 691-695. doi: 10.1038/316691a0

Sich, B., Kirch, U., Tepel, M., Zidek, W., & Schoner, W. (1996). Pulse pressure correlates in humans with a proscillaridin A immunoreactive compound. *Hypertension, 27*(5), 1073-1078. doi: 10.1161/01.hyp.27.5.1073

Singer, S. J., & Nicolson, G. L. (1972). The fluid mosaic model of the structure of cell membranes. *Science, 175*(4023), 720-731. doi: 10.1126/science.175.4023.720

Skou, J. C. (1957). The influence of some cations on an adenosine triphosphatase from peripheral nerves. *Biochim Biophys Acta, 23*(2), 394-401. doi: 10.1016/0006-3002(57)90343-8

Skou, J. C. (1988). The Na,K-pump. *Methods Enzymol, 156*, 1-25. doi: 10.1016/0076-6879(88)56004-4

Skou, J. C., & Esmann, M. (1992). The Na,K-ATPase. *J Bioenerg Biomembr, 24*(3), 249-261. doi: 10.1007/BF00768846

Smart, E. J., Ying, Y., Donzell, W. C., & Anderson, R. G. (1996). A role for caveolin in transport of cholesterol from endoplasmic reticulum to plasma membrane. *J Biol Chem, 271*(46), 29427-29435. doi: 10.1074/jbc.271.46.29427

Sodhi, K., Maxwell, K., Yan, Y., Liu, J., Chaudhry, M. A., Getty, M., . . . Shapiro, J. I. (2015). pNaKtide inhibits Na/K-ATPase reactive oxygen species amplification and attenuates adipogenesis. *Sci Adv, 1*(9), e1500781. doi: 10.1126/sciadv.1500781

Sodhi, K., Nichols, A., Mallick, A., Klug, R. L., Liu, J., Wang, X., . . . Shapiro, J. I. (2018). The Na/K-ATPase Oxidant Amplification Loop Regulates Aging. *Sci Rep, 8*(1), 9721. doi: 10.1038/s41598-018-26768-9

Sodhi, K., Srikanthan, K., Goguet-Rubio, P., Nichols, A., Mallick, A., Nawab, A., . . . Shapiro, J. I. (2017). pNaKtide Attenuates Steatohepatitis and Atherosclerosis by Blocking Na/K-ATPase/ROS Amplification in C57Bl6 and ApoE Knockout Mice Fed a Western Diet. *Sci Rep, 7*(1), 193. doi: 10.1038/s41598-017-00306-5

Sodhi, K., Wang, X., Chaudhry, M. A., Lakhani, H. V., Zehra, M., Pratt, R., . . . Shapiro, J. I. (2020). Central Role for Adipocyte Na,K-ATPase Oxidant Amplification Loop in the Pathogenesis of Experimental Uremic Cardiomyopathy. *J Am Soc Nephrol, 31*(8), 1746-1760. doi: 10.1681/ASN.2019101070

Song, E., Ouyang, N., Horbelt, M., Antus, B., Wang, M., & Exton, M. S. (2000). Influence of alternatively and classically activated macrophages on fibrogenic activities of human fibroblasts. *Cell Immunol, 204*(1), 19-28. doi: 10.1006/cimm.2000.1687

Sordella, R., Jiang, W., Chen, G. C., Curto, M., & Settleman, J. (2003). Modulation of Rho GTPase signaling regulates a switch between adipogenesis and myogenesis. *Cell, 113*(2), 147-158. doi: 10.1016/s0092-8674(03)00271-x

Soriano, P., Montgomery, C., Geske, R., & Bradley, A. (1991). Targeted disruption of the c-src proto-oncogene leads to osteopetrosis in mice. *Cell, 64*(4), 693-702. doi: 10.1016/0092-8674(91)90499-o

Srikanthan, K., Feyh, A., Visweshwar, H., Shapiro, J. I., & Sodhi, K. (2016). Systematic Review of Metabolic Syndrome Biomarkers: A Panel for Early Detection, Management, and Risk

Stratification in the West Virginian Population. *Int J Med Sci, 13*(1), 25-38. doi: 10.7150/ijms.13800

Steger, D. J., Grant, G. R., Schupp, M., Tomaru, T., Lefterova, M. I., Schug, J., . . . Lazar, M. A. (2010). Propagation of adipogenic signals through an epigenomic transition state. *Genes Dev, 24*(10), 1035-1044. doi: 10.1101/gad.1907110

Sun, K., Tordjman, J., Clement, K., & Scherer, P. E. (2013). Fibrosis and adipose tissue dysfunction. *Cell Metab, 18*(4), 470-477. doi: 10.1016/j.cmet.2013.06.016

Sweadner, K. J. (1979). Two molecular forms of (Na+ + K+)-stimulated ATPase in brain. Separation, and difference in affinity for strophanthidin. *J Biol Chem, 254*(13), 6060-6067.

Sweadner, K. J. (1985). Enzymatic properties of separated isozymes of the Na,K-ATPase. Substrate affinities, kinetic cooperativity, and ion transport stoichiometry. *J Biol Chem, 260*(21), 11508-11513.

Sweadner, K. J. (1991). Overview: subunit diversity in the Na,K-ATPase. *Soc Gen Physiol Ser, 46*, 63-76.

Tang, Q. Q., Zhang, J. W., & Daniel Lane, M. (2004). Sequential gene promoter interactions of C/EBPbeta, C/EBPalpha, and PPARgamma during adipogenesis. *Biochem Biophys Res Commun, 319*(1), 235-239. doi: 10.1016/j.bbrc.2004.04.176

Tang, W., Zeve, D., Suh, J. M., Bosnakovski, D., Kyba, M., Hammer, R. E., . . . Graff, J. M. (2008). White fat progenitor cells reside in the adipose vasculature. *Science, 322*(5901), 583-586. doi: 10.1126/science.1156232

Tang, Z. L., Scherer, P. E., & Lisanti, M. P. (1994). The primary sequence of murine caveolin reveals a conserved consensus site for phosphorylation by protein kinase C. *Gene, 147*(2), 299-300. doi: 10.1016/0378-1119(94)90087-6

Thomas, R. C. (1969). Membrane current and intracellular sodium changes in a snail neurone during extrusion of injected sodium. *J Physiol, 201*(2), 495-514. doi: 10.1113/jphysiol.1969.sp008769

Tian, J., Gong, X., & Xie, Z. (2001). Signal-transducing function of Na+-K+-ATPase is essential for ouabain's effect on [Ca2+]i in rat cardiac myocytes. *Am J Physiol Heart Circ Physiol, 281*(5), H1899-1907. doi: 10.1152/ajpheart.2001.281.5.H1899

Tian, J., Li, X., Liang, M., Liu, L., Xie, J. X., Ye, Q., . . . Xie, Z. (2009). Changes in sodium pump expression dictate the effects of ouabain on cell growth. *J Biol Chem, 284*(22), 14921-14929. doi: 10.1074/jbc.M808355200

Tian, J., Liu, J., Garlid, K. D., Shapiro, J. I., & Xie, Z. (2003). Involvement of mitogen-activated protein kinases and reactive oxygen species in the inotropic action of ouabain on cardiac myocytes. A potential role for mitochondrial K(ATP) channels. *Mol Cell Biochem, 242*(1-2), 181-187.

Tian, J., Shidyak, A., Periyasamy, S. M., Haller, S., Taleb, M., El-Okdi, N., . . . Shapiro, J. I. (2009). Spironolactone attenuates experimental uremic cardiomyopathy by antagonizing marinobufagenin. *Hypertension, 54*(6), 1313-1320. doi: 10.1161/HYPERTENSIONAHA.109.140038

Tontonoz, P., Hu, E., & Spiegelman, B. M. (1995). Regulation of adipocyte gene expression and differentiation by peroxisome proliferator activated receptor gamma. *Curr Opin Genet Dev, 5*(5), 571-576. doi: 10.1016/0959-437x(95)80025-5

Trevisi, L., Visentin, B., Cusinato, F., Pighin, I., & Luciani, S. (2004). Antiapoptotic effect of ouabain on human umbilical vein endothelial cells. *Biochem Biophys Res Commun, 321*(3), 716-721. doi: 10.1016/j.bbrc.2004.07.027

Vasilets, L. A., Takeda, K., Kawamura, M., & Schwarz, W. (1998). Significance of the glutamic acid residues Glu334, Glu959, and Glu960 of the alpha subunits of Torpedo Na+, K+ pumps for transport activity and ouabain binding. *Biochim Biophys Acta, 1368*(1), 137-149. doi: 10.1016/s0005-2736(97)00195-8

Visse, R., & Nagase, H. (2003). Matrix metalloproteinases and tissue inhibitors of metalloproteinases: structure, function, and biochemistry. *Circ Res, 92*(8), 827-839. doi: 10.1161/01.RES.0000070112.80711.3D

Wang, H., Haas, M., Liang, M., Cai, T., Tian, J., Li, S., & Xie, Z. (2004). Ouabain assembles signaling cascades through the caveolar Na+/K+-ATPase. *J Biol Chem, 279*(17), 17250-17259. doi: 10.1074/jbc.M313239200

Wang, J. G., Staessen, J. A., Messaggio, E., Nawrot, T., Fagard, R., Hamlyn, J. M., . . . Manunta, P. (2003). Salt, endogenous ouabain and blood pressure interactions in the general population. *J Hypertens, 21*(8), 1475-1481. doi: 10.1097/00004872-200308000-00010

Wang, W., Ishibashi, J., Trefely, S., Shao, M., Cowan, A. J., Sakers, A., . . . Seale, P. (2019). A PRDM16-Driven Metabolic Signal from Adipocytes Regulates Precursor Cell Fate. *Cell Metab, 30*(1), 174-189 e175. doi: 10.1016/j.cmet.2019.05.005

Wang, X., Cai, L., Xie, J. X., Cui, X., Zhang, J., Wang, J., . . . Xie, Z. (2020). A caveolin binding motif in Na/K-ATPase is required for stem cell differentiation and organogenesis in mammals and C. elegans. *Sci Adv, 6*(22), eaaw5851. doi: 10.1126/sciadv.aaw5851

Wang, X. M., Zhang, Y., Kim, H. P., Zhou, Z., Feghali-Bostwick, C. A., Liu, F., . . . Choi, A. M. (2006). Cav1: a critical regulator of lung fibrosis in idiopathic pulmonary fibrosis. *J Exp Med, 203*(13), 2895-2906. doi: 10.1084/jem.20061536

Whayne, T. F., Jr. (2018). Clinical Use of Digitalis: A State of the Art Review. *Am J Cardiovasc Drugs, 18*(6), 427-440. doi: 10.1007/s40256-018-0292-1

Williams, T. M., & Lisanti, M. P. (2005). Cav1 in oncogenic transformation, cancer, and metastasis. *Am J Physiol Cell Physiol, 288*(3), C494-506. doi: 10.1152/ajpcell.00458.2004

Winer, J. P., Janmey, P. A., McCormick, M. E., & Funaki, M. (2009). Bone marrow-derived human mesenchymal stem cells become quiescent on soft substrates but remain responsive to chemical or mechanical stimuli. *Tissue Eng Part A, 15*(1), 147-154. doi: 10.1089/ten.tea.2007.0388

Wu, Z., Rosen, E. D., Brun, R., Hauser, S., Adelmant, G., Troy, A. E., . . . Spiegelman, B. M. (1999). Cross-regulation of C/EBP alpha and PPAR gamma controls the transcriptional pathway of adipogenesis and insulin sensitivity. *Mol Cell, 3*(2), 151-158. doi: 10.1016/s1097-2765(00)80306-8

Xie, J., Ye, Q., Cui, X., Madan, N., Yi, Q., Pierre, S. V., & Xie, Z. (2015). Expression of rat Na-K-ATPase alpha2 enables ion pumping but not ouabain-induced signaling in alpha1-deficient porcine renal epithelial cells. *Am J Physiol Cell Physiol, 309*(6), C373-382. doi: 10.1152/ajpcell.00103.2015

Xie, J. X., Li, X., & Xie, Z. (2013). Regulation of renal function and structure by the signaling Na/K-ATPase. *IUBMB Life, 65*(12), 991-998. doi: 10.1002/iub.1229

Xie, Z. (2003). Molecular mechanisms of Na/K-ATPase-mediated signal transduction. *Ann N Y Acad Sci, 986*, 497-503. doi: 10.1111/j.1749-6632.2003.tb07234.x

Xie, Z., & Cai, T. (2003). Na+-K+--ATPase-mediated signal transduction: from protein interaction to cellular function. *Mol Interv, 3*(3), 157-168. doi: 10.1124/mi.3.3.157

Xie, Z., Kometiani, P., Liu, J., Li, J., Shapiro, J. I., & Askari, A. (1999). Intracellular reactive oxygen species mediate the linkage of Na+/K+-ATPase to hypertrophy and its marker genes in cardiac myocytes. *J Biol Chem, 274*(27), 19323-19328. doi: 10.1074/jbc.274.27.19323

Yamada, E. (1955). The fine structure of the renal glomerulus of the mouse. *J Histochem Cytochem, 3*(4), 309. doi: 10.1177/3.4.309

Yan, Y., Haller, S., Shapiro, A., Malhotra, N., Tian, J., Xie, Z., . . . Liu, J. (2012). Ouabain-stimulated trafficking regulation of the Na/K-ATPase and NHE3 in renal proximal tubule cells. *Mol Cell Biochem, 367*(1-2), 175-183. doi: 10.1007/s11010-012-1331-x

Yan, Y., Shapiro, A. P., Haller, S., Katragadda, V., Liu, L., Tian, J., . . . Liu, J. (2013). Involvement of reactive oxygen species in a feed-forward mechanism of Na/K-ATPase-mediated signaling transduction. *J Biol Chem, 288*(47), 34249-34258. doi: 10.1074/jbc.M113.461020

Yan, Y., Wang, J., Chaudhry, M. A., Nie, Y., Sun, S., Carmon, J., . . . Liu, J. (2019). Metabolic Syndrome and Salt-Sensitive Hypertension in Polygenic Obese TALLYHO/JngJ Mice: Role of Na/K-ATPase Signaling. *Int J Mol Sci, 20*(14). doi: 10.3390/ijms20143495

Yeh, W. C., Cao, Z., Classon, M., & McKnight, S. L. (1995). Cascade regulation of terminal adipocyte differentiation by three members of the C/EBP family of leucine zipper proteins. *Genes Dev, 9*(2), 168-181. doi: 10.1101/gad.9.2.168

Yu, H., Cui, X., Zhang, J., Xie, J. X., Banerjee, M., Pierre, S. V., & Xie, Z. (2018). Heterogeneity of signal transduction by Na-K-ATPase alpha-isoforms: role of Src interaction. *Am J Physiol Cell Physiol, 314*(2), C202-C210. doi: 10.1152/ajpcell.00124.2017

Yuan, Z., Cai, T., Tian, J., Ivanov, A. V., Giovannucci, D. R., & Xie, Z. (2005). Na/K-ATPase tethers phospholipase C and IP3 receptor into a calcium-regulatory complex. *Mol Biol Cell, 16*(9), 4034-4045. doi: 10.1091/mbc.e05-04-0295

Zamani, N., & Brown, C. W. (2011). Emerging roles for the transforming growth factor-{beta} superfamily in regulating adiposity and energy expenditure. *Endocr Rev, 32*(3), 387-403. doi: 10.1210/er.2010-0018

Zeituni, E. M., Wilson, M. H., Zheng, X., Iglesias, P. A., Sepanski, M. A., Siddiqi, M. A., . . . Farber, S. A. (2016). Endoplasmic Reticulum Lipid Flux Influences Enterocyte Nuclear Morphology and Lipid-dependent Transcriptional Responses. *J Biol Chem, 291*(45), 23804-23816. doi: 10.1074/jbc.M116.749358

Zhang, J., Lee, M. Y., Cavalli, M., Chen, L., Berra-Romani, R., Balke, C. W., . . . Blaustein, M. P. (2005). Sodium pump alpha2 subunits control myogenic tone and blood pressure in mice. *J Physiol, 569*(Pt 1), 243-256. doi: 10.1113/jphysiol.2005.091801

Zhao, Y. Y., Liu, Y., Stan, R. V., Fan, L., Gu, Y., Dalton, N., . . . Chien, K. R. (2002). Defects in Cav1 cause dilated cardiomyopathy and pulmonary hypertension in knockout mice. *Proc Natl Acad Sci U S A, 99*(17), 11375-11380. doi: 10.1073/pnas.172360799

APPENDIX A

LETTER FROM OFFICE OF RESEARCH INTEGRITY

MARSHALL UNIVERSITY.
www.marshall.edu

Office of Research Integrity

April 1, 2021

Minqi Huang
Applied Engineering Complex, Rm 4127
Marshall Institute for Interdisciplinary Research (MIIR)
Marshall University

Dear Minqi:

This letter is in response to the submitted thesis abstract entitled *"Na/K-ATPase α1 Regulates Adipogenesis via its Conserved Caveolin-binding Motif."* After assessing the abstract it has been deemed not to be human subject research and therefore exempt from oversight of the Marshall University Institutional Review Board (IRB). The Institutional Animal Care and Use Committee (IACUC) has reviewed and approved the study under protocol #609. The applicable human and animal federal regulations have set forth the criteria utilized in making this determination. If there are any changes to the abstract you provided then you would need to resubmit that information to the Office of Research Integrity for review and a determination.

I appreciate your willingness to submit the abstract for determination. Please feel free to contact the Office of Research Integrity if you have any questions regarding future protocols that may require IRB review.

Sincerely,

Bruce F. Day, ThD, CIP
Director

WE ARE...MARSHALL.
One John Marshall Drive • Huntington, West Virginia 25755 • Tel 304/696-4303
A State University of West Virginia • An Affirmative Action/Equal Opportunity Employer

112

APPENDIX B

ABBREVIATIONS

2-DG - 2-Deoxy-D-glucose

2-NBDG - 2-(N-(7-Nitrobenz-2-oxa-1,3-diazol-4-yl)Amino)-2-Deoxyglucose

3D - three-dimensional

ADIPOQ - gene encodes adiponectin

ATP - adenosine triphosphate

Atp1a1 - gene encode Na/K-ATPase α1

ATPase - adenosine triphosphatase

bFGF - basic fibroblast growth factor

C/EBP - CCAAT enhancer binding protein

C57BL6 – a commonly used strain of inbred mice

CAV - gene encodes caveolin protein

Cav1 – caveolin-1

CBM – caveolin binding motif

CCL2 – gene encodes monocyte chemoattractant protein-1

CD36 - cluster of differentiation 36

cDNA - Complementary DNA

Cl - chlorine

CLS - Crown-like structures

COL1A1 – gene encodes collagen type I, α1

CRISPRCas9 - clustered regularly interspaced short palindromic repeats-CRISPR associated

protein 9

CSD - caveolin scaffolding domain

C-terminus - carboxyl-terminus

CTS - Cardiotonic steroids

DMEM - Dulbecco's Modified Eagle Medium

DNA - deoxyribonucleic acid

EC_{50} - concentration of a drug that gives half-maximal response

ECAR - extracellular acidification rate

EchoMRI – a body composition analyzer

ECM - extracellular matrix

EDTA - ethylenediaminetetraacetic acid

EGFR - Epidermal Growth Factor Receptor

EGTA - ethylene glycol-bis(β-aminoethyl ether)-N,N,N′,N′-tetraacetic acid

EM - Electron Microscopy

EO - endogenous ouabain

ERK - extracellular signal-regulated kinases

F - fluorine

F4/80 - EGF-like module-containing mucin-like hormone receptor-like 1

FACS - fluorescence-activated cell sorting

FASN - fatty acid synthase

FBS - fetal bovine serum

FCCP - carbonyl cyanide-4-(trifluoromethoxy)phenylhydrazone

FFA - free fatty acid

FITC - fluorescein isothiocyanate

FN1 – gene encode fibronectin

FRET - Fluorescence Resonance Energy Transfer

GDP - gross domestic product

GFP - green fluorescent protein

GFR - glomerular filtration rate

GLUT4 - insulin-sensitive glucose transporter

GST - Glutathione-S-Transferase

GTP - guanosine triphosphate

H&E - Hematoxylin & Eosin

HEPES - 4-(2-hydroxyethyl)-1-piperazineethanesulfonic acid

HIF - hypoxia-inducible factor

HIF1A - gene encode HIF-1α

IACUC - Institutional Animal Care and Use Committee

IBMX - 3-Isobutyl-1-methylxanthine

IC_{50} - the concentration of an inhibitor where the response is reduced by half

IL-6 - interleukin 6

IP3R - inositol trisphosphate receptor

iPSC - induced pluripotent stem cell

IR - insulin receptor

IRS - insulin receptor substrate

ITP - immune thrombocytopenia

K - potassium

K^+ - potassium ion

KEGG - Kyoto Encyclopedia of Genes and Genomes

Kg - kilogram

LD - lipid droplet

LoxP - locus of X-over P1

MAPK - Mitogen-activated protein kinase

MBS - 25mM MES (2-(N-morpholino)ethanesulfonic acid

mCBM - F97A and F100A double mutant α1 Na/K-ATPase

MCP-1 - monocyte chemoattractant protein-1

MES - 2-(N-morpholino)ethanesulfonic acid

Mg - magnesium

Mg – magnesium

Mg^{2+} - Magnesium ion

mitoNeoD - A Mitochondria-Targeted Superoxide Probe

MitoTEMPO - a mitochondria-targeted superoxide dismutase

MMP - matrix metalloproteinases

mRNA - messenger RNA

MSC - mesenchymal stem cell

Na - sodium

Na/K-ATPase – sodium-potassium adenosine triphosphatase

Na^+ - sodium ion

NADP - Nicotinamide adenine dinucleotide phosphate

NADPH - reduced form of NADP

NaN_3 - sodium azide

NCX - sodium-calcium exchanger

NHE3 - Sodium–hydrogen antiporter 3

NIH - National Institutes of Health

NKA - Na/K-ATPase

nM - nanomolar

N-terminus - NH2-terminus

OCR - oxygen consumption rate

PBS – phosphate-buffered saline

PDGFRA - gene encodes Platelet Derived Growth Factor Receptor Alpha

PDGFRB - gene encodes Platelet Derived Growth Factor Receptor Beta

PE - Phycoerythrin

PKFM – phosphofructokinase

PPARγ - proliferator-activated receptor-γ

RHO - The Rho family of GTPases

RHOGAP - RHO GTPase-activating proteins

RIPA - radioimmunoprecipitation assay

RNA - ribonucleic acid

RNA-seq - RNA sequencing

ROCK - RHO GTPase-RHO-associated kinase

ROS - reactive oxidative species

RT-qPCR - real-time polymerase chain reaction

SB431542 – a specific inhibitor of transforming growth factor-β superfamily type I

SDS - sodium dodecyl sulfate

SE - standard error of the mean

sgDNA - guide RNA

Src - Proto-oncogene tyrosine-protein kinase Src

ssODN - single-stranded oligo donor

TBST - tris-buffered saline and Tween 20

TCA cycle - tricarboxylic acid cycle cycle

TGE motif - Threonine-Glycine-Glutamic motif

TGF - transforming growth factor

TLR4 - toll-like receptor 4

TNFα - tumor necrosis factor alpha

Tris - tris(hydroxymethyl)aminomethane

Trizol - a chemical solution used in the extraction of DNA and RNA

UTP - uridine triphosphate

Vmax - maximum turnover rate

WAT - white adipose tissue

Wnt - Wingless and Int-1

WT – wild type

μl - microlitter

μM - micromolar